# Reduced Deformation Transport of Flexible Objects using Decentralized Robot Networks

Yoshua Redrie Gombo

A dissertation
submitted in partial fulfillment of the
requirements for the degree of

Doctor of Philosophy

University of Washington

2023

Reading Committee:

Santosh Devasia, Chair

Xu Chen

Shuonan Dong

Program Authorized to Offer Degree:
Department of Mechanical Engineering

University of Washington

**Abstract**

Reduced Deformation Transport of Flexible Objects
using Decentralized Robot Networks

Yoshua Redrie Gombo

Chair of the Supervisory Committee:
Santosh Devasia
Department of Mechanical Engineering

This dissertation presents and evaluates new control approaches for flexible object transport using robot networks. Recent works have investigated bio-inspired strategies to transport objects using decentralized robot networks that only use local measurements without the need for communication between robots. However, current decentralized theories focus on ensuring state consensus at the end of the transition and not during transition. Deviation of states during transition causes large deformation, which can lead to damage of the object transported. With current methods, deformation can only be reduced by increasing the transport time. In contrast, this dissertation develops a delayed self-reinforcement (DSR) approach for transport tasks to reduce deformation during transport of flexible objects, without increasing transport time. An advantage of the DSR method is that it only uses a delayed self reinforcement of each robot's actions utilizing prior available data and does not require additional information from the network. This dissertation presents the novel fully decentralized approach using DSR for transporting flexible objects with robot networks, which substantially reduces deformation.

# TABLE OF CONTENTS

# LIST OF FIGURES

# ACKNOWLEDGMENTS

I would to express my sincere appreciation to Professor Santosh Devasia for guiding and supporting me throughout my graduate studies. His patience and encouragement have inspired me to improve as both an engineer and a researcher. Additionally, my gratitude extends to my colleagues and friends in the Precision Controls lab at the University of Washington, whose assistance and contributions were invaluable to the completion of this dissertation. Lastly, I am thankful for the prayers of my family throughout this journey.

# DEDICATION

to my mother and father who always hold me in their prayers.

# Chapter 1

# INTRODUCTION

The use of a multiple robot systems (robot networks) has gained more interest recently due to its advantages as compared to a single robot, which offers flexibility and scalability to do different tasks. For this reason, robot networks have been used in several applications, such as in a platoon of vehicles [4], surveillance and exploration [5], and object transport [2, 6–8]. In general, two typical control schemes used for robot networks are centralized and decentralized. Centralized approaches have been used to achieve precision collaborative control of robot networks [9, 10]. However, the challenge of centralized approaches is the need for sufficient communication bandwidth between the robots and the central controller to maintain situational awareness and generate control actions, which might not be available in all settings [11]. On the other hand, a decentralized approach has several advantages including (i) robustness to failure of one or more robots [12, 13], (ii) scalability of number of robots in the network [7, 14], and (iii) versatility to transport different objects [13, 15] as compared to a centralized approach. Therefore, there is a growing interest in decentralized approaches for robot networks, especially in the application of object transport [16, 17].

Observation in nature indicates that ants seem to use local force measurement in their movement to transport foods, rather than communicating explicitly, e.g., [18]. Similarly, in a transport task the elasticity of the object can be used to transmit information (i.e., forces and positions) among neighbors in the network, instead of communicating with each other directly. Such methods can be used to achieve transport of flexible objects from one position to another, say within some specified transport time. However, the main challenge in decentralized methods is that the deviation between robot states during transition are relatively large, resulting in large deformation which can lead to damaging the object. For

example when transporting uncured-composite aircraft wings, large deformations can lead to structural damage. A current solution to reduce deformation is by slowing down, e.g. increasing transport time, which is not ideal in some cases. Therefore, the main goal of the dissertation is to develop an approach to reduce deformation of flexible object transport in a decentralized manner, without increasing the transport time or changing the network structure. In the following, the current limitation of decentralized-based transport system is presented using an illustrative example and a brief discussion of the research goal with main contributions are also discussed.

## *1.1 Problem Statement*

In this section, an example of network-based transport system is presented, followed by its current limitation.

### *1.1.1 Network-based update for object transport*

Consider a network-based transport system in Fig. 1.1 to illustrate the drawback of such systems. The example system consists of four robots carrying a flexible object shown as the

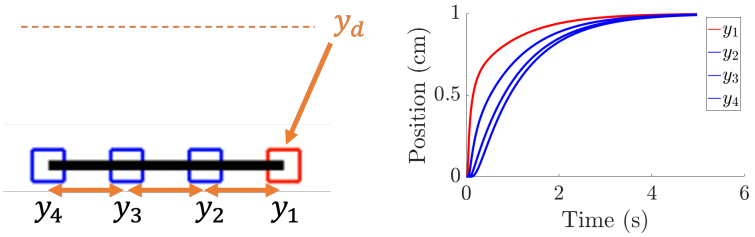


(a) Transport system (b) Typical response

Figure 1.1: Network-based decentralized transport. (a) An example of object transport using a network of four robots with position $y_i$ with $i \in \{1, 2, 3, 4\}$. The red box indicates the leader robot which has information of desired trajectory $y_d$ and the blue boxes are the follower robots. The object transported is shown as the black line. (b) Typical position of each robot in the network in a response to a step in position $y_d = 1cm$.

black line. Only the leader (shown in red) has the information of the desired trajectory $y_d$, and the followers (shown in blue) only respond to local measurement (force) given changes in their neighbors position. Then, the network-based update law in discrete time can be written as,

$$y_k[m+1] = \begin{cases} y_k[m] - \gamma f_k[m] & \text{if } k \text{ is a follower} \\ y_k[m] - \gamma f_k[m] - \gamma k_L(y_k[m] - y_d[m]) & \text{if } k \text{ is a leader,} \end{cases} \tag{1.1}$$

where $y_k$ is the position of robot $k$, $f_k$ is the local force measurement at the contact point of robot $k$, $k_L$ is the alignment strength between leader robot and desired trajectory $y_d$, $\gamma$ is the update gain, and $m$ indicates a discrete time instants ($m\delta_t$) with $\delta_t$ as the sampling time. Note that the update of each robot only depends on its local force measurement, thus the system is decentralized.

### *1.1.2 Current limitation*

Let the deformation metric be quantified as difference between robots' positions, i.e.,

$$\bar{D} = \max_m \big\{ D[m] = \max_{i,j} |y_i[m] - y_j[m]| \big\}, \tag{1.2}$$

where $i, j \in \{1, 2, 3, 4\}$. The typical position response of each robot is shown in Fig. 1.1b, which shows convergence only at the end of transition, but the deviation of positions between robots are relatively large during transition. This implies that the object is deformed during transition, which can lead to damage. A way to reduce deformation is by changing the update gain $\gamma$ in Eq. (1.1), but it requires increasing the transport time. For instance as shown in Fig. 1.2, the maximum deformation is reduced to $0.550cm$ with transport time of $20s$ as compared to $0.612cm$ with transport time of $2s$. Hence, there is a trade-off between transport time and deformation as shown in Fig. 1.3. Decreasing the update gain $\gamma$ does reduce deformation, however the transport speed increases and vice versa.

The current limitation of the current decentralized approaches is that reducing the object deformation with current methods requires an increase in the transport time. Thus, this

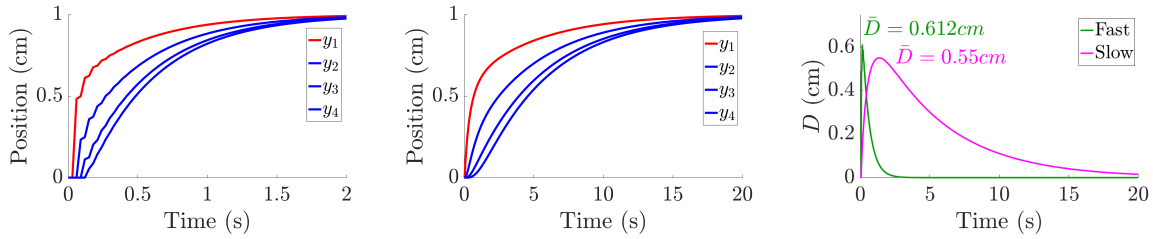


(a) Faster response (b) Slower response (c) Deformation over time

Figure 1.2: (a) A faster response by increasing the update gain $\gamma$ in Eq. (1.1). Note that all robots reach $y_d = 1cm$ in $2s$ time. (b) Conversely, a slower response by decreasing $\gamma$ but the task in completed in $20s$ for the same $y_d = 1cm$. (c) A comparison between the two responses showing the deformation as in Eq. (1.2), where the maximum deformation is higher when moving faster ($\bar{D} = 0.612cm$) than moving slower ($\bar{D} = 0.550cm$) per Eq. (1.2).

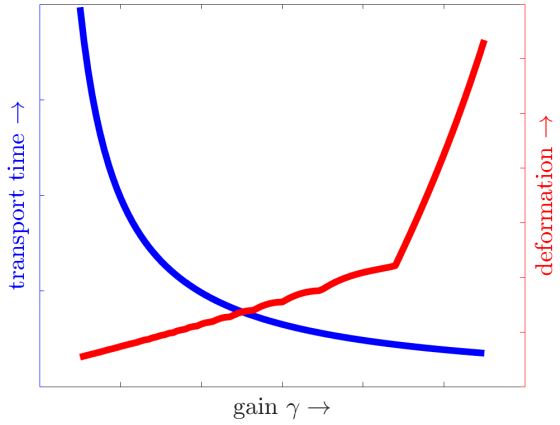


Figure 1.3: Typical trade off between transport time and deformation as in Eq. (1.2) with respect to update gain $\gamma$.

motivates the main research goal that is to develop an approach for transporting flexible objects using robot networks in a decentralized manner, while avoiding excess deformation without increasing transport time.

## *1.2 Research Goal*

The main research goal which is to transport flexible objects using robot networks in a decentralized manner, while avoiding excess deformation without increasing transport time. This leads to the formulation of research questions (**RQ**s) and main contributions (**MC**s) described in the subsequent subsections in the following.

### *1.2.1 RQ1: Does accelerated methods decrease deformation during transition?*

Increasing state transition time allows each robot in the network to response faster, thus reaching faster convergence. This can be achieved by using accelerated-gradient-based method as shown in [19] and can potentially yield to decrease in deformation. Therefore, the objective of research question 1 (**RQ1**) is to investigate if accelerated methods decrease deformation of the object during transition.

**MC1: Development and evaluation of an accelerated-gradient-based method for object transport.**

The first main contribution (**MC1**) of the dissertation addresses research question 1 (**RQ1**) and has been published in [1]. For a robot network, increasing state transition time can potentially decrease deviation between robots state, thus reducing object deformation during transition. The convergence rate of the standard decentralized update law shown in Eq. (1.1) only depends on the update parameter $\gamma$. However, there is a limit on the parameter $\gamma$ which affects the stability of the network. An alternative way to increase speed of convergence is by using an accelerated-gradient-based method [1, 19]. For object transport tasks, the accelerated method is formulated by modifying the standard update law in Eq. (1.1) to obtain,

$$\begin{aligned} y_k[m+1] = y_k[m] - \gamma f_k[m] - \gamma k_L(y_k[m] - y_d[m]) \\ + \beta_2(y_k[m] - y_k[m-1]) - \beta_1(f_k[m] - f_k[m-1]), \end{aligned} \tag{1.3}$$

where $\beta_1$ and $\beta_2$ are the accelerated gains, $k_L \neq 0$ if $k$ is a leader and zero otherwise . The

added terms in Eq. (1.3) allow the rate of convergence to be speed up by selecting gains $\beta_1$ and $\beta_2$.

However, as shown in the results in [1], faster transition does not necessarily decrease deformation. Indeed, for a specific desired trajectory, e.g. a constant speed (ramp in position), the deformation does decreases, but for another trajectory, e.g., a step in position, the deformation is still large. This leads to the next research question (**RQ2**), that is to investigate an alternative approach to reduce deformation during transition.

### *1.2.2 RQ2: How to reduce deformation during transition without increasing transport time?*

Faster transition does not necessarily reduce deformation. Although, it increases rate of convergence of the robot network to a new consensus value, the deformation is still large or even more at some cases as shown in Fig. 1.2c. An approach to decrease deformation is by considering an ideal centralized-based approach, which is implemented in a decentralized manner using delayed-self-reinforcement (DSR) method. The DSR approach enables all robots to have similar responses during transition, resulting in small deviations between states of the robot and thus decreasing deformation. Hence, the objective of research question 2 (**RQ**2) is to investigate if the DSR approach reduces deformation during transition.

**MC2.1: Development of a reduced-deformation approach using DSR for translational transport.**

The first part of main contribution 2 of the dissertation (**MC2.1**) is the development of DSR based approach for translational transport, which has been published in [2]. The delayed-self-reinforcement (DSR) approach uses outdated feedback measurements of each robot to achieve similar responses among the robots in the network, similar to the accelerated approach shown in Eq. (1.3). In fact, the DSR approach is a special case of accelerated approach with the gain $\beta_2 = 1$. The DSR-based update law can be written as,

$$\begin{aligned} y_k[m+1] = y_k[m] - \gamma f_k[m] - \gamma k_L(y_k[m] - y_d[m]) \\ + (y_k[m] - y_k[m-1]) - \beta(f_k[m] - f_k[m-1]), \end{aligned} \tag{1.4}$$

where $\beta$ is the DSR gain. The results in [2] show that with DSR, the deformation of the object during transition decreases significantly due to the fact that each robot moves in a similar way.

The main contribution published in [2] focuses on the translation motion where the zero deformation state are similar for all robots. However, rotation transport poses another challenge due to change is object orientation. Orientation changes caused by rotations of the leader robots can cause larger deformations when compared to translational transport case since the desired movement of other robots in the network tend to increase with distance from the center of rotation and depends on the object geometry, whereas during translation only all robots have similar desired displacements. This leads to the development of the second part of main contribution 2, that is to reduce deformation for translational and rotational transport.

**MC2.2: Development of a reduced-deformation approach using DSR for translational and rotational transport.**

The second part of main contribution 2 (**MC2.2**) is to develop DSR-based approach for translational and rotational transport. This work has been accepted to a peer-reviewed journal shown in [3]. Rotational motion affects the dynamics of the object to be time-varying due to change in orientation. As a consequence, the zero deformation state for each robot is also changing with respect to object's geometry and orientation. Since the rate of object orientation directly affecting the deformation of the object during rotation, the main contribution is to establish stability conditions on the control parameters for the DSR approach while also quantifying the deformation bounds that depends on the rate of orientation changes.

### *1.2.3 RQ3: Can the transport task be fully-decentralized?*

Bio-inspired decentralized approaches for transporting objects with robot networks seek to use locally-sensed information without the need for communication. However, the parameter

selection to achieve a specified network performance (e.g., to achieve a desired network settling time $T_s$) depends on the specific network and therefore tends to be a centralized decision. Such centralized parameter selection is not biomimetic and might not be viable if communication is not available between agents to achieve consensus on the parameter selection. Therefore, the objective of research question 3 (**RQ3**) is to investigate a fully-decentralized approach for the transport tasks to select the control parameters in decentralized manners.

**MC3: Development of decentralized parameters selection for transport tasks.** The third main contribution (**MC3**) addresses research question 3 (**RQ3**) and the article is ready to be submitted to a peer-reviewed journal [20]. The goal is to develop a decentralized parameter selection approach using local measurements, which does not require prior knowledge of the network connectivity structure or object properties. The proposed delayed self-reinforcement (DSR) approach decentralizes the ideal case (where each robot has information about the transport task) with only already-available, sensed interaction forces with the object.

## 1.3 Research Timeline

The summary of the research timeline is shown in the Fig. 1.4 below.

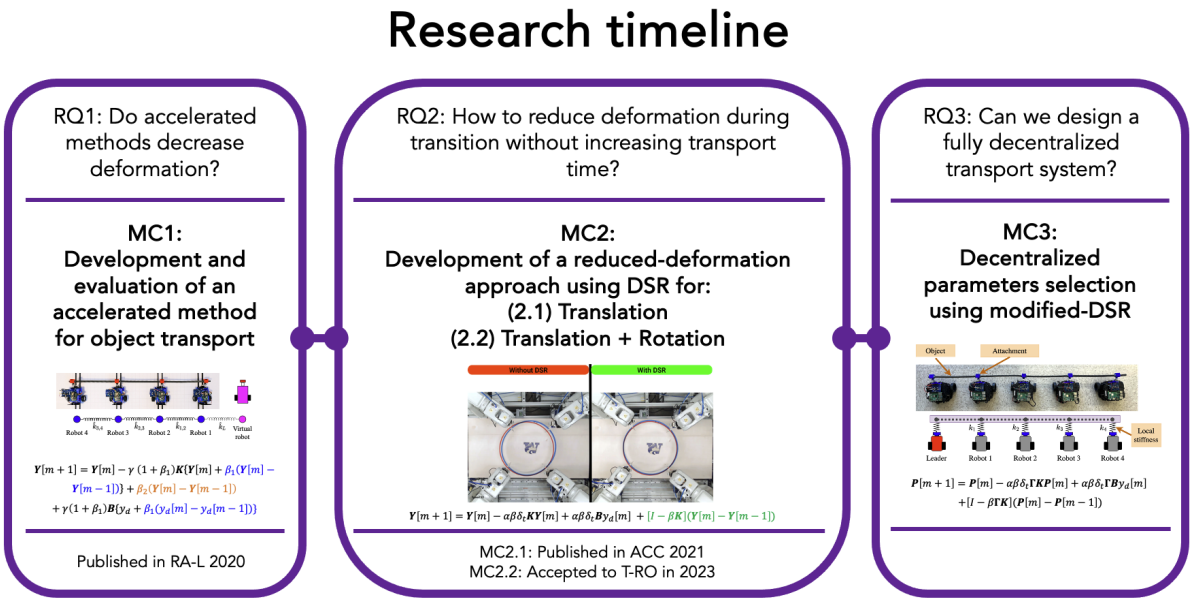


Figure 1.4: Research timeline with main contributions and publications [1–3].

## 1.4 Structure of the Thesis

The rest of this dissertation is organized as follows. Chapter 2 provides background of each main contribution, including the a brief review on accelerated-gradient-based and delayed-self-reinforcement (DSR) approaches. Chapter 3 presents the main contribution 1 (**MC1**), that is the development of accelerated-gradient-based approach. Next, Chapter 4 which presents the first part of main contribution 2 (**MC2.1**), that is to use DSR to reduce deformation during translational transport. Chapter 5 presents the continuation of main contribution 2 (**MC2.2**) to extend the DSR approach for translational and rotational transport. Chapter 6 presents the efforts for the main contribution 3 (**MC3**), a decentralized parameters selection for transport tasks. And lastly, Chapter 7 discusses potential direction towards

future work regarding the transport task using robot networks.

# Chapter 2
# BACKGROUND

This chapter presents a brief review and background of main contributions (**MC1**, **MC2**, **MC3**) of this dissertation. Each corresponding background are taken from the published articles in [1, 2], the accepted article in [3] and the ready-to-submit article in [20].

## *2.1 Background on object transport*

### *2.1.1 Transport: manipulation and locomotion*

In general, a transport task includes (i) locomotion, i.e., the motion of the object from one position to another and (ii) manipulation, i.e., the handling aspect such as holding and orienting the object [21, 22]. Manipulation aspect of the transport, e.g., holding an object using friction can require centralized coordination to partition the required holding forces amongst the different robots, with a zero net resultant force [8, 23]. If the object does not have to be held up by the robots, then other strategies such as pushing-and-pulling, grasping or caging can be used for the locomotion aspect of transport, e.g., see [24]. Since it is possible to decouple the manipulation and locomotion tasks [21, 22], this dissertation focuses on the locomotion aspect of the transport by attaching the robots to the object using connectors that create pin-joint and cantilever-type connectors to hold the object.

### *2.1.2 Decentralized versus centralized*

Centralized approaches have been used to achieve precision collaborative control of robot networks [9, 10]. However, the challenge of centralized approaches is the need for sufficient communication bandwidth between the robots and the central controller to maintain situational awareness and generate control actions, which might not be available in all settings [11].

Moreover, detailed models of the object being transported (that couples the interactions between the robots) might not be available to implement centralized collaborative controllers. Approximate models can be used, but inaccuracy of object models lead to errors in robot control inputs, which can cause asynchronous motions among robots and potentially damage the object.

On the other hand, a decentralized approach has several advantages including (i) robustness to failure of one or more robots [12, 13], (ii) scalability of number of robots in the network [7, 14], and (iii) versatility to transport different objects [13, 15] as compared to a centralized approach. Therefore, decentralized approaches are more preferable to be used for object transport with robot networks [16, 17]. In the application of an object transport task, local force and velocity measurements from the interaction with the object have been used to update each robot's motion and alignment in a decentralized manner [7]. If the mass of the object is relatively small compared to the robot, or if the accelerations are small, then the forces caused by the inertial dynamics [8, 25, 26] are less significant than the forces caused by robots' elastic interactions [5, 27], and local position-based robot control updates with force feedback can be used for object manipulation, e.g., [28, 29]. The work in this dissertation uses similar local (force) measurements to update robot's next position in a decentralized manner.

## *2.2 MC1: Development and evaluation of an accelerated-gradient-based method for object transport.*

The overall goal is to move flexible objects rapidly without increasing deformation using robot networks. Large deformations in the object can lead to damage. Nevertheless, the flexibility of the object can be used to transmit information about the displacements and forces from neighbors for co-ordination of the task, rather than requiring communication with each other. Similar behavior is seen in nature, where ants appear to use local force and displacement measurements instead of using direct communication to transport food, e.g., [18]. As opposed to rigid objects, flexible objects can convey the intent of neighboring

robots through both local forces and deformation. Therefore, changes to the desired shape of highly flexible objects has been measured and used as feedback for decentralized control of robot teams during transport, e.g., [5, 27]. Similarly, local force measurements on flexible objects have been used to update the force applied by each robot in a decentralized manner in [8, 30]. The speed of transport, i.e., convergence of the robot team and the flexible object to a new position, depends on the specific connectivity-graph of the team. It is shown in this work that the fastest transport to a new position is limited by the need to ensure overall stability [31]. Moreover, the transport speed tends to decrease as the number of robots increases, especially if the number of inter-robot connections remain small [32]. This limit motivates the current investigation into alternate update laws to speed up the transport for the same connectivity between the robot team and the flexible object, without increasing object deformation.

This work uses the accelerated-gradient approach to improve the convergence of the robot team and thereby achieve faster transport. Note that the robot team's update law can be considered to be the gradient of a potential, e.g., [8]. Hence, this work proposes the use of accelerated-gradient-based approaches, which have been used to speed up gradient-based optimization [19], to speed up transport using robot teams. Nevertheless, it is important that the increase in transport speed does not lead to excessive deformation. For example, when transporting flexible objects, such as large uncured-composite aircraft wings in a manufacturing setting, large deformations can lead to damage. Therefore, this contribution work selects the parameters of the accelerated gradient-based update approach to increase the transport speed without increasing the deformations of the flexible object. An advantage of the proposed gradient-based approach is that it can be implemented with only local force information using an accelerated delayed self reinforcement (A-DSR), without the need for additional information.

### *2.3 MC2.1: Development of a reduced-deformation approach using DSR for translational transport.*

The main goal is to transport flexible objects cohesively (i.e., all robots move in a similar manner) using decentralized robot networks. Network control theories can be used to rapidly transition from one equilibrium (where all the robots in the network are in consensus) to another, i.e., a new consensus value, which also can be applied for transporting an object using robot networks. However, current network theories focus on the speed of convergence to a new consensus value [19, 33], and they do not aim to ensure that the robot responses remain cohesive during transition. For a transport task, the lack of cohesion during transition can lead to large deformation and cause damage to the object being transported. While centralized communication can yield to low-deformation transport [9, 10], there is a growing interest in decentralized transport using a robot network that only uses local sensing due to robustness to one or more robot failures [12,13], adaptability to varying number of robots [7, 14], and versatility to transport different objects [13, 15], without the need for centralized control and communication [11]. The main contributions of this chapter are to propose a cohesive transport approach for flexible structures with decentralized robot networks, and to establish stability conditions for a discrete-time implementation using local force sensing.

Observation in nature indicates that ants seem to use local force measurement in their movement to transport foods, rather than communicating explicitly, e.g., [18]. Similarly, in a transport task the elasticity of the object can be used to transmit information (i.e., forces and positions) among neighbors in network, instead of communicating with each other. For example, as shown in [7,8,30,34] measurements of the local force exerted between the flexible object and robot can be used to infer the local deformation and accomplish the transport task in a decentralized manner. Alternatively, changes in the desired shape of the object can also be measured to develop a decentralized feedback control for object transport, e.g., [5,27]. While such methods can be used to achieve transport of flexible objects from one position to another, say within some specified settling time, there is no direct control over the resulting

deformations on the object. In the presence of only a few leaders (who have access to desired transport trajectory), there can be substantial deviation in the robot positions away from the leaders resulting in distortion and potential damage. For example when transporting uncured-composite aircraft wings, large deformations can lead to structural damage. If all the robots are leaders with access to the desired transport trajectory, then the network response would be cohesive, but this leads to a centralized approach, and such communication might not be always feasible, e.g., if one of the robots is directly controlled by a human and the others follow based on neighbor-based observations or local sensing of the object. This motivates the effort to improve cohesion during decentralized transport of flexible objects.

## *2.4 MC2.2: Development of a reduced-deformation approach using DSR for translational and rotational transport.*

Decentralized object transport involves a team of robots carrying an object in a cooperative manner from one place to another. If the robots are not physically attached to the object then they rely on pushing actions [7,15,35], and if the robots physically grasp the object, then they can both push and pull the object [8,11,13,25]. In either case, direct communication between robots is needed to allocate the required forces amongst the robots. The main contribution considers decentralized transport of flexible objects without the need for communication between robots. Such decentralized approaches are found in nature, e.g., when ants use local measurements (small vibrations and forces) to cooperatively transport food, instead of using direct communication [18, 36, 37]. Similar biomimetic approaches using local measurements have been used for the transport of flexible-objects using decentralized robot networks [1, 7, 11, 12, 17]. In these approaches, each robot measures its local deformation and then seeks to reduce it. The object acts as a medium to convey information between robots, and coordinate the transport. The connectivity of robots in the network is established through the object, as illustrated in Fig. 2.1. Thus, local measurements can be used in lieu of inter-robot communications for object transport with decentralized robot networks.

The goal is to avoid excessive deformation of the flexible object during transport since

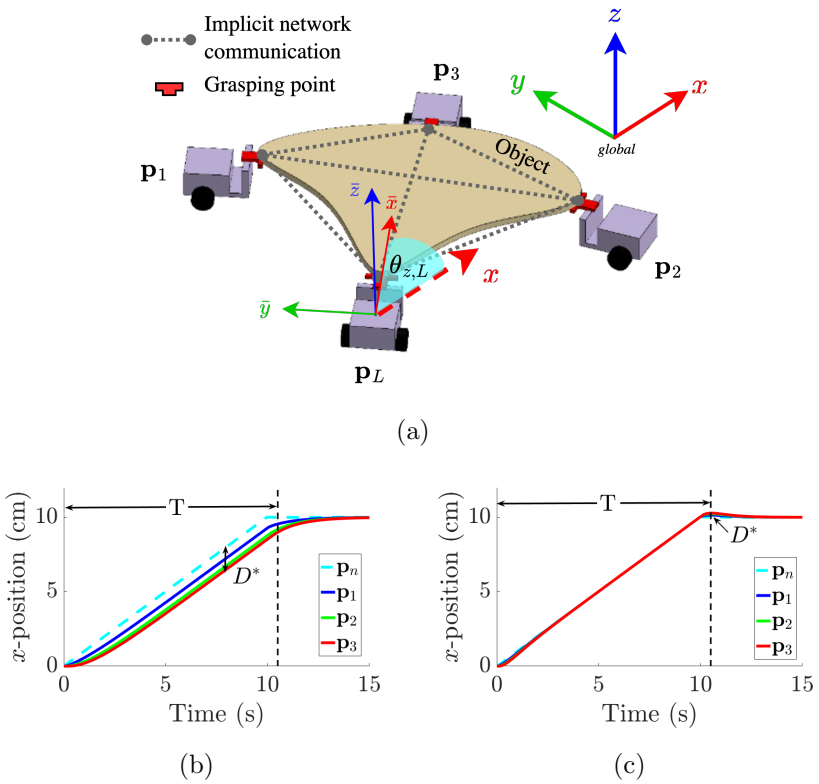


Figure 2.1: (Top) An implicit network is formed between the robots due to the connectivity through the flexible object (a). Each robot uses locally measured force or deformation to infer information about the overall intended task as well as external perturbations, which eliminates the need for direct communication with each other to coordinate the transport. The position $\mathbf{p}_i$ of the $i^{th}$ robot in global frame $(x, y, z)$ is $(p_{x,i}, p_{y,i}, p_{z,i})$ and in the local frame $(\bar{x}, \bar{y}, \bar{z})$ is $(\bar{p}_{x,i}, \bar{p}_{y,i}, \bar{p}_{z,i})$. The local frame is attached to the leader robot $(i = L)$ and oriented at $\Theta_L = [\theta_{x,L}, \theta_{y,L}, \theta_{z,L}]^\intercal$ with respect to the global frame. (Bottom) Example transport trajectories without DSR (b) and with DSR (c). Both cases have the same leader trajectory $\mathbf{p}_L$ and transport time $T$ between initial and final configurations. However, the maximum deformation $D^*$ is smaller with DSR.

it can lead to damage, e.g., when transporting uncured-composite parts during aerospace manufacturing [38]. The object deformation tends to increase with distance from the lead robots that have access to the desired transport trajectory during autonomous operations or are being directly controlled by a human. Moreover, orientation changes caused by rotations of the lead robots can cause larger deformations when compared to translational transport

case since the desired movement of other robots in the network tend to increase with distance from the center of rotation and depends on the object geometry, which in turn, requires centralized information of the object's geometry. In contrast, all robots have similar desired displacements during translation. While the robot-network structure can be optimized to minimize the object deformation, the research challenge is that, in general, reducing the object deformation $D^*$ also requires an increase in the transport transition time $T$ (i.e., the transition time between the initial and final configurations) for a given transport trajectory $\mathbf{p}_L$. This motivates the current work to develop an approach that decreases the object deformation $D^*$ without increasing the transport time $T$ for the same desired trajectory $\mathbf{p}_L$, as shown in Fig. 2.1. The desired trajectory $\mathbf{p}_L$ is available only to the leader robots and not to the follower robots, which use locally sensed forces to infer the required change in position. The main contribution is to develop a decentralized approach for transport tasks that uses previous local force measurements to add a delayed self-reinforcement (DSR) to the robots' actions, resulting in smaller object deformation, even during orientation changes. An advantage is that the DSR approach does not require changes to the network structure, i.e., neither the connectivity between the robots nor an increase in the number of robots nor increased inter-robot communication.

The work in this main contribution is an evolution of prior work of the main contribution 2.1 (**MC2.1**) also shown in [2], which presented experimental results that DSR can reduce deformation during purely translational transport where the motion of the robots is cohesive, i.e., each robot moves in the same manner. Moreover, the dynamics of translational transport is time-invariant. In contrast, the current work develops a new decentralized DSR theory for orientation changes, when the robot motions are no longer cohesive, since the desired position-changes for the robots can vary depending on the robot's geometric location. Additionally, analysis is developed for the resulting time-varying dynamics (i) to establish conditions on the control parameters for stability of the DSR approach and (ii) to quantify the performance in terms of deformation bounds.

### *2.5 MC3: Development of decentralized parameters selection for transport tasks.*

Decentralized approaches for transporting flexible objects with robot networks seek to use only locally-sensed information without communication between robots [39]. Such decentralized behavior is observed in natural systems, for instance, when ants cooperatively transport food. Studies have shown that ants only use local small vibrations and forces from the interactions with the object to infer the collective intent of the group, rather than communicating directly with each other [36, 40]. Similarly, in bio-inspired object transport, the goal is to use a team of robots for transporting objects from one place to another by using only local measurements without communication. However, local communication is often needed to partition the net force amongst all the robots [8, 15] and to ensure that the net force aligns with the desired transport direction [41, 42], as illustrated in Fig. 2.2. The need for communication can be avoided when the object is flexible since the local interaction forces implicitly contain information about the forces acting on the object. Specifically, local measured forces can be used to find robot motion updates to achieve decentralized implementation of the cooperative transport [7, 12, 35]. Nevertheless, even with such decentralized implementation of the transport task, centralized information is still needed to design the gain for each individual robot update [21, 43]. This work considers decentralized methods to select update gains for each robot for achieving specified performance, without the need for centralized information about the robot-object network structure or stiffness properties of the flexible object.

The parameter selection in robot networks also tends to be centralized in order to meet the desired transport performance criteria, such as settling time and stability. In general, the network settling time $T_s$ can be designed to be much slower than the settling time of each individual robot $T_r$ and the update sampling time $\delta_t$, to ensure network convergence, i.e.,

$$T_r < \delta_t << T_s. \tag{2.1}$$

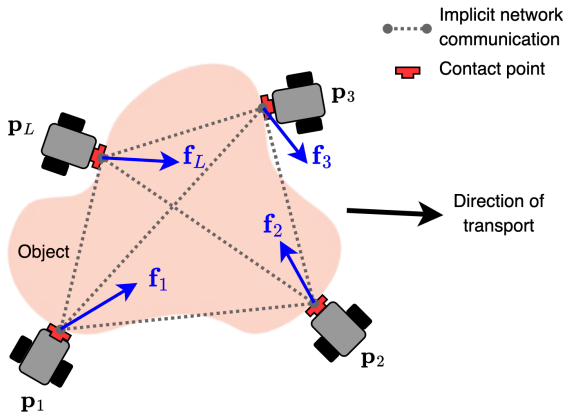


Figure 2.2: Example transport network with four robots $\mathbf{p}_i$ for $i \in \{L, 1, 2, 3\}$, transporting an object. The schematic shows that each robot applies prerequisite force $\mathbf{f}_i$ for $i \in \{L, 1, 2, 3\}$ such that the net force $\sum_i \mathbf{f}_i$ aligns with the direction of transport.

However in the standard decentralized approaches, selecting the network settling time $T_s$ is depending upon the second smallest eigenvalue of the network connectivity matrix, i.e., the Laplacian matrix [44]. Obtaining this information tends to be challenging without centralized knowledge concerning the network connectivity structure. Furthermore, the control parameters need to be selected to ensure stability of the transport. Yet, finding the bounds of stable control parameters relies on centralized information, specifically the largest eigenvalue of the network connectivity matrix. This holds true even for the recently developed approach that uses delayed self-reinforcement (DSR) to reduce deformation during transport [1,2]. Although the DSR-based transport approach effectively reduces deformation during transport and allows the robots to achieve the desired network settling time $T_s$, the design of the DSR algorithm, including the optimal parameter selection, requires the knowledge of network connectivity structure. Such centralized parameter selections are not viable for large networks with varying number of robots and for transporting different types of objects. In addition, these approaches do not reflect the novelty of the fully decentralized behavior observed in biological systems. This motivates the current work to develop a decentralized parameter

selection approach using local measurements, which does not require prior knowledge of the network connectivity structure or object properties.

# Chapter 3

# MC1: DEVELOPMENT AND EVALUATION OF AN ACCELERATED-GRADIENT-BASED METHOD FOR OBJECT TRANSPORT

This chapter forms the main contribution 1 (**MC1**) of this dissertation, that is to use accelerated - delayed self reinforcement (A-DSR) to achieve faster transport using robot networks, and has been published in [1]. This work proposes the use of accelerated-gradient-based approaches, which have been used to speed up gradient-based optimization [19], to speed up transport using robot networks. Nevertheless, it is important that the increase in transport speed does not lead to excessive deformation. For example, when transporting flexible objects, such as large uncured-composite aircraft wings in a manufacturing setting, large deformations can lead to damage. Therefore, the work in this chapter selects the parameters of the accelerated gradient-based update approach to increase the transport speed without increasing the deformations of the flexible object. An advantage of the proposed gradient-based approach is that it can be implemented with only local force information using an accelerated delayed self reinforcement (A-DSR), without the need for additional information.

## *3.1 Preliminaries and problem statement*

### *3.1.1 Preliminaries*

The decentralized robot team here is a set of robots that interact with each other by sensing local forces through the object being transported, without the need for direct communication between them, as illustrated in Figure 3.1. The team includes a leader robot $r_L$ that has access to the desired position trajectory $\mathbf{z}_d = [z_{d,1}, z_{d,2}, z_{d,3}]^T \in \mathbb{R}^3$ (with the superscript

$T$ indicating matrix transpose), which can be provided by an external source such as a human. This access to the desired trajectory $\mathbf{z}_d$ is included in the model as a virtual robot, which is at the desired position $\mathbf{z}_d$ at all times and is connected to the leader robot $r_L$ via virtual springs of stiffness $\left\{\hat{k}_{L,j}\right\}_{j=1}^{3}$ that denotes the alignment strength between the leader's position $\mathbf{z}_L = [z_{L,1}, z_{L,2}, z_{L,3}]^T \in \mathbb{R}^3$ and the virtual robot's position $\mathbf{z}_d$.

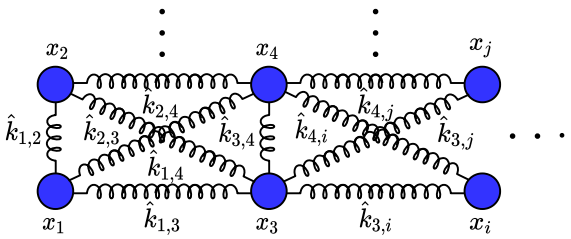


Figure 3.1: Schematic transport model with $n$ robots at nodes $x_k$ on the flexible object where $1 \leq k \leq n$.

*Background: gradient-based position update*

Decentralized transport using local force feedback can be modeled as a network-based update [7, 8]. The relation between force $\mathbf{F} \in \mathbb{R}^{3n}$ and position $\mathbf{Z} \in \mathbb{R}^{3n}$ of the flexible object at nodes attached to the robots in Figure 3.1 can be related through the gradient of the potential energy $\hat{\Phi}(\mathbf{Z})$ due to object's elastic deformation as

$$\mathbf{F} = \nabla\hat{\Phi}(\mathbf{Z}), \tag{3.1}$$

where $\mathbf{Z} = [\mathbf{z}_1, \ldots, \mathbf{z}_n]^T$, the position $\mathbf{z}_k \in \mathbb{R}^3$ of the $k^{th}$ robot at node $x_k$ is a vector of its three components $\mathbf{z}_k = [z_{k,1}, z_{k,2}, z_{k,3}]^T$ measured from an initial undeformed configuration of the flexible object. The total potential $\Phi$, which includes the potential of the virtual springs is given by

$$\Phi(\mathbf{Z}) = \hat{\Phi}(\mathbf{Z}) + \frac{1}{2}\sum_{j=1}^{3}[z_{L,j} - z_{d,j}]^T\hat{k}_{L,j}[z_{L,j} - z_{d,j}]. \tag{3.2}$$

Note that if all robots are at the same desired position $\mathbf{z}_k = \mathbf{z}_{k,d} = \mathbf{z}_d$ for $1 \leq k \leq n$ with the position of all robots $\mathbf{Z} = \mathbf{Z}_d = [\mathbf{z}_{1,d}, \ldots \mathbf{z}_{n,d}]^T$, then the elastic deformation and the

potential energy $\hat{\Phi}(\mathbf{Z})$ are zero, resulting in zero total potential, i.e., $\Phi(\mathbf{Z}_d) = 0$. Therefore, the position update of the robot seeks to minimize the potential energy $\Phi$ using its gradient as

$$\mathbf{Z}[m+1] = \mathbf{Z}[m] - \gamma \nabla \Phi(\mathbf{Z}[m]), \tag{3.3}$$

where the position updates are completed within the time interval $\delta_t$, $\mathbf{Z}[m] \in \mathbb{R}^{3n}$ represents the position $\mathbf{Z}$ at discrete time instants, i.e., $\mathbf{Z}[m] = \mathbf{Z}(m\delta_t)$, and $\gamma$ is the update gain.

*Implementation using local sensing*

For an individual robot $r_k$, Eq. (3.3) can be written in terms of the local force $\mathbf{f}_k = [f_{k,1}, f_{k,2}, f_{k,3}]^T \in \mathbb{R}^3$ depending on whether the robot is a leader or not, as

$$\mathbf{z}_k[m+1] = \begin{cases} \mathbf{z}_k[m] - \gamma \mathbf{f}_k[m] & \text{if } k \neq L \\ \mathbf{z}_k[m] - \gamma \mathbf{f}_k[m] - \gamma \hat{\mathbf{k}}_L(\mathbf{z}_L[m] - \mathbf{z}_d[m]) & \text{if } k = L, \end{cases} \tag{3.4}$$

where $\hat{\mathbf{k}}_L$ is a $3 \times 3$ diagonal matrix with $\hat{k}_{L,j}$ $(1 \leq j \leq 3)$ along the diagonal. Since the current work aims to keep the deformation in the object small, the force-position relation in Eq. (3.1) is considered to be linear, i.e.,

$$\mathbf{F} = \hat{\mathbf{K}}\mathbf{Z}, \tag{3.5}$$

where the stiffness matrix $\hat{\mathbf{K}}$ is positive semidefinite, i.e., $\mathbf{Z}^T\hat{\mathbf{K}}\mathbf{Z} \geq 0$ for any robot-team position. Then, the update dynamics in Eq. (3.3) can be rewritten as

$$\mathbf{Z}[m+1] = \mathbf{P}\mathbf{Z}[m] + \gamma \mathbf{B}\mathbf{z}_d[m], \quad \mathbf{P} = \mathbf{I} - \gamma \mathbf{K} \tag{3.6}$$

where $\mathbf{K}$, referred to as the pinned Laplacian [44], is identical to the stiffness matrix $\hat{\mathbf{K}}$ except along the diagonal terms associated with the leader where $\mathbf{K}_{(L^*+j),(L^*+j)} = \hat{\mathbf{K}}_{(L^*+j),(L^*+j)} + \hat{k}_{L,j}$ for $L^* = 3(L-1)$ and $1 \leq j \leq 3$. The matrix $\mathbf{B}$ is nonzero only at rows associated with the leader robot, i.e., $\mathbf{B}_{(L^*+j),j} = \hat{k}_{L,j}$ for $1 \leq j \leq 3$ and zero elsewhere.

**Assumption 1** *In the following, it is assumed that there are no rigid body modes (translations or rotations of the flexible body) remaining when the virtual robot is at a fixed position* $\mathbf{z}_d$*, i.e., the eigenvalues* $\lambda_{\mathbf{K},k}$ *of the pinned Laplacian* $\mathbf{K}$ *are nonzero.*

*Bound on update gain for stability*

For a fixed desired position trajectory $\mathbf{z}_d$, the robot position $\mathbf{Z}_d$ is an equilibrium since it results in an update $\mathbf{z}_k[m+1] = \mathbf{z}_k[m]$ in Eq. (3.4) and the local force $\mathbf{f}_k = \mathbf{0}$. The transport dynamics in Eq. (3.6) is stable if the spectral radius (maximum magnitude of the eigenvalues $\lambda_{\mathbf{P},k}$) of the matrix $\mathbf{P} = \mathbf{I} - \gamma\mathbf{K}$ is less than one, i.e.,

$$\rho(\mathbf{P}) = \max_k |\lambda_{\mathbf{P},k}| = \max_k |1 - \gamma\lambda_{\mathbf{K},k}| < 1 \tag{3.7}$$

where $\lambda_{\mathbf{K},k} = a_k + b_k\sqrt{-1}$ are the eigenvalues of the pinned Laplacian $\mathbf{K}$. The stability condition in Eq. (3.7) is met if the update gain $\gamma$ satisfies [31]

$$0 < \gamma < \min_{1\le k\le n} \frac{2a_k}{a_k^2 + b_k^2} = \overline{\gamma}. \tag{3.8}$$

### *3.1.2 Problem statement*

The update gain can be selected from the stable range in Eq. (3.8) to speed up the convergence of the robot team $\mathbf{Z}$ to a desired position $\mathbf{Z}_d$, i.e., to achieve a desired transport time. However, there is no control over the resulting deformation in the flexible object during the transition to the desired position of $\mathbf{Z}_d$. Therefore, the research problem is to decrease the deformation of the flexible object without changing the transport time. Alternatively, the proposed approach seeks to decrease the transport time without increasing the deformation. This improvement is to be achieved without changing the robot-connectivity structure $\mathbf{K}$ and without centralized approaches such as broadcasting the desired trajectory $\mathbf{z}_d$ to all robots.

## *3.2 Proposed approach*

### *3.2.1 Accelerated Delayed Self Reinforcement (A-DSR)*

The generalized accelerated-gradient update is given by modifying the standard gradient-based update in Eq. (3.3), as in [19, 45] to

$$\begin{aligned}\mathbf{Z}[m+1] &= \mathbf{Z}[m] - \gamma\nabla\Phi\big\{\mathbf{Z}[m] + \beta_1\big(\mathbf{Z}[m] - \mathbf{Z}[m-1]\big)\big\} \\ &\quad + \beta_2\big(\mathbf{Z}[m] - \mathbf{Z}[m-1]\big) \qquad (3.9) \\ &= \mathbf{Z}[m] - \gamma(1+\beta_1)\mathbf{K}\big\{\mathbf{Z}[m] + \beta_1\big(\mathbf{Z}[m] - \mathbf{Z}[m-1]\big)\big\} \\ &\quad + \gamma(1+\beta_1)\mathbf{B}\big\{\mathbf{z}_d[m] + \beta_1\big(\mathbf{z}_d[m] - \mathbf{z}_d[m-1]\big)\big\} \\ &\quad + \beta_2\big(\mathbf{Z}[m] - \mathbf{Z}[m-1]\big). \qquad (3.10)\end{aligned}$$

The A-DSR update in Eq. (3.10) can be computed by each robot $r_k$ using local force $\mathbf{f}_k$ as,

$$\begin{aligned}\mathbf{z}_k[m+1] =& \mathbf{z}_k[m] - \gamma(1+\beta_1)^2\mathbf{f}_k[m] + \gamma(1+\beta_1)\beta_1\mathbf{f}_k[m-1] \\ &+ \beta_2(\mathbf{z}_k[m] - \mathbf{z}_k[m-1]) \\ &- \gamma(1+\beta_1)^2\hat{\mathbf{k}}_k^*(\mathbf{z}_L[m] - \mathbf{z}_d[m]) \\ &+ \gamma(1+\beta_1)\beta_1\hat{\mathbf{k}}_k^*(\mathbf{z}_L[m-1] - \mathbf{z}_d[m-1]), \qquad (3.11)\end{aligned}$$

where $\hat{\mathbf{k}}_k^* = \hat{\mathbf{k}}_L$ if robot $r_k$ is a leader ($k = L$), and $\hat{\mathbf{k}}_k^* = \mathbf{0}$ if robot $r_k$ is not a leader ($k \neq L$). Note that this update can be implemented by each robot using current and delayed self reinforcement with previously collected information, as illustrated in Figure 3.2, hence it is referred to as A-DSR.

### *3.2.2 Stability conditions for A-DSR*

The proposed A-DSR dynamics in Eq. (3.10) can be expressed further in a state-space form as,

$$\mathbf{S}[m+1] = \mathbf{A}_s\mathbf{S}[m] + \mathbf{B}_s\mathbf{s}_d[m], \qquad (3.12)$$

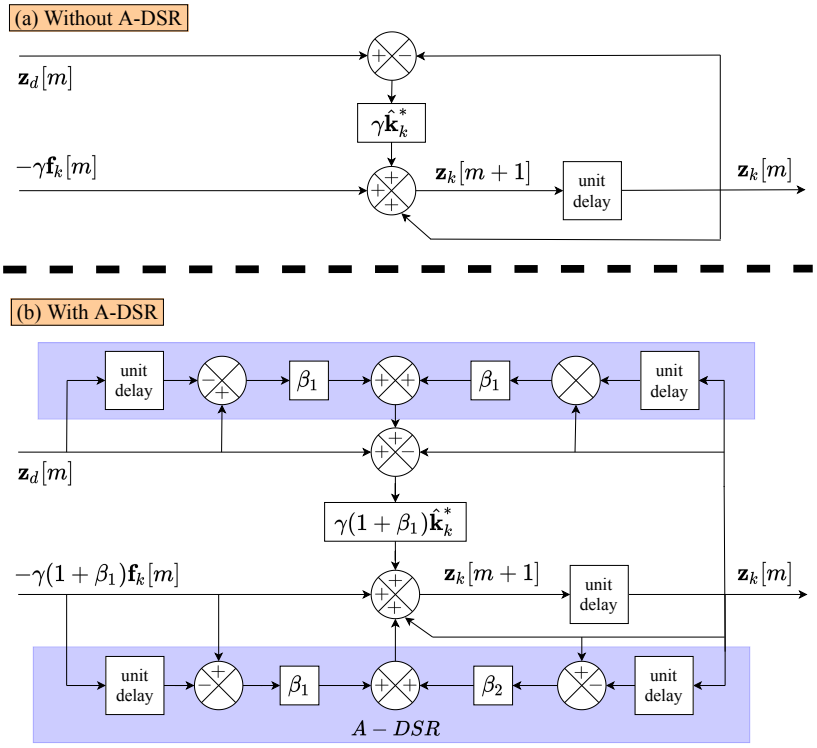


Figure 3.2: Implementation of transport update for robot $r_k$ using locally-sensed force $\mathbf{f}_k$ and position $\mathbf{z}_k$. Top (a): without A-DSR approach as in Eq. (3.4). Bottom (b): with A-DSR as in Eq. (3.11), which includes delayed self reinforcement by each robot using previously collected information.

where

$$
\begin{aligned}
\mathbf{S}[m+1] &= \begin{bmatrix} \mathbf{Z}[m] \\ \mathbf{Z}[m+1] \end{bmatrix} \in \mathbb{R}^{6n}, \quad \mathbf{S}[m] = \begin{bmatrix} \mathbf{Z}[m-1] \\ \mathbf{Z}[m] \end{bmatrix}, \\
\mathbf{A}_s &= \begin{bmatrix} \mathbf{0} & \mathbf{I} \\ \beta_1\gamma(1+\beta_1)\mathbf{K} - \beta_2\mathbf{I} & (1+\beta_2)\mathbf{I} - \gamma(1+\beta_1)^2\mathbf{K} \end{bmatrix}, \\
\mathbf{B}_s &= \begin{bmatrix} \mathbf{0} & \mathbf{0} \\ -\gamma\beta_1(1+\beta_1)\mathbf{B} & \gamma(1+\beta_1)^2\mathbf{B} \end{bmatrix}, \\
\mathbf{s}_d[m] &= \begin{bmatrix} \mathbf{z}_d[m-1] \\ \mathbf{z}_d[m] \end{bmatrix} \in \mathbb{R}^6.
\end{aligned}
\tag{3.13}
$$

The proposed A-DSR approach is stable if the update parameters $(\gamma, \beta_1, \beta_2)$ are selected such that the spectral radius $\rho(\mathbf{A}_s)$ is less than one, i.e.,

$$\rho(\mathbf{A}_s) = \max_k |\lambda_{\mathbf{A}_s,k}| < 1. \tag{3.14}$$

where $\lambda_{\mathbf{A}_s,k}$ are eigenvalues of the matrix $\mathbf{A}_s$.

**Remark 1 (With and without A-DSR)** *The update with A-DSR in Eq.* (3.10) *is the same as the update without A-DSR in Eq.* (3.6) *if* $\beta_1 = \beta_2 = 0$. *Therefore, the proposed A-DSR approach can only improve the performance of the robot team as compared to the case without A-DSR, due to the additional flexibility in the choice of* $\beta_1$ *and* $\beta_2$.

**Remark 2 (Nonlinear case)** *The A-DSR approach in Eq.* (3.9) *and the update using local force in Eq.* (3.11) *are still valid when the force-position expression in Eq.* (3.1) *is nonlinear. Moreover, if a linearization as in Eq.* (3.5) *is possible, then the stability of the linearized update dynamics also ensures local stability of the nonlinear update dynamics about the undeformed position* $\mathbf{Z} = \mathbf{0}$.

**Remark 3 (Multiple leaders)** *The virtual robot can be connected to multiple leader robots resulting in the modified update in Eq.* (3.4) *for each leader robot, and a modification of the total potential in Eq.* (3.2) *to include the potential energy of the additional virtual springs. In the extreme case when all robots are leaders, with access to the desired trajectory, all robots can follow it in the same manner and therefore, the deformation can be substantially reduced. However, such a system is centralized.*

### *3.3 Experimental system*

This section presents the experimental setup to evaluate the proposed approach. Furthermore, the evaluation metrics and selection of update parameters are discussed. The following three cases are used in the comparative evaluations.

- **Case 1: Without A-DSR**, the baseline case as in Eq. (3.4).
- **Case 2: With A-DSR** as in Eq. (3.11) with the update parameters $(\gamma, \beta_1, \beta_2)$ selected to minimize the deformation with the same transport time as in Case 1.
- **Case 3: With fast A-DSR** as in Eq. (3.11) with the update parameters $(\gamma, \beta_1, \beta_2)$ selected to minimize the transport time with the same deformation as in Case 1.

### *3.3.1 System description*

In this experiment, a transport task along a single axis, i.e., $\mathbf{z}_k = [0, 0, z_k]^T$, $\mathbf{f}_k = [0, 0, f_k]^T$ with $z_k \in \mathbb{R}, f_k \in \mathbb{R}$, is considered to demonstrate the efficacy of the proposed approach. The experimental system consists of four custom mobile robots shown in Figure 3.3. Each robot is equipped with magnetic encoders on the wheels for absolute position feedback, a micro-controller for on-board computation of control inputs and load cells as a force sensing mechanism, as shown in Figure 3.4. Each robot has a grasping hook on the front that enables attachment to the flexible object. To visualize the deformation during transport, the object is chosen to be highly flexible, comprising of a coiled spring with diameter of 1.30cm and length of 90cm.

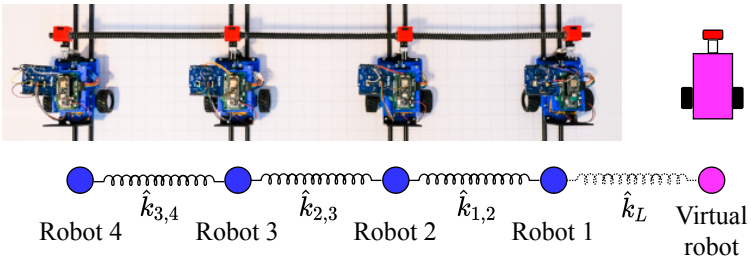


Figure 3.3: Top: Experimental setup of flexible load transport. Bottom: Schematic model of transport.

The schematic robot transport is shown in Figure 3.3. Each robot is connected to its nearest neighbor, and only the leader (robot 1) has knowledge of the desired position illustrated by the virtual robot shown in pink. The effective stiffness coefficients, i.e., $\hat{k}_{k,j} \in \mathbb{R}$,

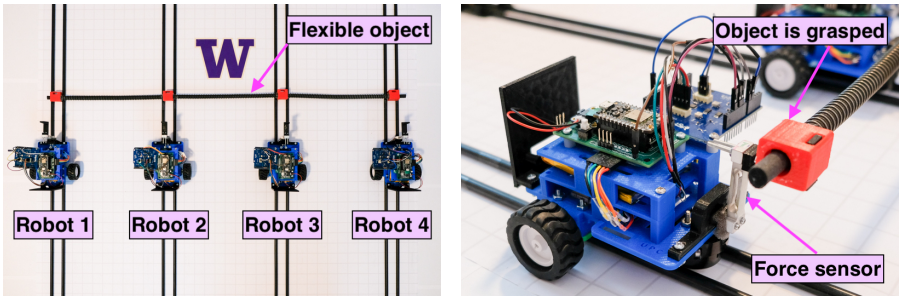


(a) Overall system (b) Single robot detail

Figure 3.4: Experimental setup with (a) highly-flexible object and 4 robots to visualize impact of transport speed on deformation and (b) local force sensing mechanism on the grasped object.

of the flexible object (spring) are measured experimentally. For example, to measure $\hat{k}_{1,2}$, robot 1 is moved for a known distance $z_1$ without moving the other robots (nor connecting robot 1 to the virtual source) and the resulting force $f_1$ is measured to yield $\hat{k}_{1,2} = f_1/z_1$. To measure $\hat{k}_{2,3}$, robot 2 is moved for a known distance $z_2$ without moving the other robots and the resulting force $f_2$ is measured to yield $\hat{k}_{2,3} = (f_2/z_2) - \hat{k}_{1,2}$. The same procedure is used to obtain the rest of the effective stiffness coefficients, which are all the same and given by $\hat{k}_{k,k+1} = 0.05$ N/cm, for $1 \leq k \leq 3$, because all the connecting springs have the same length. Note that the desired position $\mathbf{z}_d = [0, 0, z_d]^T$ with $z_d \in \mathbb{R}$ of the virtual source is available only to the leader robot, which, for the setup shown in Figure 3.3 is robot 1 with a virtual spring $\hat{k}_L = 0.05 \in \mathbb{R}$. Hence the pinned Laplacian $\mathbf{K}$ and matrix $\mathbf{B}$ in Eq. (3.6)

with $\mathbf{F} = [f_1, f_2, f_3, f_4]^T \in \mathbb{R}^4$ and $\mathbf{Z} = [z_1, z_2, z_3, z_4]^T \in \mathbb{R}^4$ can be written as,

$$\mathbf{K} = \begin{bmatrix} \hat{k}_{1,2} + \hat{k}_L & -\hat{k}_{1,2} & 0 & 0 \\ -\hat{k}_{1,2} & \hat{k}_{1,2} + \hat{k}_{2,3} & -\hat{k}_{2,3} & 0 \\ 0 & -\hat{k}_{2,3} & \hat{k}_{2,3} + \hat{k}_{3,4} & -\hat{k}_{3,4} \\ 0 & 0 & -\hat{k}_{3,4} & \hat{k}_{3,4} \end{bmatrix}$$

$$= \begin{bmatrix} 0.10 & -0.05 & 0 & 0 \\ -0.05 & 0.10 & -0.05 & 0 \\ 0 & -0.05 & 0.10 & 0.05 \\ 0 & 0 & -0.05 & 0.05 \end{bmatrix},$$

$$\mathbf{B} = \begin{bmatrix} \hat{k}_L & 0 & 0 & 0 \end{bmatrix}^T = \begin{bmatrix} 0.05 & 0 & 0 & 0 \end{bmatrix}^T. \tag{3.15}$$

Note that the pinned Laplacian $\mathbf{K}$ in the equation above is symmetric, thus the eigenvalues $\lambda_{\mathbf{K},k}$, $1 \leq k \leq 4$ are real and positive.

### *3.3.2 Robot's control implementation*

Each robot $r_k$ aims to reach the new position $z_k[m+1]$ by the next discrete sampling time $m+1$ as per Eqs. (3.4) and (3.11). The individual control of the robot position uses locally-sensed force $f_k$ and position $z_k$ measured using an encoder to find the next position $z_k[m+1]$, as illustrated in Figure 3.2. The updated position $z_k[m+1]$ of robot $r_k$ for the next time instant $t_{m+1} = (m+1)\delta_t$ is achieved within the sampling-time period $\delta_t = 0.1$s, using a velocity-based feedback control to maintain the velocity at $v_k(t) = (z_k[m+1] - z_k[m])/\delta_t$, as shown in Figure 3.5. While high-frequency measurement noise can be filtered, small offset errors can have a significant impact towards the end of the transport when the robots are coming to a halt. In such cases, deadzones can be used to change the control strategy when the force levels become small, e.g., as in [46], and is used in these experiments to stop the robots at the end of the transport, for both cases, with and without A-DSR.

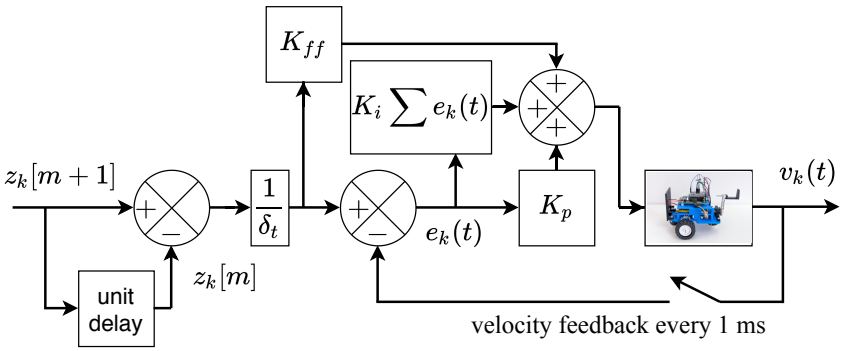


Figure 3.5: Velocity-based feedback control system of robot $r_k$ to achieve the state $z_k[m+1]$ used for both approaches, without A-DSR as in Eq. (3.4) and with A-DSR as in Eq. (3.11). Control consists of feedforward (gain $K_{ff}$) and proportional feedback (gain $K_p$) and integral feedback (gain $K_i$).

### *3.3.3 Evaluation metrics*

The following metrics are used for the comparative evaluations, with and without A-DSR.

**Maximum deformation** $\overline{D}$ is measured as the maximum difference between the first and the last robot positions, estimated using encoders on each robot's wheels, as

$$\overline{D} = \max_{m} \Big| \; D[m] = (z_1[m] - z_4[m]) \; \Big|. \tag{3.16}$$

**Task completion time** $T_s$ is the time needed for all the robots to reach and stay within 2% of the final desired position $z_d$.

**Maximum force** $\overline{f}$ applied by any robot to the object while it is being transported, over all time steps $m$, where the individual force $f_k[m]$ applied by robot $r_k$ is measured using the load cell attached in the front of the robot, i.e.,

$$\overline{f} = \max_{k=\{1,2,3,4\}} \Big( \max_{m} \Big| f_k[m] = \sum_{n=1}^{4} \hat{k}_{k,n} \left( z_k[m] - z_n[m] \right) \Big| \Big). \tag{3.17}$$

### *3.3.4 Selection of update parameters*

*Without A-DSR case*

There is a trade-off between maximum deformation $\overline{D}$ and the task completion time, i.e., settling time $\tau$ (for a step change in desired trajectory $z_d$) as illustrated in Figure 3.6 over the range of possible stable update gain $\gamma$ found from Eq. (3.8). The baseline task completion time is chosen to be as fast as possible (i.e., a larger update gain) without oscillations (non-negative eigenvalues $\lambda_{\mathbf{P},k}$) by choosing the update gain $\gamma$ as $\gamma_{opt} = 1/\overline{\lambda}_{\mathbf{K}} = 1/0.177 = 5.66$, where $\overline{\lambda}_{\mathbf{K}} = 0.177$ is the largest eigenvalue of the pinned Laplacian $\mathbf{K}$ in Eq. (3.15). The corresponding spectral radius $\rho(\mathbf{P})$ as in Eq. (3.7) of the $\mathbf{P}$ matrix is $\rho(\mathbf{P}) = |1 - \gamma\underline{\lambda}_{\mathbf{K}}| = |1 - (5.66)(0.006)| = 0.966$, where $\underline{\lambda}_{\mathbf{K}} = 0.006$ is the smallest eigenvalue of the pinned Laplacian $\mathbf{K}$ in Eq. (3.15). With the computed spectral radius $\rho(\mathbf{P}) = 0.966$ and the update gain $\gamma = 5.66$, the settling time $\tau$ to reach and stay within 2% for a step change in the desired trajectory $z_d$ cannot be bigger than, $\tau \approx -4\ \delta_t / ln\,(\rho(\mathbf{P})) = -4\ (0.1\text{s})/ln\,(0.966) = 11.6\text{s}$. This is close to the settling time of 11.5s found in simulation. The resulting maximum deformation was $\overline{D} = 0.57\text{cm}$ for the step input.

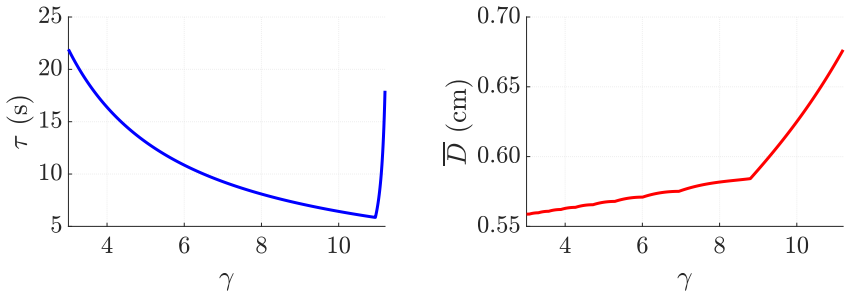


(a) (b)

Figure 3.6: Impact of update gain $\gamma$ selection on settling time $\tau$ and maximum deformation $\overline{D}$ for the case without A-DSR.

*With A-DSR case*

The A-DSR parameters ($\gamma$, $\beta_1$, $\beta_2$) can be selected to reduce the maximum deformation $\overline{D}$ without increasing the settling time $\tau$ when compared to the case without A-DSR. The update gain can be used to trade-off between the settling time $\tau$ and the maximum deformation $\overline{D}$ with A-DSR. Note that for a fixed $\beta = \beta_1 = \beta_2$, the settling time $\tau$ tends to decrease and the maximum deformation $\overline{D}$ tends to increase with increasing update gain $\gamma$ similar to the case without A-DSR as shown in Figure 3.7. Moreover, the additional flexibility in choosing potentially different parameters $\beta_1, \beta_2$ can improve the performance further, provided the parameter selection satisfies the spectral radius condition in Eq. (3.14) for stability. The optimal A-DSR parameters $(\gamma, \beta_1, \beta_2)$ to reduce the maximum deformation $\overline{D}$, found through a numerical search with simulations of the discrete dynamics in Eq. (3.11) for different parameters $(\gamma, \beta_1, \beta_2)$, are $\gamma = 0.19,\ \beta_1 = 4.91,$ and $\beta_2 = 0.95$. This resulted in settling time $\tau = 10.5$s and maximum deformation $\overline{D} = 0.49$cm for the step input.

*With fast A-DSR case*

The A-DSR parameters ($\gamma$, $\beta_1$, $\beta_2$) can be selected to reduce the settling time $\tau$ without increasing the maximum deformation $\overline{D}$ from the case without A-DSR. The A-DSR parameters, found using a numerical search, are $\gamma = 0.18,\ \beta_1 = 4.99,$ and $\beta_2 = 0.95$. This resulted in settling time $\tau = 9.8$s and maximum deformation $\overline{D} = 0.50$cm for the step input.

**Remark 4 (Update parameters comparison)** *The update parameters $(\gamma, \beta_1, \beta_2)$ are similar for both the A-DSR and fast A-DSR case. Thus, a similar A-DSR update can be used to either reduce the maximum deformation $\overline{D}$ or reduce the settling time $\tau$.*

### *3.4 Results and discussion*

This section presents comparative evaluation of simulation and experiment of the flexible object transport task. In the experiment, the desired position trajectory $z_d$ is chosen to be

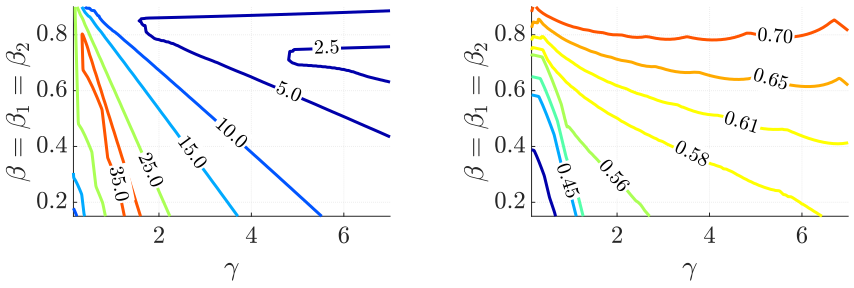


(a) (b)

Figure 3.7: Variation of settling time $\tau$ (left) and maximum deformation $\overline{D}$ (right) with different update gain $\gamma$ with $\beta_1 = \beta_2 = \beta$ for a step change in desired position trajectory $z_d$.

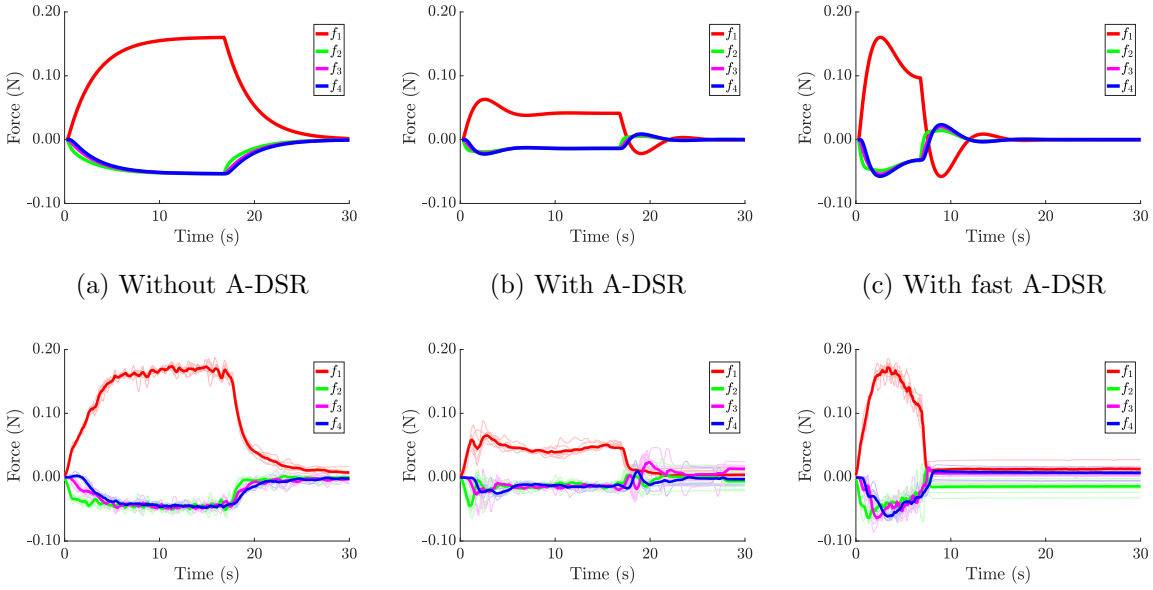


(a) Without A-DSR (b) With A-DSR (c) With fast A-DSR

(d) Without A-DSR (e) With A-DSR (f) With fast A-DSR

Figure 3.8: Simulation (top: (a), (b), (c)) and experiment (bottom: (d), (e), (f)) results showing the force $f_k$ for $k = \{1, 2, 3, 4\}$, measured as in Eq. (3.17) over time in response to a ramp input for all cases with and without A-DSR, as well as with fast A-DSR case. The experimental results are presented over 7 trials (shown in thin lines), and the means are plotted using thick lines.

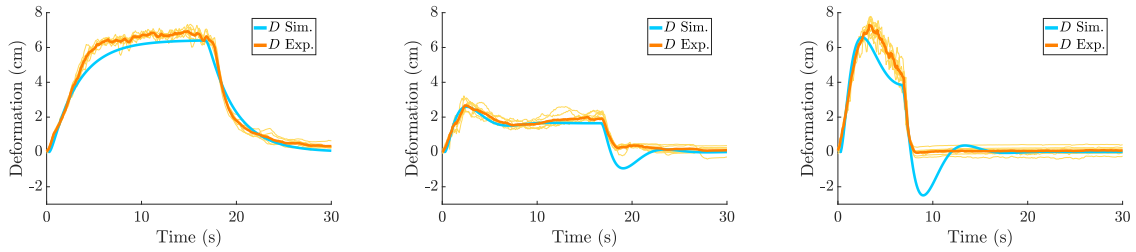


(a) Without A-DSR (b) With A-DSR (c) With fast A-DSR

Figure 3.9: Simulation and experiment results showing the total deformation in the elastic object $D$ defined in Eq. (3.16) over time in response to a ramp input for all cases with and without A-DSR, as well as with fast A-DSR case. The experimental results are presented over 7 trials (shown in thin lines), and the means are plotted using thick lines.

a ramp input from 0cm to 50cm. The ramp rate was kept sufficient low so the robots would not drag each other.

Two sets of experiments were performed. The first set of experiments was to compare the maximum deformations $\overline{D}$ of the cases with and without A-DSR, for the same task completion time $T_s$, i.e., with the same desired trajectory slope of 3cm/s (beyond which the lead robot would drag others for the case without A-DSR). Then, the resulting deformation was compared with and without A-DSR. The second set of experiments was to compare the task completion time $T_s$ of the cases with and without A-DSR, for the same maximum deformation $\overline{D}$. This was done by increasing the slope of the desired trajectory for the case with A-DSR until the maximum deformation $\overline{D}$ was similar to the case without A-DSR. Then, the resulting task completion time $T_s$ was compared without and with (fast) A-DSR.

The results are presented using evaluation metrics discussed in Section 3.3.3, which are maximum deformation $\overline{D}$, task completion time $T_s$ and maximum force $\overline{f}$, as shown in Table 3.1. The resulting system responses are also presented; for force $f_k$ as in Eq. (3.17) which displays the measured local force of each robot as shown in Figure 3.8, and for the total deformation $D$ in Eq. (3.16) as shown in Figure 3.9. Moreover, experimental results

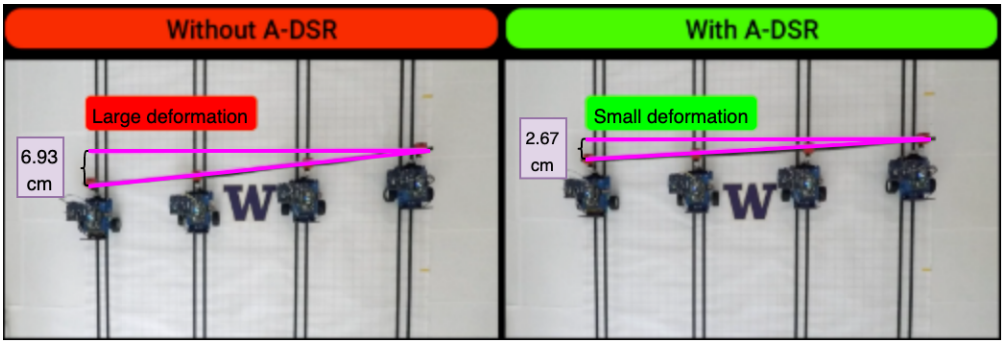


(a) Deformation comparison

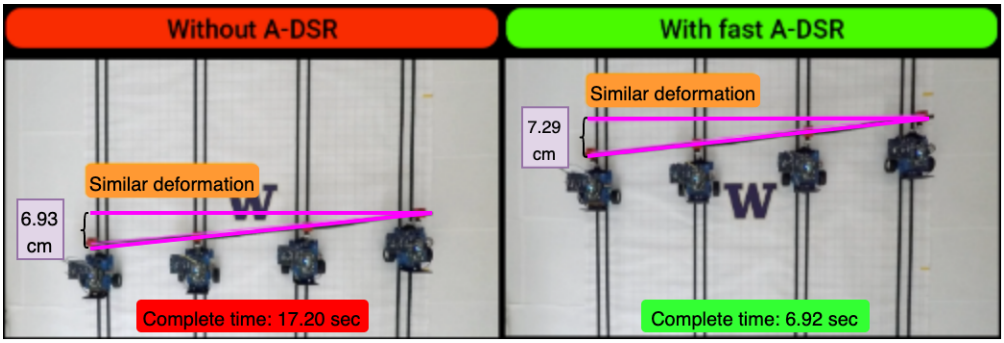


(b) Completion time comparison

Figure 3.10: Snapshots of video for both experimental sets: (a) with and without A-DSR to compare maximum deformation $\overline{D}$, and (b) with and without fast A-DSR to compare task completion time $T_s$.

from seven trials are also presented below.

### *3.4.1 Smaller deformation for similar task completion time*

The use of A-DSR shows significant reduction of 60% in simulation and $61 \pm 1.4\%$ in experiment in maximum deformation $\overline{D}$ for the same task completion time $T_s$. Similarly, the reduction in maximum force $\overline{f}$ is also significant, 62% in simulation and $64 \pm 5.8\%$ in experiment (Table 3.1). The improvements can be observed from the force $f_k$ and total deformation $D$ responses over time in Figures 3.8 and 3.9 respectively, where the force $f_k$ and deformation $D$ are reduced significantly for the case with A-DSR. These figures show

that the experimental results closely match the predictions from simulations. A snapshot from the experimental video, shown in Figure 3.10, also provides a visualization on how the use of A-DSR reduces the maximum deformation $\overline{D}$ as compared to case without A-DSR.

### *3.4.2 Smaller task completion time for similar deformation*

The proposed A-DSR approach can also reduce the task-completion time while maintaining a similar deformation level when compared to the baseline (without A-DSR) case. Results in Table 3.1 show that the task completion time $T_s$ is reduced from 16.67s to 6.67s in simulation and from $17.16 \pm 0.05$s to $6.92 \pm 0.02$s, resulting in a significant time saving of $59 \pm 0.3\%$ to complete the task. The improvements are also seen in Figures 3.8 and 3.9 as both force $f_k$ and total deformation $D$ settled faster with the fast A-DSR case compared to case without A-DSR. Figure 3.10 further shows that with the fast A-DSR, the system was able to complete the task faster as compared to the case without A-DSR. As a result, the robots can move faster (up to 2.5 times the speed of the case without A-DSR) without increasing the deformation.

**Remark 5 (Spectral radius comparison)** *The spectral radius (e.g., $\rho(\mathbf{P})$ in Eq. (3.7) or $\rho(\mathbf{A}_s)$ in Eq. (3.14)) is a measure of distance from instability (e.g., when eigenvalues are on the unit circle) and is thus an indicator of structural robustness. The spectral radii for the cases with and without A-DSR are similar as seen in Table 3.1, and hence the improvement in performance with A-DSR is not at the cost of structural robustness. Moreover, if needed, the selection of the A-DSR parameters could seek to improve the structural robustness, i.e., minimize the spectral radius $\rho(\mathbf{A}_s)$ for the same task completion time $T_s$ or the same maximum deformation $\overline{D}$ as the baseline case, without A-DSR.*

## *3.5 Conclusion*

In this chapter, an approach was proposed to improve the performance of flexible-object transport with a decentralized robot team. In particular, the approach used accelerated

delayed self-reinforcement (A-DSR) of local force measurements to reduce the deformation during transport with the same completion time as the baseline approach without A-DSR. Moreover, A-DSR allowed reduction in completion time for the same maximum deformation. Simulation results were provided to verify the theoretical findings of the proposed approach. Finally, experimental results using four robots transporting a flexible object (spring) were presented to demonstrate the applicability of the proposed A-DSR approach.

| Label | $\overline{D}$ (cm) | $\overline{f}$ (N) | $T_s$ (sec) | $\rho$ |
|---|---|---|---|---|
| **Simulation** | | | | |
| Without A-DSR | 6.40 | 0.16 | 16.67 | 0.9659 |
| With A-DSR | 2.58 | 0.06 | 16.67 | 0.9578 |
| Improvement | 60% | 62% | - | |
| With fast A-DSR | 6.64 | 0.16 | 6.67 | 0.9575 |
| Improvement | - | - | 60% | |
| **Experiment** | | | | |
| Without A-DSR $\mu$ ($\pm\sigma$) | 6.93 ($\pm$0.10) | 0.17 ($\pm$0.01) | 17.16 ($\pm$0.05) | - |
| With A-DSR $\mu$ ($\pm\sigma$) | 2.67 ($\pm$0.10) | 0.06 ($\pm$0.01) | 16.93 ($\pm$0.06) | - |
| Improvement $\mu$ ($\pm\sigma$) | 61% ($\pm$1.4 %) | 64% ($\pm$5.8%) | - | - |
| With fast A-DSR $\mu$ ($\pm\sigma$) | 7.29 ($\pm$0.15) | 0.17 ($\pm$0.02) | 6.92 ($\pm$0.02) | - |
| Improvement $\mu$ ($\pm\sigma$) | - | - | 59% ($\pm$0.3 %) | - |

Table 3.1: Top: Evaluation metrics from simulations and spectral radius $\rho$ from Eqs. (3.7) and (3.14). Bottom: Mean $\mu$ and standard deviation $\sigma$ results across 7 trials of experiment. Both results are shown for the three evaluation metrics: maximum deformation ($\overline{D}$), maximum force ( $\overline{f}$), and task completion time ($T_s$). Improvement, for each case, with respect to the case without A-DSR, is highlighted in green.

# Chapter 4

# MC2.1: DEVELOPMENT OF A REDUCED-DEFORMATION APPROACH USING DSR FOR TRANSLATIONAL TRANSPORT

This chapter forms the main contribution 2.1 (**MC2.1**) of this dissertation, that is to use delayed self-reinforcement (DSR) to achieve cohesive transport using robot networks, and has been published in [2]. The work in this chapter aims to reduce deformations of the object being transported by developing methods for cohesive positioning of the robot network. Recent studies have shown that control laws can be developed to improve cohesion of decentralized networks using Delayed Self-Reinforcement (DSR) [47]. The main contribution of this chapter is to develop an approach to transport objects using the cohesive method in [47], without the need for inter-robot communications - rather, only the local force measurements are required. Specifically, this work (i) shows that the DSR approach can be used to achieve cohesive transport using only local force measurements, without the need of inter-robot communication, and (ii) establishes stability conditions for the discrete-time implementation of the proposed cohesive transport approach. Furthermore, experimental results are used to show that the proposed approach improves network cohesion, and leads to low-deformation transport of flexible objects.

## 4.1 Problem formulation

In this section, the deformation control issue with local force-based decentralized transport dynamics is presented along a single axis-$y$. Similar approaches can be used for the other axes of motion.

### *4.1.1 Local-force feedback as a network-based update*

The robots are attached to a flexible object, e.g., as shown in Fig. 4.1. The position $y_k \in \mathbb{R}$ of each robot $k$ in the network is updated using local force measurements $f_k \in \mathbb{R}$ as well as a virtual force $\tilde{f}_k = \hat{k}_{k,d}(y_k - y_d) \in \mathbb{R}$ if robot $k$ is a leader, as

$$y_k[m+1] = y_k[m] - \gamma \hat{f}_k[m], \tag{4.1}$$

$$\hat{f}_k[m] = f_k[m] + \tilde{f}_k[m], \tag{4.2}$$

where the update sampling-time period is $\delta_t$, $y_k[m]$ represents the position of robot $k$ at discrete time instants, e.g., $y_k[m] = y_k(m\delta_t)$, $\gamma$ is the update gain, and the desired position from the virtual source $y_d \in \mathbb{R}$ is known (i.e., $\hat{k}_{k,d} \neq 0$) only if robot $k$ is a leader, e.g., $k = 1$ in the example in Fig. 4.1. Each robot position $y_k$ is measured from an initial undeformed configuration (with all $y_k = 0$) of the flexible object.

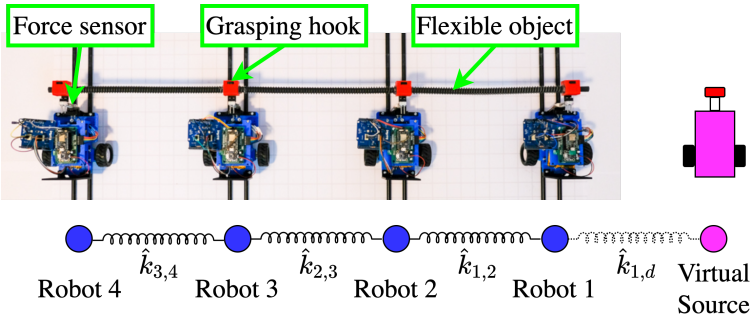


Figure 4.1: Top: Experimental setup of flexible load transport. Bottom: Schematic network model where the leader, robot $k = 1$, aims to match the position of the virtual source (pink).

The local force-based robot position update in Eq. (4.1) achieves object transport, i.e.,

for a fixed desired position $y_d$, the network reaches equilibrium when each robot reaches the desired position, i.e., $y_k = y_d$ for all $k$ and the object has no distortion, i.e., $f_k = 0$. To clarify, note that the local force $f_k$ measured by robot $k$ can be written linearly in terms of the position $y_j$ of all robots connected to robot $k$, provided the local deformation of the flexible object remains small, as

$$f_k[m] = \sum_{j=1}^{n} \hat{k}_{k,j}(y_k[m] - y_j[m]), \tag{4.3}$$

where $\hat{k}_{k,j} = \hat{k}_{j,k} \geq 0$ is the effective stiffness of the flexible object between two neighboring robots $j$ and $k$, $n$ is the number of robots, and $\hat{k}_{j,j} = 0$ for all $1 \leq j \leq n$. Then, the update law in Eq. (4.1) can be written in matrix form as

$$\mathbf{Y}[m+1] = (\mathbf{I} - \gamma\mathbf{K})\mathbf{Y}[m] + \gamma\mathbf{B}y_d[m], \tag{4.4}$$

where $\mathbf{Y} = [y_1, y_2, \ldots, y_k, \ldots, y_n]^T \in \mathbb{R}^n$ is the $n$ dimensional vector of the individual robots positions $y_k$, $B_k = \hat{k}_{k,d}$ is the $k^{th}$ element of $n$ dimensional vector $\mathbf{B} \in \mathbb{R}^n$ which is nonzero only if the robot $k$ is a leader and the symmetric matrix $\mathbf{K}$ is the pinned Laplacian with elements

$$\begin{aligned} \mathbf{K}_{k,j} &= \hat{k}_{k,d} + \textstyle\sum_{m=1}^{n} \hat{k}_{k,m} \quad \geq 0 \quad \text{if } k = j \\ &= -\hat{k}_{k,j} \qquad\qquad\qquad\qquad \text{otherwise,} \end{aligned} \tag{4.5}$$

with real nonzero eigenvalues $\lambda_{\mathbf{K},j} > 0$ for $1 \leq j \leq n$. It can be shown that for an update gain $\gamma$ satisfying

$$0 < \gamma < \left( \overline{\gamma} \ = 2/\overline{\lambda}_{\mathbf{K}} \ = 2/\max_j(\lambda_{\mathbf{K},j}) \right), \tag{4.6}$$

the eigenvalues of $(\mathbf{I} - \gamma\mathbf{K})$ are inside the unit circle. Therefore, the transport dynamics in Eq. (4.4) is stable, and the desired transport of the object can be achieved, i.e., for a fixed desired position $y_d$, the robot positions in $\mathbf{Y}$ converge to the desired value [44]

$$\lim_{m\to\infty} \mathbf{Y}[m] \ = \mathbf{1}_n y_d \tag{4.7}$$

with $\mathbf{1}_n$ representing the $n$ dimensional vector of all ones.

### *4.1.2 Problem: improve cohesion for similar settling time*

The settling time $T_s$ to a new desired position $y_d$ can be selected by choosing the update gain $\gamma$. In particular, the settling time $T_s$ to reach and stay within 2% of a step change in the desired displacement $y_d$ can be estimated as

$$T_s \approx \frac{-4\ \delta_t}{\ln\left(\lambda^*_{\mathbf{K}}\right)} \quad \text{where } \lambda^*_{\mathbf{K}} = \arg\max_{\lambda_{\mathbf{K},j}} |1 - \gamma\lambda_{\mathbf{K},j}|. \tag{4.8}$$

However, for a given settling time (i.e., given selection of the update gain $\gamma$), the deformations during transport can not be controlled further. Typically, faster settling (i.e., a smaller settling time $T_s$) also results in larger deformation. The research problem addressed here is to improve cohesion, i.e., to reduce the maximum deformation $\overline{D}$ of the object during transport,

$$\overline{D} = \max_m \left[ D[m] = \max_{k,j} \left| \left(y_j[m] - y_k[m]\right) \right| \right], \tag{4.9}$$

without increasing the settling time $T_s$.

## *4.2 Transport using cohesive DSR*

### *4.2.1 Cohesive transport using local force measurements*

The robot-position update to transport the object is chosen as a discrete-time approximation of an ideal cohesive network. For example, in the continuous time case, if each robot had access to the desired position $y_d$, i.e., in a centralized approach, then the ideal cohesive update can be written as,

$$\dot{\mathbf{Y}}(t) = -\alpha\mathbf{Y}(t) + \alpha\mathbf{1}_n y_d(t), \tag{4.10}$$

where the gain $\alpha > 0$ can be tuned to achieve a desired settling time and all robot move in a similar manner. The lack of access to centralized information about the desired position $y_d$ can be alleviated by multiplying both sides with the scaled pinned Laplacian $\beta\mathbf{K}$, substituting

$\mathbf{K1}_n$ with $\mathbf{B}$ [47], and adding $\dot{\mathbf{Y}}$ to both sides and rearranging the equation to obtain

$$\dot{\mathbf{Y}}(t) = -\alpha\beta\mathbf{K}\mathbf{Y}(t) + \alpha\beta\mathbf{B}y_d(t) + [\mathbf{I} - \beta\mathbf{K}]\dot{\mathbf{Y}}(t), \tag{4.11}$$

$$\approx -\alpha\beta\mathbf{K}\mathbf{Y}(t) + \alpha\beta\mathbf{B}y_d(t) + [\mathbf{I} - \beta\mathbf{K}]\,\frac{\mathbf{Y}(t) - \mathbf{Y}(t-\tau)}{\tau}. \tag{4.12}$$

With the time delay $\tau = \delta_t$ and the update kept constant between sampling periods, the update law in Eq. (4.12) for robot positions becomes

$$\begin{aligned}\mathbf{Y}[m+1] =& \mathbf{Y}[m] - \alpha\beta\delta_t\mathbf{K}\mathbf{Y}[m] + \alpha\beta\delta_t\mathbf{B}y_d[m] \\ &+ [\mathbf{I} - \beta\mathbf{K}]\,(\mathbf{Y}[m] - \mathbf{Y}[m-1])\,.\end{aligned} \tag{4.13}$$

Then for each robot $k$, the update law becomes

$$\begin{aligned}y_k[m+1] =& y_k[m] - \alpha\beta\delta_t f_k[m] + \alpha\beta\delta_t\hat{k}_{k,d}\big(y_d[m] - y_k[m]\big) \\ &+(1 - \beta\hat{k}_{k,d})\big(y_k[m] - y_k[m-1]\big) \\ &- \beta\big(f_k[m] - f_k[m-1]\big).\end{aligned} \tag{4.14}$$

Note that this cohesive transport law is decentralized. For each robot, in addition to the virtual source position $y_d$ if the robot is a leader, the update only requires current information and delayed self reinforcement (DSR) by a time step of: (i) local force measurements $f_k$ and (ii) its own position $y_k$.

### *4.2.2 Stability of cohesive DSR*

Stability conditions can be established by finding the roots of the characteristic equation of the cohesive dynamics in Eq. (4.13), i.e.,

$$\det\Big(\mathbf{I}z^2 - (\mathbf{I} - \alpha\beta\delta_t\mathbf{K}_J + [\mathbf{I} - \beta\mathbf{K}_J])\,z + [\mathbf{I} - \beta\mathbf{K}_J]\Big) = 0, \tag{4.15}$$

where $\mathbf{K}_J = {\mathbf{P}_\mathbf{K}}^{-1}\mathbf{K}\mathbf{P}_\mathbf{K}$ is the diagonalization of the pinned Laplacian $\mathbf{K}$ with eigenvalues $\lambda_{\mathbf{K},k}$ along the diagonal. In particular, the cohesive dynamics in Eq. (4.13) is stable if and

only if, for each eigenvalue $\lambda_{\mathbf{K},k}$ of the pinned Laplacian $\mathbf{K}$, the roots of $D(z)$ where

$$\begin{aligned} D(z) =& z^2 - (1 - \alpha\beta\delta_t\lambda_{\mathbf{K},k} + [1 - \beta\lambda_{\mathbf{K},k}])\, z \\ &+ [1 - \beta\lambda_{\mathbf{K},k}] = 0 \end{aligned} \tag{4.16}$$

have magnitude less than one. Thus, stability can be evaluated by computing the roots of Eq. (4.16). Nevertheless, for design purposes, it is preferable to establish analytical conditions on the DSR parameters for stability, as shown next.

**Lemma 1** *The proposed cohesive DSR based dynamics in Eq.* (4.13) *is stable if and only if the gains* $\alpha, \beta$ *satisfy the following conditions for the largest eigenvalue* $\overline{\lambda}_{\mathbf{K}}$ *of the pinned Laplacian* $\mathbf{K}$*:*

$$\begin{aligned} &(i) \quad 0 < \alpha \\ &(ii) \quad 0 < \beta < \frac{4}{\overline{\lambda}_{\mathbf{K}}(\alpha\delta_t + 2)}. \end{aligned} \tag{4.17}$$

*Proof:* Proof of Lemma 1 follows from Jury stability test and is omitted here for brevity.

**Remark 6** *The delay in Eq.* (4.12) *can be defined over multiple samples, i.e.,* $\tau = N\delta_t$ *where* $N \geq 1$ *is an integer number. However a larger delay* $\tau$ *(larger* $N$*) reduces the effectiveness of the approximate derivative in Eq.* (4.12) *and thereby, reduces the ability to track faster signals in a cohesive manner [47].*

## *4.3 Experiment and parameter selection*

### *4.3.1 System description*

To easily visualize the deformation during transport, a highly flexible object (a long spring coiled with diameter of 1.30 *cm* and length of 90 *cm*) was selected for transport using a robot network as shown in Fig. 4.1. Only the leader (robot 1) has knowledge of the desired position illustrated by the virtual source shown in pink in Fig. 4.1. Each robot $k$ measures

the local force $f_k$ using a force sensor between the robot and the object, and senses its position $y_k$ using magnetic encoders on the wheels, and uses an on-board micro-controller to compute the next position $y_k[m+1]$. The updated position $y_k[m+1]$ is achieved within the sampling-time period $\delta_t = 0.03\ s$, using a velocity feedback control to maintain the velocity at $v_{d,k}(t) = (y_k[m+1] - y_k[m])/\delta_t$ as shown in Fig. 4.2.

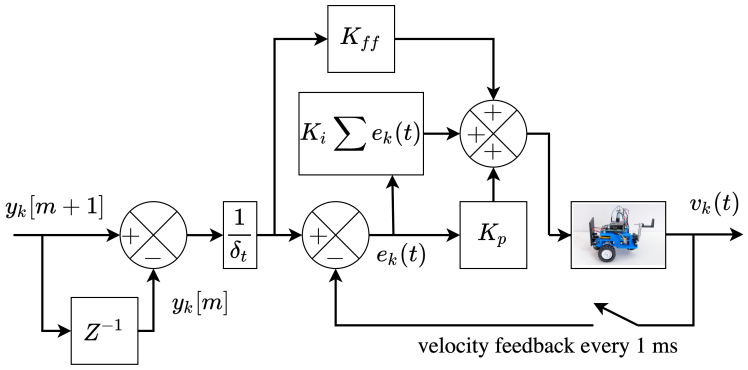


Figure 4.2: Velocity-based feedback control system of robot $k$ to achieve the position $y_k[m+1]$ using a proportional (gain $K_p$) and integral (gain $K_i$) feedback controller along with feedforward control (gain $K_{ff}$).

The system dynamics in Eq. (4.1) was found by estimating the elastic object stiffness $\hat{k}_{i,j}$ experimentally. In particular, for estimating $\hat{k}_{1,2}$, robot 1 was moved for a known distance $y_1$ without moving the other robots (nor connecting robot 1 to the virtual source) and the resulting force $f_1$ was measured to yield $\hat{k}_{1,2} = f_1/y_1$. Then, to estimate stiffness $\hat{k}_{2,3}$, robot 2 was moved for a known distance $y_2$ without moving the other robots and the resulting force $f_2$ was measured to yield $\hat{k}_{2,3} = (f_2/y_2) - \hat{k}_{1,2}$. The same procedure is used to obtain the rest of the effective stiffness coefficients, which are all the same and given by $\hat{k}_{i,i+1} = 0.05\ N/cm$, for $1 \leq i \leq 3$, which is to be expected since the connecting springs have similar lengths. For the setup shown in Fig. 4.1, the stiffness of the connection with virtual source is chosen to be same as the other spring elements, i.e., $\hat{k}_{1,d} = 0.05$. The resulting pinned

Laplacian $\mathbf{K}$ and matrix $\mathbf{B}$ were

$$\mathbf{K} = \begin{bmatrix} \hat{k}_{1,2} + \hat{k}_{1,d} & -\hat{k}_{1,2} & 0 & 0 \\ -\hat{k}_{1,2} & \hat{k}_{1,2} + \hat{k}_{2,3} & -\hat{k}_{2,3} & 0 \\ 0 & -\hat{k}_{2,3} & \hat{k}_{2,3} + \hat{k}_{3,4} & -\hat{k}_{3,4} \\ 0 & 0 & -\hat{k}_{3,4} & \hat{k}_{3,4} \end{bmatrix}$$

$$= \begin{bmatrix} 0.10 & -0.05 & 0 & 0 \\ -0.05 & 0.10 & -0.05 & 0 \\ 0 & -0.05 & 0.10 & 0.05 \\ 0 & 0 & -0.05 & 0.05 \end{bmatrix}, \tag{4.18}$$

$$\mathbf{B} = \begin{bmatrix} \hat{k}_{1,d} & 0 & 0 & 0 \end{bmatrix}^T = \begin{bmatrix} 0.05 & 0 & 0 & 0 \end{bmatrix}^T. \tag{4.19}$$

### *4.3.2 Selection of control parameters*

To avoid optimization over each desired trajectory $y_d$, the control parameters are selected to minimize the deformation for a specified settling time $T_s$ for a unit step change in the desired position $y_d$.

*Case without DSR*

The update gain $\gamma$ is found numerically for a specified network settling time $T_s$ when the position changes by a unit step. For update gains $\gamma$ satisfying the stability condition in Eq. (4.6), the settling times $T_s$ were estimated using Eq. (4.8), and are shown in Fig. 4.3a. Interpolation of this data can be used to find the update gain $\gamma$ for a specified settling time $T_s$. In the following, the settling time $T_s = 10\ s$ is chosen in order to bound the maximum speed input to the robot $v_{d,k} = v_{nodsr}$ below the acceptable speed limit $v_{max} = 5\ cm/s$ as shown in Fig. 4.4b. The corresponding update gain $\gamma = 1.93$ and the step response is shown in Fig. 4.4a.

*Case with cohesive DSR*

To enable comparative evaluation, the cohesive DSR parameters $(\alpha, \beta)$ are selected to match the settling time $T_s$ of the case without DSR, and the maximum speed input $v_{d,k}$ is below $v_{nodsr}$ for the case without DSR. Since it is possible to obtain multiple combinations of the parameters $(\alpha, \beta)$ that satisfy the settling time $T_s$ and the maximum speed input $v_{d,k}$ conditions, the optimal parameters are selected such that the spectral radius $\sigma$ is minimized (to maximize structural robustness), i.e.,

$$\begin{gathered} \sigma^* = \min_{\alpha,\beta} \left( \sigma(\alpha, \beta) = \max_j |z_j| \right), \\ \text{subject to } v_{d,k} \leq v_{nodsr} \end{gathered} \tag{4.20}$$

where $z_j$ is the $j^{th}$ root of the characteristic equation $D(z)$ as in Eq. (4.16). The parameters $(\alpha, \beta)$ for the same range of settling time $T_s$ as in the case without DSR are shown in Fig. 4.3b. In the following, the settling time $T_s = 10\ s$ is chosen to match the case without DSR and the corresponding parameters are

$$\alpha = 0.39 \ \approx 0.4, \qquad \beta = 10.92 \ \approx 10.9. \tag{4.21}$$

The step response is also shown in Fig. 4.4a. Note that the maximum speed input to the robot $v_{d,k}$ is also well below $v_{nodsr}$ as shown in Fig. 4.4b.

**Remark 7** *When the sampling time $\delta_t$ becomes small as compared to the transport time, the discrete time cohesive dynamics in Eq.* (4.13) *should be similar to the continuous-time ideal cohesive dynamics in Eq.* (4.10)*. Therefore, the settling time becomes $T_s = 4/\alpha$ and can be selected using the parameter $\alpha$. With the settling time chosen as $T_s = 10\ s$, the estimate of $\alpha = 4/T_s = 0.4$ is close to the result from the numerical search $\alpha = 0.39$ in Eq.* (4.21)*.*

**Remark 8** *The spectral radius, provided the associated second-order dynamics in Eq.* (4.16) *is not overdamped, is the maximum value of $|1 - \beta\lambda_{\mathbf{K},k}|$, which is minimized over all eigenvalues $\lambda_{\mathbf{K},k}$, by selecting $\beta = \frac{2}{\underline{\lambda}_{\mathbf{K}} + \bar{\lambda}_{\mathbf{K}}} = \frac{2}{0.006 + 0.176} = 10.95$, which is close to the result from the numerical search, $\beta = 10.92$ in Eq.* (4.21)*.*

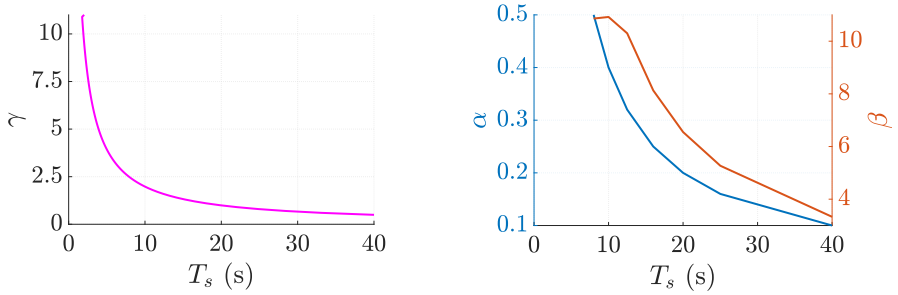


Figure 4.3: Selection of control parameters with respect to settling time $T_s$: (left) The update gain $\gamma$ for the case without DSR, (right) DSR parameters $\alpha$ and $\beta$ for the case with cohesive DSR.

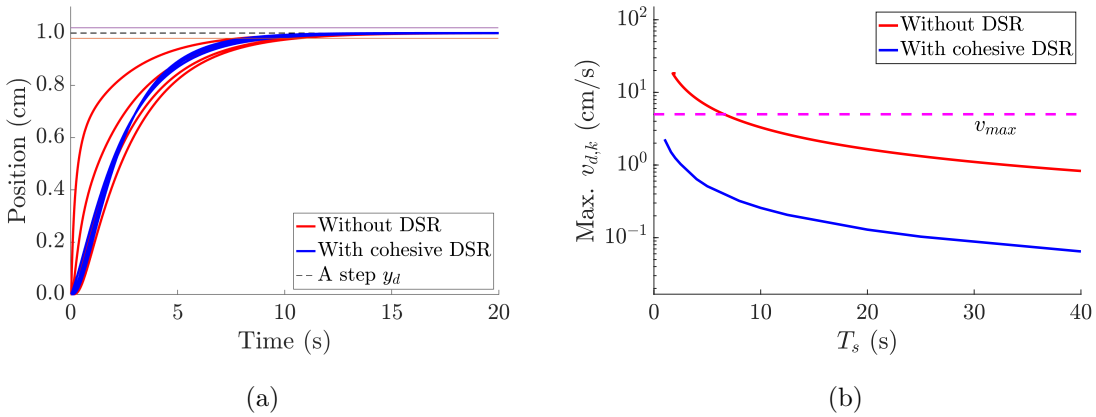


Figure 4.4: **(a) Increase in cohesion with DSR.** Position responses for a step change in position $y_d$ for both (i) without DSR ($\gamma = 1.93$) as in Eq. (4.4) and (ii) with cohesive DSR ($\alpha = 0.39$, $\beta = 10.92$) as in Eq. (4.13) which show that both settle within $T_s = 10$ $s$. **(b) Reduction of maximum input speed with DSR for the same settling time.** Selection of settling time $T_s$ such that the maximum speed $v_{d,k}$ of the robot is below the acceptable speed limit $v_{max}$.

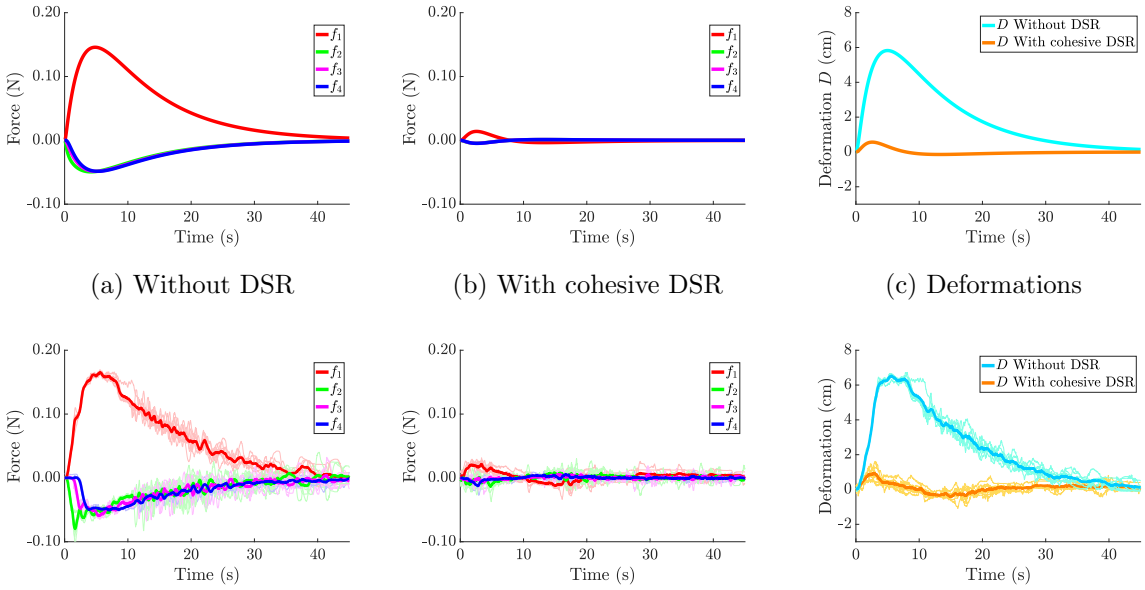


(a) Without DSR (b) With cohesive DSR (c) Deformations

(d) Without DSR (e) With cohesive DSR (f) Deformations

Figure 4.5: Comparative evaluation of force $f_k$ as in Eq. (4.3) and deformation $D$ as in Eq. (4.9) with and without cohesive DSR, and similarity of simulations (top row) and experimental results (bottom row). Experiment results are shown for 7 trials (shown in thin lines), and the means are shown in thick lines.

## *4.4 Results*

### *4.4.1 Selection of the desired transport trajectory*

A large change in position $y_d$ from 0 $cm$ to 50 $cm$ was chosen to help visualize the transport of the flexible body. To ensure that the deformations are not too large (i.e., to avoid other robots dragging each other), the desired transport trajectory $y_d$ was chosen as a step that is filtered using a first-order, low-pass filter with cutoff frequency $\omega_c$ and implemented using Tustin's approximation, as

$$y_d[m] = \frac{2 - \omega_c \delta_t}{2 + \omega_c \delta_t} y_d[m-1] + \frac{\omega_c \delta_t}{2 + \omega_c \delta_t} \left( y_{ds}[m] + y_{ds}[m-1] \right), \tag{4.22}$$

where $y_{ds}[m] = 50$ if $m > 0$ and zero otherwise. The effect of the cutoff frequency $\omega_c$ on maximum deformation $\overline{D}$ in Eq. (4.9) is shown in Fig. 4.6a. The cutoff frequency $\omega_c$ was

selected as $\omega_c = 0.1\ rad/s$ so that the maximum deformation $\overline{D}$ is below 7 $cm$ and the maximum speed input to the robot $v_{d,k} \leq (v_{max} = 5\ cm/s)$ to avoid dragging of the robots by each other for the case without DSR. Note that the desired trajectory $y_d$ reaches the final value of 50 $cm$ in about $T_{sf} = 4/\omega_c = 40\ s$ as seen in Fig. 4.6b.

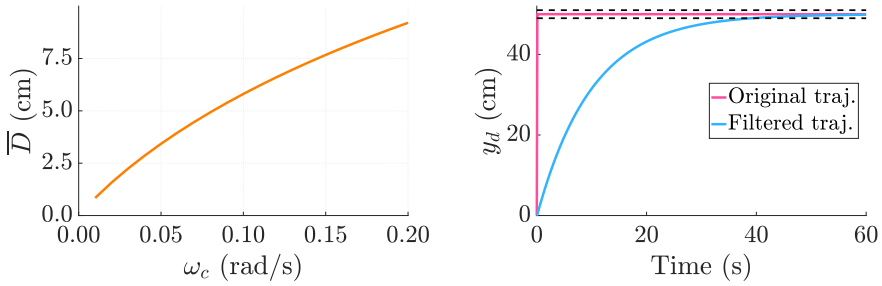


(a) (b)

Figure 4.6: (a) The effect of cutoff frequency $\omega_c$ on maximum deformation $\overline{D}$. (b) The desired trajectory $y_d$ obtained by passing a step trajectory $y_{ds}$ through a first-order, low-pass filter with cutoff frequency $\omega_c = 0.1\ rad/s$ as in Eq. (4.22).

### *4.4.2 Results and discussion*

Comparative evaluations, with and without the DSR approach, are presented below. The results are evaluated based on the maximum deformation $\overline{D}$ in Eq. (4.9) and also the maximum force $\overline{f}$ defined as

$$\overline{f} = \max_{k=\{1,2,3,4\}} \left( \max_{m} |f_k[m]| \right). \tag{4.23}$$

The simulation and experimental results are shown in Fig. 4.5, and quantified in Table 4.1. The responses from the experiments and simulations are similar to each other in Fig. 4.5, which indicates that the models are close to the experimental system. The cohesive DSR approach reduces the maximum deformation $\overline{D}$ substantially, by 90% in simulation and $85 \pm 0.05\%$ in experiment. Similarly, the corresponding maximum forces $\overline{f}$ are also reduced

significantly, by 90% in simulation and $87 \pm 0.50\%$ in experiment. The reduction in deformation indicates that the robot network responses are more cohesive during transport with the cohesive DSR approach. This increased cohesion can also be observed from snapshots of experiment in Fig. 4.7.

| Label | Without DSR | Cohesive DSR | Improvement |
|---|---|---|---|
| **Simulation** | | | |
| $\overline{f}$ (N) | 0.146 | 0.014 | 90% |
| $\overline{D}$ (cm) | 5.824 | 0.563 | 90% |
| **Experiment** | | | |
| $\overline{f}$ $(\mu \pm \sigma)$ (N) | 0.165 $\pm$0.008 | 0.021 $\pm$0.004 | 87 $\pm$0.50% |
| $\overline{D}$ $(\mu \pm \sigma)$ (cm) | 6.530 $\pm$0.010 | 0.940 $\pm$0.010 | 85 $\pm$0.05% |

Table 4.1: Improvement (reduction) in maximum force ( $\overline{f}$) and maximum deformation ($\overline{D}$) with cohesive DSR when compared to case without DSR. Top: Simulation results. Bottom: Experimental results with mean $\mu$ and standard deviation $\sigma$ over 7 trials.

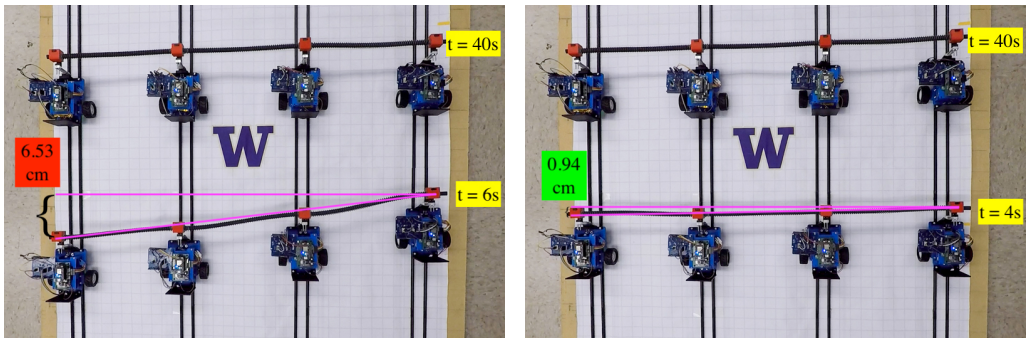


(a) (b)

Figure 4.7: Reduction in maximum deformation $\overline{D}$ with cohesive DSR approach (at time $t = 4$ $s$) compared to the case without DSR (at time $t = 6$ $s$) as seen in video snapshots of the experiment overlaid with the positions at time $t = 40$ $s$: (top) without DSR, and (bottom) with cohesive DSR. The deformations over time are shown in Fig. 4.5f. Video of the experiment can be seen here: https://youtu.be/tzDfnMbgIgA.

## *4.5 Conclusion*

In this chapter, a development of centralized-based approach to reduce deformation of flexible objects during transport using robot networks was presented. The approach was implemented using delayed-self-reinforcement (DSR) in a decentralized manner, where it used only local force measurements without additional communication, and conditions for stability were established. The proposed cohesive DSR approach was evaluated using simulation and the results closely matched the experimental results. Overall, the proposed approach led to 85% reduction in the deformation of the experimental system without increasing the time to transport the object to a new position.

# Chapter 5

# MC2.2: DEVELOPMENT OF A REDUCED-DEFORMATION APPROACH USING DSR FOR TRANSLATIONAL AND ROTATIONAL TRANSPORT

The main contribution of this work is to develop a decentralized approach that uses previous local force measurements to add a delayed self-reinforcement (DSR) to the robots' actions, resulting in smaller object deformation, even during orientation changes. This work has been accepted to a peer-reviewed journal [3].

This chapter is an evolution of prior work in [2], which presented experimental results that DSR can reduce deformation during purely translational transport where the motion of the robots is cohesive, i.e., each robot moves in the same manner. Moreover, the dynamics of translational transport is time invariant. In contrast, the current work in this chapter develops a new decentralized DSR theory for orientation changes, when the robot motions are no longer cohesive, since the desired position-changes for the robots can vary depending on the robot's geometric location. Additionally, analysis is developed for the resulting time-varying dynamics (i) to establish conditions on the control parameters for stability of the DSR approach and (ii) to quantify the performance in terms of deformation bounds. Finally, results from both simulations and experiments show that the proposed DSR approach leads to rapid, low-deformation decentralized transport when compared to standard decentralized approaches without the DSR.

## *5.1 Preliminaries and Problem formulation*

The decentralized robot network is a team of $n$ robots where the $i^{th}$ robot is located at position $\mathbf{p}_i = [x_i, y_i, z_i]^\intercal \in \mathbb{R}^3$ with orientation $\Theta_i = [\theta_{x,i}, \theta_{y,i}, \theta_{z,i}]^\intercal \in \mathbb{R}^3$ in the global

coordinates $(x, y, z)$. All the robots are rigidly attached to the flexible object, and therefore, the zero-deformation nominal position $\bar{\mathbf{p}}_n$ of the flexible object is constant with respect to the local coordinates $(\bar{x}, \bar{y}, \bar{z})$ with origin at the position $\mathbf{p}_L = [x_L, y_L, z_L]^\intercal$ of the leader robot and orientation $\Theta_L = [\theta_{x,L}, \theta_{y,L}, \theta_{z,L}]^\intercal$ in the global coordinates.

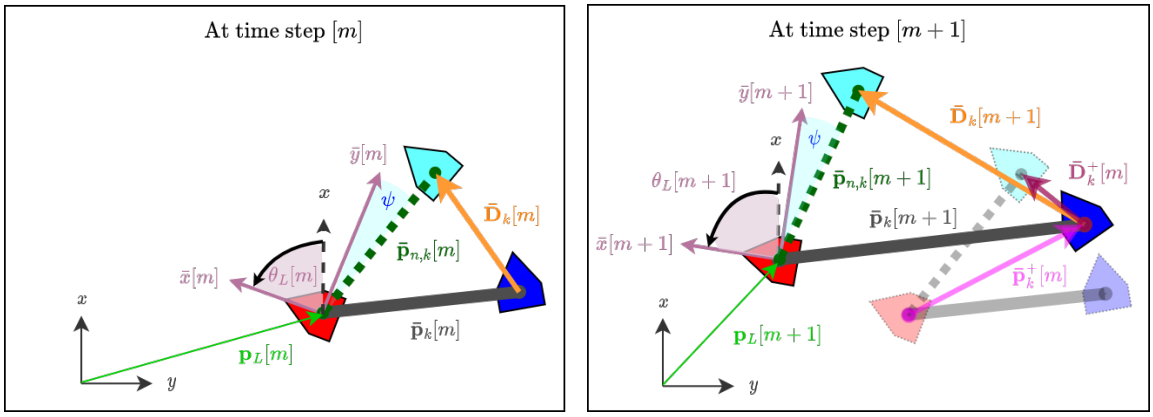


(a) (b)

Figure 5.1: Different coordinate frames of an example 2-robot planar transport system. The position of the leader robot (robot 1 shown in red) in global frame $(x, y)$ indicated as $\mathbf{p}_L$ while $\bar{\mathbf{p}}_k$ is the position of robot $k$ (shown in blue) in the leader's coordinate frame $(\bar{x}, \bar{y})$ which is rotated by $\theta_L$. **(a)** At time step $[m]$, robot $k$ seeks to move towards its nominal position $\bar{\mathbf{p}}_{n,k}$ shown in cyan to minimize the deformation $\bar{\mathbf{D}}_k$. **(b):** At the next time step $[m+1]$, the leader robot has moved to different location in global coordinate, closer to the original nominal position $\bar{\mathbf{p}}_{n,k}[m]$ in this instance. However, the nominal position $\bar{\mathbf{p}}_{n,k}$ of robot $k$ has changed, resulting in a change (increase in this instance) in the deformation $\bar{\mathbf{D}}_k$.

### *5.1.1 Leader robot update*

The role of a leader robot in the network is to steer and orient the object. The desired trajectory $\mathbf{p}_d$ information is then implicitly communicated to the followers through the object. In particular, the leader robot adjusts its configuration $\mathbf{q}_L$ (position $\mathbf{p}_L$ and orientation $\Theta_L$) based on the desired position $\mathbf{p}_d = [x_d, y_d, z_d]^\intercal$ and orientation $\Theta_d = [\theta_{x,d}, \theta_{y,d}, \theta_{z,d}]^\intercal$, in global

coordinates $(x, y, z)$, as

$$\mathbf{q}_L[m+1] = \mathbf{q}_L[m] + \gamma_L(\mathbf{q}_d[m] - \mathbf{q}_L[m]), \tag{5.1}$$

where $\mathbf{q}_L = [\mathbf{p}_L, \Theta_L]^\intercal \in \mathbb{R}^{\bar{n}}$, $\mathbf{q}_d = [\mathbf{p}_d, \Theta_d]^\intercal \in \mathbb{R}^{\bar{n}}$, $\gamma_L \in \mathbb{R}$ is the update gain, and $[m]$ represents the current discrete time instant, with $\bar{n}$ denoting the number of degree of freedom (DOF).

### *5.1.2 Follower robots update using local force measurements*

*Individual robot update*

Since the follower robots do not have access to the desired trajectory, they use measurements of local reactions (force and torque) $\hat{\mathbf{f}}_k = [\hat{f}_{x,k}, \hat{f}_{y,k}, \hat{f}_{z,k}, \hat{\tau}_{x,k}, \hat{\tau}_{y,k}, \hat{\tau}_{z,k}]^\intercal \in \mathbb{R}^{\bar{n}}$ (tared by the gravity force measured at an initial low-deformation configuration of the object), in each robot's body-fixed local coordinates $(\hat{x}_k, \hat{y}_k, \hat{z}_k)$, to update their orientation as

$$\hat{\mathbf{q}}_k^+[m] = -\gamma \hat{\mathbf{\Gamma}}_k \hat{\mathbf{f}}_k[m], \tag{5.2}$$

where $\hat{\mathbf{q}}_k^+ = [\hat{\mathbf{p}}_k^+, \hat{\Theta}_k^+]^\intercal \in \mathbb{R}^{\bar{n}}$ is a stacked vector of the position update $\hat{\mathbf{p}}_k = [\hat{x}_k, \hat{y}_k, \hat{z}_k]^\intercal$ and orientation update $\hat{\Theta}_k = [\hat{\theta}_{x,k}, \hat{\theta}_{y,k}, \hat{\theta}_{z,k}]^\intercal$ of the $k^{th}$ robot at the next time instant in the current robot's local coordinate denoted by $+$, $[m]$ indicates discrete time instants $(m\delta_t)$ with sampling period $\delta_t$, $\gamma\hat{\mathbf{\Gamma}}_k \in \mathbb{R}^{\bar{n}\times\bar{n}}$ is the update gain matrix which varies with time depending on object's orientation. The update Eq. (5.2) in the local body-fixed coordinates $(\hat{x}_k, \hat{y}_k, \hat{z}_k)$ of each robot $k$ is converted to the position update of each robot in the global coordinates $(x, y, z)$ by first rewriting the update in the leader robots coordinates $(\bar{x}, \bar{y}, \bar{z})$, as discussed below, under the following assumptions.

**Assumption 2** *Follower robots are rigidly attached to the object, and therefore, each follower robot maintains its local orientation with respect to the object.*

The gains in the individual robot's update Eq. (5.2) can vary depending on the objects stiffness in the different directions. Therefore, Assumption 2 allows the local gain matrix

to be fixed $\hat{\mathbf{\Gamma}}_k$ since the robot and the object remain aligned. If the robots are not rigidly connected, an alternative approach is to measure the angle between the robot and the flexible object to realign the stiffness matrix from object coordinate to robot body coordinates before computing the update in Eq. (5.2).

**Assumption 3** *Deformation during transport is relatively small and does not substantially alter the overall object shape.*

From Assumption 3, the configuration update $\hat{\mathbf{q}}_k^+ = [\hat{\mathbf{p}}_k^+, \hat{\Theta}_k^+]^\intercal$ and local reaction $\hat{\mathbf{f}}_k$ in the individual robot coordinates are similar in the leader robot's local coordinates $(\bar{x}, \bar{y}, \bar{z})$, i.e.,

$$\begin{aligned} \bar{\mathbf{q}}_k^+ &= \mathbf{T}_{\bar{\Theta}_k} \hat{\mathbf{q}}_k^+ + \bar{\mathbf{q}}_k \quad \approx \hat{\mathbf{q}}_k^+ + \bar{\mathbf{q}}_k \\ \bar{\mathbf{f}}_k &= \mathbf{T}_{\bar{\Theta}_k} \hat{\mathbf{f}}_k \ \approx \hat{\mathbf{f}}_k, \end{aligned} \tag{5.3}$$

where $\mathbf{T}_{\bar{\Theta}_k} \approx \mathbf{I}$ is a standard rotation transformation matrix as defined in [48] which depends on the orientation $\bar{\Theta}_k$ of each robot with respect to leader robot, from Assumption 2. For large deformations, the transformation matrix $\mathbf{T}_{\bar{\Theta}_k}$ needs to be included in the analysis, but it is simplified to identity $\mathbf{I}$ in the following since the overall objective is to maintain small deformations during transport.

*Robot network update in leader coordinates*

The stacked vector of difference in robot states at next and current time instant in the local coordinate for all $n$-follower robots, $\bar{\mathbf{Q}}^+ - \bar{\mathbf{Q}}$, in the leader robot's coordinate frame, is given by, from Eq. (5.3),

$$\bar{\mathbf{Q}}^+ - \bar{\mathbf{Q}} \ = \mathbf{R} \begin{bmatrix} \bar{\mathbf{q}}_1^+ - \bar{\mathbf{q}}_1 \\ \bar{\mathbf{q}}_2^+ - \bar{\mathbf{q}}_2 \\ \vdots \\ \bar{\mathbf{q}}_n^+ - \bar{\mathbf{q}}_n \end{bmatrix} = \mathbf{R} \begin{bmatrix} \hat{\mathbf{q}}_1^+ \\ \hat{\mathbf{q}}_2^+ \\ \vdots \\ \hat{\mathbf{q}}_n^+ \end{bmatrix}, \tag{5.4}$$

where $\bar{\mathbf{Q}} = [\bar{\mathbf{P}}_x, \bar{\mathbf{P}}_y, \bar{\mathbf{P}}_z, \bar{\mathbf{\Theta}}_x, \bar{\mathbf{\Theta}}_y, \bar{\mathbf{\Theta}}_z]^\intercal \in \mathbb{R}^{\bar{n}n}$,

$$\begin{aligned} \bar{\mathbf{P}}_i &= [\bar{p}_{i,1}, \bar{p}_{i,2}, \ldots, \bar{p}_{i,n}]^\intercal, \\ \bar{\mathbf{\Theta}}_i &= [\bar{\theta}_{i,1}, \bar{\theta}_{i,2}, \ldots, \bar{\theta}_{i,n}]^\intercal, \end{aligned} \tag{5.5}$$

with $i \in \{x, y, z\}$, $n$ is the number of robots and the superscript "+" on $\bar{\mathbf{Q}}^+$ indicates the state $\bar{\mathbf{Q}}$ at the next time instant in the current local coordinate, the orthogonal reordering matrix $\mathbf{R}$ is given by

$$\mathbf{R} = \begin{bmatrix} \mathbf{R}_{1,(n\times\bar{n}n)} \\ \mathbf{R}_{2,(n\times\bar{n}n)} \\ \vdots \\ \mathbf{R}_{\bar{n},(n\times\bar{n}n)} \end{bmatrix} \in \mathbb{R}^{\bar{n}n\times\bar{n}n}, \quad \mathbf{R}^\intercal\mathbf{R} = \mathbf{R}\mathbf{R}^\intercal = \mathbf{I}, \tag{5.6}$$

with elements given by

$$\begin{aligned} \mathbf{R}_s(j,k) &= 1, \quad \text{if } k = (j-1) * \bar{n} + s \\ &= 0, \quad \text{otherwise}, \end{aligned} \tag{5.7}$$

where $s = 1, 2, \ldots, \bar{n}$, and $\mathbf{I}$ is an identity matrix of appropriate dimension from context. Similarly, the stacked robot reaction force along each axis in the leader robot's coordinate frame is given by

$$\bar{\mathbf{F}} = \mathbf{R} \begin{bmatrix} \bar{\mathbf{f}}_1 \\ \bar{\mathbf{f}}_2 \\ \vdots \\ \bar{\mathbf{f}}_n \end{bmatrix} = \mathbf{R} \begin{bmatrix} \hat{\mathbf{f}}_1 \\ \hat{\mathbf{f}}_2 \\ \vdots \\ \hat{\mathbf{f}}_n \end{bmatrix}, \tag{5.8}$$

where $\bar{\mathbf{F}} = [\bar{\mathbf{F}}_x, \bar{\mathbf{F}}_y, \bar{\mathbf{F}}_z, \bar{\mathbf{M}}_x, \bar{\mathbf{M}}_y, \bar{\mathbf{M}}_z]^\intercal \in \mathbb{R}^{\bar{n}n}$,

$$\bar{\mathbf{F}}_i = [\bar{f}_{i,1}, \bar{f}_{i,2}, \ldots, \bar{f}_{i,n}]^\intercal \in \mathbb{R}^n, \tag{5.9}$$

$$\bar{\mathbf{M}}_i = [\bar{\tau}_{i,1}, \bar{\tau}_{i,2}, \ldots, \bar{\tau}_{i,n}]^\intercal \in \mathbb{R}^n, \tag{5.10}$$

with $i \in \{x, y, z\}$. The individual updates in Eq. (5.2), in each robot's local coordinate frame, can be stacked to obtain

$$\begin{bmatrix} \hat{\mathbf{q}}_1^+[m] \\ \hat{\mathbf{q}}_2^+[m] \\ \vdots \\ \hat{\mathbf{q}}_n^+[m] \end{bmatrix} = \begin{bmatrix} -\gamma \hat{\mathbf{\Gamma}}_1 \hat{\mathbf{f}}_1[m] \\ -\gamma \hat{\mathbf{\Gamma}}_2 \hat{\mathbf{f}}_2[m] \\ \vdots \\ -\gamma \hat{\mathbf{\Gamma}}_n \hat{\mathbf{f}}_n[m] \end{bmatrix} = -\gamma \hat{\mathbf{\Gamma}} \begin{bmatrix} \hat{\mathbf{f}}_1[m] \\ \hat{\mathbf{f}}_2[m] \\ \vdots \\ \hat{\mathbf{f}}_n[m] \end{bmatrix}, \tag{5.11}$$

where $\hat{\mathbf{\Gamma}} \in \mathbb{R}^{\bar{n}n \times \bar{n}n}$ is block diagonal

$$\hat{\mathbf{\Gamma}} = \begin{bmatrix} \hat{\mathbf{\Gamma}}_1 & & \\ & \ddots & \\ & & \hat{\mathbf{\Gamma}}_n \end{bmatrix}, \tag{5.12}$$

and each $\hat{\mathbf{\Gamma}}_i$ has positive values on its diagonal and zeros elsewhere. Using Eqs. (5.4) and (5.8), Eq. (5.11) can be rewritten in the leader robot's coordinates $(\bar{x}, \bar{y}, \bar{z})$ as

$$\mathbf{R}^{-1} \left( \bar{\mathbf{Q}}^+[m] - \bar{\mathbf{Q}}[m] \right) = -\gamma \hat{\mathbf{\Gamma}} \mathbf{R}^{-1} \bar{\mathbf{F}}[m], \tag{5.13}$$

which simplifies to

$$\bar{\mathbf{Q}}^+[m] = \bar{\mathbf{Q}}[m] - \gamma \bar{\mathbf{\Gamma}} \bar{\mathbf{F}}[m], \tag{5.14}$$

where the reordered gain matrix $\bar{\mathbf{\Gamma}}$ is

$$\bar{\mathbf{\Gamma}} = \mathbf{R} \hat{\mathbf{\Gamma}} \mathbf{R}^{-1}. \tag{5.15}$$

*Robot network update in global coordinates*

The stacked states of the robots $\bar{\mathbf{Q}}$, the nominal states $\bar{\mathbf{Q}}_n$ where the object is undeformed, and the stacked reactions $\bar{\mathbf{F}}$ in the leader's coordinate frame can be converted to the global coordinate frame using the leader-to-global transformation matrix $\mathbf{T}$, that is

$$\begin{aligned} \mathbf{Q}[m] &= \mathbf{T}[m] \bar{\mathbf{Q}}[m] + \mathbf{B}_1 \mathbf{q}_L[m], \\ \mathbf{Q}_n[m] &= \mathbf{T}[m] \bar{\mathbf{Q}}_n[m] + \mathbf{B}_1 \mathbf{q}_L[m], \\ \mathbf{F}[m] &= \mathbf{T}[m] \bar{\mathbf{F}}[m], \end{aligned} \tag{5.16}$$

where the orthogonal transformation matrix is defined with respect to the leader's orientation as

$$\mathbf{T} = \mathbf{R}(\mathbf{I}_{n\times n} \otimes \mathbf{T}_{\Theta_L})\mathbf{R}^{-1}, \quad \mathbf{T}\mathbf{T}^\intercal = \mathbf{T}^\intercal\mathbf{T} = \mathbf{I}, \tag{5.17}$$

where $\otimes$ indicates a Kronecker product and $\mathbf{T}_{\Theta_L}$ is a standard orthogonal rotation matrix from Section 2.2. in [48] as

$$\mathbf{T}_{\Theta_L} = \begin{bmatrix} \mathbf{T}_z\mathbf{T}_y\mathbf{T}_x & \mathbf{0}_{3\times3} \\ \mathbf{0}_{3\times3} & \mathbf{I}_{3\times3} \end{bmatrix}, \quad \mathbf{T}_{\Theta_L}^\intercal\mathbf{T}_{\Theta_L} = \mathbf{T}_{\Theta_L}\mathbf{T}_{\Theta_L}^\intercal = \mathbf{I}, \tag{5.18}$$

where

$$\mathbf{T}_z = \begin{bmatrix} c_z & -s_z & 0 \\ s_z & c_z & 0 \\ 0 & 0 & 1 \end{bmatrix}, \quad \mathbf{T}_y = \begin{bmatrix} c_y & 0 & -s_y \\ 0 & 1 & 0 \\ s_y & 0 & c_y \end{bmatrix}, \tag{5.19}$$

$$\mathbf{T}_x = \begin{bmatrix} 1 & 0 & 0 \\ 0 & c_x & -s_x \\ 0 & s_x & c_x \end{bmatrix}, \quad \text{where} \quad \begin{matrix} c_i = cos(\theta_{i,L}), \\ s_i = sin(\theta_{i,L}), \end{matrix} \tag{5.20}$$

with $i \in \{x, y, z\}$, $\mathbf{q}_L$ is the state of leader robot in the global coordinate, $\mathbf{R}$ is defined in Eq. (5.6), and

$$\mathbf{B}_1 = (\mathbf{I}_{\bar{n}\times\bar{n}} \otimes \mathbf{1}_n) \in \mathbb{R}^{\bar{n}n\times\bar{n}}, \tag{5.21}$$

where $\mathbf{1}_n$ is an $n$-sized column vector of ones. State of the robots at the next time instant $\bar{\mathbf{Q}}^+[m]$ in the current local coordinate frame $(\bar{x}, \bar{y}, \bar{z})$, is converted to the state in global coordinate frame at the next time instant $\mathbf{Q}[m+1]$ using leader-to-global transformation $\mathbf{T}$ in Eq. (5.17) with respect to leader robot's position $\mathbf{p}_L$, e.g.,

$$\mathbf{Q}[m+1] = \mathbf{T}[m]\bar{\mathbf{Q}}^+[m] + \mathbf{B}_1\mathbf{q}_L[m]. \tag{5.22}$$

Similarly, the state $\bar{\mathbf{Q}}[m+1]$ in the local coordinate frame $(\bar{x}, \bar{y}, \bar{z})$ at the next time instant $[m+1]$ can also be converted to the state $\mathbf{Q}[m+1]$ in the global coordinates using leader-to-global transformation $\mathbf{T}$ at the next time instant $[m+1]$ as

$$\mathbf{Q}[m+1] = \mathbf{T}[m+1]\bar{\mathbf{Q}}[m+1] + \mathbf{B}_1\mathbf{q}_L[m+1]. \tag{5.23}$$

Then, equating Eqs. (5.22) and (5.23) above to solve for $\bar{\mathbf{Q}}^{+}[m]$ results in

$$\begin{aligned}\bar{\mathbf{Q}}^{+}[m] =&\mathbf{T}^{-1}[m]\big\{\mathbf{T}[m+1]\bar{\mathbf{Q}}[m+1] \\ &+\mathbf{B}_1(\mathbf{q}_L[m+1]-\mathbf{q}_L[m])\big\},\end{aligned} \tag{5.24}$$

and substituting Eq. (5.24) into Eq. (5.14) yields

$$\begin{aligned}&\mathbf{T}^{-1}[m]\big\{\mathbf{T}[m+1]\bar{\mathbf{Q}}[m+1]+\mathbf{B}_1(\mathbf{q}_L[m+1]-\mathbf{q}_L[m])\big\} = \\ &\bar{\mathbf{Q}}[m]-\gamma\bar{\mathbf{\Gamma}}\bar{\mathbf{F}}[m],\end{aligned} \tag{5.25}$$

which can be simplified to

$$\begin{aligned}\bar{\mathbf{Q}}[m+1] =&\mathbf{T}^{-1}[m+1]\Big\{\mathbf{T}[m]\Big[\bar{\mathbf{Q}}[m]-\gamma\bar{\mathbf{\Gamma}}\bar{\mathbf{F}}[m]\Big] \\ &+\mathbf{B}_1(\mathbf{q}_L[m]-\mathbf{q}_L[m+1])\Big\}.\end{aligned} \tag{5.26}$$

Using the transformation in Eq. (5.16), the above equation can be rewritten in the global coordinate frame as,

$$\begin{aligned}&\mathbf{T}^{-1}[m+1](\mathbf{Q}[m+1]-\mathbf{B}_1\mathbf{q}_L[m+1]) = \\ &\mathbf{T}^{-1}[m+1]\Big\{\mathbf{T}[m]\Big[\mathbf{T}^{-1}[m](\mathbf{Q}[m]-\mathbf{B}_1\mathbf{q}_L[m]) \\ &-\gamma\bar{\mathbf{\Gamma}}\mathbf{T}^{-1}[m]\mathbf{F}[m]\Big]+\mathbf{B}_1(\mathbf{q}_L[m]-\mathbf{q}_L[m+1])\Big\},\end{aligned} \tag{5.27}$$

which simplifies to

$$\mathbf{Q}[m+1] =\mathbf{Q}[m]-\gamma\mathbf{\Gamma}[m]\mathbf{F}[m], \tag{5.28}$$

where the transformed gain matrix $\mathbf{\Gamma}$ is

$$\mathbf{\Gamma}[m] = \mathbf{T}[m]\bar{\mathbf{\Gamma}}\mathbf{T}^{-1}[m]. \tag{5.29}$$

### *5.1.3 Deformation based update*

The stacked reaction force $\bar{\mathbf{F}}$ in the update Eq. (5.14) can be written in terms of object stiffness $\bar{\mathbf{K}} \in \mathbb{R}^{\bar{n}n\times\bar{n}n}$ and deviation of the robots' state $\bar{\mathbf{Q}}$ from the nominal state $\bar{\mathbf{Q}}_n$ as

$$\bar{\mathbf{F}} = \bar{\mathbf{K}}(\bar{\mathbf{Q}}-\bar{\mathbf{Q}}_n) \ = \bar{\mathbf{K}}\bar{\mathbf{D}}, \tag{5.30}$$

where $\bar{\mathbf{D}}$ represents the object deformation, and $\bar{\mathbf{K}}$ is the object stiffness, which can be obtained using the Finite Element Method (FEM) if object's properties are known [49]. Using the local-to-global transformation matrix $\mathbf{T}$ in Eq. (5.17) the reaction force $\mathbf{F}$ can be written in the global coordinate as,

$$\mathbf{F} = \mathbf{T}\bar{\mathbf{K}}\mathbf{T}^{-1}(\mathbf{Q} - \mathbf{Q}_n) = \mathbf{T}\bar{\mathbf{K}}\mathbf{T}^{-1}\mathbf{D} = \mathbf{K}\mathbf{D}. \tag{5.31}$$

The reaction force and deformation relationship in Eq. (5.31) can be used to rewrite the update law in terms of the change in the object deformation $\mathbf{D}$ by subtracting both sides of Eq. (5.28) with its nominal position $\mathbf{Q}_n$ at each respected time step as,

$$\begin{aligned}\mathbf{Q}[m+1] - \mathbf{Q}_n[m+1] - \mathbf{Q}_n[m] = \mathbf{Q}[m] - \mathbf{Q}_n[m+1] \\ - \mathbf{Q}_n[m] - \gamma\mathbf{\Gamma}[m]\mathbf{T}[m]\bar{\mathbf{K}}\mathbf{T}^{-1}[m]\mathbf{D}[m],\end{aligned} \tag{5.32}$$

which can be simplified to

$$\begin{aligned}\mathbf{D}[m+1] =& \mathbf{D}[m] - \gamma\mathbf{\Gamma}[m]\mathbf{K}[m]\mathbf{D}[m] \\ & - \mathbf{Q}_n[m+1] + \mathbf{Q}_n[m] \\ =& \left(\mathbf{I} - \gamma\mathbf{\Gamma}[m]\mathbf{K}[m]\right)\mathbf{D}[m] + \mathbf{Q}_n[m] - \mathbf{Q}_n[m+1].\end{aligned} \tag{5.33}$$

Since the nominal configuration of the flexible object, measured with respect to the orientation $(\bar{x}, \bar{y}, \bar{z})$ of the leader robot does not vary with time instant, $\bar{\mathbf{Q}}_n[m+1] = \bar{\mathbf{Q}}_n[m] = \bar{\mathbf{Q}}_n$, as seen in From Fig. 5.1, using the leader-to-global transformation $\mathbf{T}$ in Eq. (5.16), results in

$$\begin{aligned}\mathbf{Q}_n[m] - \mathbf{Q}_n[m+1] =& (\mathbf{T}[m] - \mathbf{T}[m+1])\bar{\mathbf{Q}}_n \\ & + \mathbf{B}_1(\mathbf{q}_L[m] - \mathbf{q}_L[m+1]).\end{aligned} \tag{5.34}$$

Substituting Eq. (5.34) into Eq. (5.33) yields the deformation dynamics

$$\mathbf{D}[m+1] = \mathbf{H}[m]\mathbf{D}[m] + \mathbf{U}_d[m], \tag{5.35}$$

where

$$\begin{aligned}\mathbf{H}[m] &= \mathbf{I} - \gamma\mathbf{L}[m] \quad \text{with} \quad \mathbf{L}[m] = \mathbf{\Gamma}[m]\mathbf{K}[m], \\ \mathbf{U}_d[m] &= \left(\mathbf{T}[m] - \mathbf{T}[m+1]\right)\bar{\mathbf{Q}}_n + \mathbf{B}_1(\mathbf{q}_L[m] - \mathbf{q}_L[m+1]).\end{aligned} \tag{5.36}$$

**Remark 9 (Time varying dynamics)** *The deformation dynamics in Eq.* (5.35) *is time-varying since both the gain matrix* $\mathbf{\Gamma}$ *and stiffness matrix* $\mathbf{K}$ *in the dynamics matrix* $\mathbf{H}$ *in Eq.* (5.36) *are time varying, i.e., from Eqs.* (5.29) *and* (5.31)*,*

$$\begin{aligned} \mathbf{K}[m] &= \mathbf{T}[m]\bar{\mathbf{K}}\mathbf{T}^{-1}[m], \\ \mathbf{\Gamma}[m] &= \mathbf{T}[m]\bar{\mathbf{\Gamma}}\mathbf{T}^{-1}[m], \end{aligned} \tag{5.37}$$

*where the time dependency comes from the transformation matrix* $\mathbf{T}$ *due to orientation changes.*

**Remark 10 (Dynamics matrix H)** *The dynamics matrix* $\mathbf{H}$ *seeks to decrease the deformation* $\mathbf{D}$ *in Eq.* (5.35)*. In particular, when there is no change in leader's position* $\mathbf{p}_L$ *and orientation* $\Theta_L$*, the deformation* $\mathbf{D}[m]$ *approaches zero as time* $m$ *increases.*

**Remark 11 (Deformation versus speed)** *The deformation* $\mathbf{D}[m+1]$ *at the next time step* $[m+1]$ *is driven by the change in the leader's state* $(\mathbf{q}_L[m]-\mathbf{q}_L[m+1])$ *as well as changes in the desired nominal position of the object* $(\mathbf{T}[m]-\mathbf{T}[m+1])\,\bar{\mathbf{Q}}_n$*, which are small if the leader's position and orientation are changing slowly. Therefore, the potential deformation increase will be small during slow transport due to a small disturbance* $\mathbf{U}_d$ *.*

### *5.1.4 Problem: decrease deformation*

The deformation $\mathbf{D}[m+1]$ at time step $[m+1]$ can increase due to the transport-dependent term $\mathbf{U}_d[m]$ in the update Eq. (5.35), although the update seeks to reduce the deformation through the $\mathbf{H}[m]$ term. The increase in deformation at each step can be made smaller by going slower since $\mathbf{U}_d[m] \to \mathbf{0}$ as the transport becomes slower. The research problem is to reduce the deformation without increasing the transport time. This is to be done in a decentralized manner without changing the robot-object (network) structure.

## *5.2 Proposed Approach using DSR*

In this section, the proposed DSR approach for reducing object deformation during transport is discussed. Furthermore, the stability and performance of the proposed approach are analyzed.

### *5.2.1 Ideal transport*

The proposed DSR approach is derived from the ideal update for transport, which can reduce and maintain a sufficiently small deformation within a specified settling time. In particular, if each follower robot in the network has direct access to its own undeformed nominal state $\mathbf{Q}_n$ and its changes $\dot{\mathbf{Q}}_n$, then the ideal update $\dot{\mathbf{Q}}$ can be written in continuous time domain as

$$\dot{\mathbf{Q}}(t) - \dot{\mathbf{Q}}_n(t) = -\alpha \left[\mathbf{Q}(t) - \mathbf{Q}_n(t)\right], \tag{5.38}$$

where $\alpha > 0$ is the update gain, which can be selected such that the robot network gets sufficiently close to its undeformed nominal state $\mathbf{Q}_n$ within a specified settling time, and $\mathbf{Q}$ is the state of the robots.

**Remark 12 (Ideal transport is centralized)** *The ideal update law in Eq.* (5.38) *maintains deformations to be small. However, it is centralized since the nominal position* $\mathbf{Q}_n$ *and its time derivatives need to be known by all robots. Moreover, the nominal position* $\mathbf{Q}_n$ *of each robot depends on the object's geometry during orientation changes.*

### *5.2.2 Decentralizing the ideal transport using force feedback*

Towards deriving the decentralized update, multiplying both sides of the ideal update in Eq. (5.38) with a scaled stiffness matrix $\beta\mathbf{\Gamma}(t)\mathbf{K}(t)$ and adding the derivative of state with respect to time $\dot{\mathbf{Q}}(t)$ to both sides results in

$$\begin{aligned} &\dot{\mathbf{Q}}(t) + \beta\mathbf{\Gamma}(t)\mathbf{K}(t)\left[\dot{\mathbf{Q}}(t) - \dot{\mathbf{Q}}_n(t)\right] \\ &\qquad = \dot{\mathbf{Q}}(t) - \alpha\beta\mathbf{\Gamma}(t)\mathbf{K}(t)\left[\mathbf{Q}(t) - \mathbf{Q}_n(t)\right], \end{aligned} \tag{5.39}$$

which can be rearranged and rewritten as,

$$\begin{aligned}\dot{\mathbf{Q}}(t) =&\dot{\mathbf{Q}}(t) - \alpha\beta\mathbf{\Gamma}(t)\mathbf{K}(t)\left[\mathbf{Q}(t) - \mathbf{Q}_n(t)\right] \\ &- \beta\mathbf{\Gamma}(t)\mathbf{K}(t)\left[\dot{\mathbf{Q}}(t) - \dot{\mathbf{Q}}_n(t)\right].\end{aligned} \tag{5.40}$$

The right-hand side derivative is approximated using delayed self-reinforcement (DSR) as [47]

$$\begin{aligned}\dot{\mathbf{Q}}(t) \approx&\frac{\mathbf{Q}(t) - \mathbf{Q}(t - t_\delta)}{t_\delta} - \alpha\beta\mathbf{\Gamma}(t)\mathbf{K}(t)\mathbf{D}(t) \\ &- \beta\mathbf{\Gamma}(t)\mathbf{K}(t)\left[\frac{\mathbf{D}(t) - \mathbf{D}(t - t_\delta)}{t_\delta}\right],\end{aligned} \tag{5.41}$$

where time delay $t_\delta = N\delta_t$ is an integer $N$ times the sampling period $\delta_t$. Recasting Eq. (5.41) in a discretized form yields

$$\begin{aligned}\mathbf{Q}[m+1] =&\mathbf{Q}[m] - \alpha\beta\delta_t\mathbf{\Gamma}[m]\mathbf{K}[m]\mathbf{D}[m] \\ &- \beta\mathbf{\Gamma}[m]\mathbf{K}[m]\left[\frac{\mathbf{D}[m] - \mathbf{D}[m-N]}{N}\right] \\ &+ \frac{\mathbf{Q}[m] - \mathbf{Q}[m-N]}{N}.\end{aligned} \tag{5.42}$$

### *5.2.3 Force-based decentralized DSR update for transport*

The decentralized update law in Eq. (5.42) can be written using the force-deformation relationship in Eq. (5.31) as,

$$\begin{aligned}\mathbf{Q}[m+1] = \mathbf{Q}[m] - \alpha\beta\delta_t\mathbf{\Gamma}[m]\mathbf{F}[m] + \frac{\mathbf{Q}[m] - \mathbf{Q}[m-N]}{N} \\ - \beta\mathbf{\Gamma}[m]\left[\frac{\mathbf{F}[m] - \mathbf{F}[m-N]}{N}\right].\end{aligned} \tag{5.43}$$

For each individual robot $k$, the decentralized DSR-based update law becomes,

$$\begin{aligned}\mathbf{q}_k[m+1] = \mathbf{q}_k[m] - \alpha\beta\delta_t\mathbf{\Gamma}_k[m]\mathbf{f}_k[m] \\ + \frac{\mathbf{q}_k[m] - \mathbf{q}_k[m-N]}{N} \\ - \beta\mathbf{\Gamma}_k[m]\left[\frac{\mathbf{f}_k[m] - \mathbf{f}_k[m-N]}{N}\right],\end{aligned} \tag{5.44}$$

where $\mathbf{q}_k = [\mathbf{p}_k, \Theta_k]^\intercal \in \mathbb{R}^{\bar{n}}$ is a stacked vector of the position update $\mathbf{p}_k = [p_{x,k}, p_{y,k}, p_{z,k}]^\intercal$ and orientation update $\Theta_k = [\theta_{x,k}, \theta_{y,k}, \theta_{z,k}]^\intercal$ of the $k^{th}$ robot in the global coordinate frame.

**Remark 13 (Decentralized implementation)** *While the design of the DSR transport law in Eq.* (5.44) *is centralized, the implementation is decentralized because the state update at the next time step* $\mathbf{q}_k[m+1]$ *only depends on the information of its own state* $\mathbf{q}_k[m]$ *and local reaction measurement* $\mathbf{f}_k[m]$ *at the current time step* $[m]$ *along with its delayed versions at time step* $[m-N]$*. Thus, it does not require communication among the robots during implementation.*

**Remark 14 (Derivative approximation as a filter)** *The derivative approximation acts as a filtered derivative in Eq.* (5.40)*. It tends to be accurate for low frequencies. At high frequencies, the derivative approximation is filtered and the DSR transport law in Eq.* (5.43) *becomes similar to the standard update law in Eq.* (5.28)*.*

### *5.2.4 Stability with DSR*

The update law in Eq. (5.43) can be written in terms of deformation $\mathbf{D}$ by subtracting both sides of the equation with their nominal state $\mathbf{Q}_n$ at each respected time step and substituting the force terms with Eq. (5.31) as,

$$\begin{aligned}\mathbf{D}[m+1] = &(\mathbf{I} - \alpha\beta\delta_t\mathbf{\Gamma}[m]\mathbf{K}[m])\mathbf{D}[m] \\ &+ (\mathbf{I} - \beta\mathbf{\Gamma}[m]\mathbf{K}[m])\left[\frac{\mathbf{D}[m] - \mathbf{D}[m-N]}{N}\right] \\ &+ \mathbf{Q}_n[m] - \mathbf{Q}_n[m+1] + \frac{\mathbf{Q}_n[m] - \mathbf{Q}_n[m-N]}{N}.\end{aligned} \tag{5.45}$$

The $N$ delay form can be rewritten as a single delay by stacking $N+1$ current and past deformation states as

$$\mathbf{S}[m] = \begin{bmatrix} \mathbf{D}[m-N] \\ \vdots \\ \mathbf{D}[m-1] \\ \mathbf{D}[m] \end{bmatrix}, \tag{5.46}$$

to rewrite the system with the DSR update law in Eq. (5.45) as

$$\mathbf{S}[m+1] = \mathbf{A}[m]\mathbf{S}[m] + \mathbf{B}\mathbf{U}[m], \tag{5.47}$$

where the time-varying dynamic matrix $\mathbf{A}[m] \in \mathbb{R}^{\bar{n}n(N+1)\times\bar{n}n(N+1)}$ is

$$\mathbf{A}[m] = \begin{bmatrix} \mathbf{0} & \mathbf{I} & \dots & \mathbf{0} \\ \vdots & & \ddots & \vdots \\ \mathbf{0} & \dots & & \mathbf{I} \\ \mathbf{a}_1[m] & \mathbf{0} & \dots & \mathbf{a}_2[m] \end{bmatrix} \tag{5.48}$$

$$\begin{aligned} \mathbf{a}_1[m] &= -\frac{(\mathbf{I} - \beta\mathbf{\Gamma}[m]\mathbf{K}[m])}{N} \\ \mathbf{a}_2[m] &= (\mathbf{I} - \alpha\beta\delta_t\mathbf{\Gamma}[m]\mathbf{K}[m]) + \frac{\mathbf{I} - \beta\mathbf{\Gamma}[m]\mathbf{K}[m]}{N} \\ \mathbf{B} &= [\,\mathbf{0}\ \dots\ \mathbf{0}\quad \mathbf{I}\,]^\intercal \\ \mathbf{U}[m] &= \mathbf{Q}_n[m] - \mathbf{Q}_n[m+1] + \frac{\mathbf{Q}_n[m] - \mathbf{Q}_n[m-N]}{N}, \end{aligned} \tag{5.49}$$

and each block element of $\mathbf{A}$ has dimension of $\mathbb{R}^{\bar{n}n\times\bar{n}n}$.

*Stability of the time-varying system*

Conditions on the transport are established for stability of the time-varying DSR update law in Eq. (5.47). Since the input perturbation $\mathbf{U}[m]$ does not impact stability of the linear system, in the following stability analysis, the input perturbation is assumed to be zero $\mathbf{U}[m] = \mathbf{0}$ with a fixed-nominal position $\mathbf{Q}_n[m+1] = \mathbf{Q}_n[m] = \mathbf{Q}[m-N] = \mathbf{Q}_n$. As a result, for stability analysis the dynamics in Eq. (5.47) becomes

$$\mathbf{S}[m+1] = \mathbf{A}[m]\mathbf{S}[m]. \tag{5.50}$$

The stability conditions are developed in following three parts.

1. **Frozen-time stability:** The dynamic matrix $\mathbf{A}[m]$ in Eq. (5.50) is uniformly bounded in time and frozen-time stable, i.e., for a fixed time-step $m$, the eigenvalues of $\mathbf{A}[m]$ are inside the disc with radius $1 - 2\epsilon$.

2. **Slowly varying system:** The dynamic matrix $\mathbf{A}[m]$ is slowly varying with time-step $m$ if the speed of transport is not fast.

3. **Lyapunov stability:** The slowly-varying system in Eq. (5.50) is shown to be stable using the Lyapunov method.

**Part 1 (Frozen-time stability):** The following lemmas show that the matrices $\mathbf{A}[m]$ are uniformly bounded in time $[m]$ and to establish conditions on the gain parameters $(\alpha, \beta)$ to ensure that, for each fixed time $[m]$, the eigenvalues of dynamic matrix $\mathbf{A}[m]$ are inside a disc with specified radius $(1 - 2\epsilon) < 1$.

**Lemma 2 (A is bounded)** *Matrices $\mathbf{A}[m]$, $\forall\, m$ are uniformly bounded in time, i.e., there exists $a_M$ such that, for all $m$,*

$$\sup_m \|\mathbf{A}[m]\|_2 = a_M < \infty. \tag{5.51}$$

*Proof:* The dynamic matrix $\mathbf{A}[m]$ varies in time due to changes in gain matrix $\mathbf{\Gamma}$ and stiffness matrix $\mathbf{K}$, which in turn, arise due to the variation in the orthogonal transformation matrix $\mathbf{T}$ in Eq. (5.37), which is uniformly bounded in time by its spectral radius $\rho(\cdot)$ since

$$\sup_m \|\mathbf{T}[m]\|_2 = \sup_m \left\{ \sqrt{\rho(\mathbf{T}^\intercal[m]\mathbf{T}[m])} = \sqrt{\rho(\mathbf{I})} \right\} = 1. \tag{5.52}$$

Similarly, the inverse of $\mathbf{T}$ is also uniformly bounded,

$$\sup_m \|\mathbf{T}^{-1}[m]\|_2 = \sup_m \left\{ \sqrt{\rho(\mathbf{T}[m]\mathbf{T}^\intercal[m])} = \sqrt{\rho(\mathbf{I})} \right\} = 1. \tag{5.53}$$

As a consequence, the gain matrix $\mathbf{\Gamma}[m]$ and the and stiffness matrix $\mathbf{K}$ in Eq. (5.37) are uniformly bounded since

$$\begin{aligned} \sup_m \|\mathbf{\Gamma}[m]\|_2 &\leq \sup_m \left\{ \|\mathbf{T}[m]\|_2 \|\bar{\mathbf{\Gamma}}\|_2 \|\mathbf{T}^{-1}[m]\|_2 \right\} = \rho(\bar{\mathbf{\Gamma}}), \\ \sup_m \|\mathbf{K}[m]\|_2 &\leq \sup_m \left\{ \|\mathbf{T}[m]\|_2 \|\bar{\mathbf{K}}\|_2 \|\mathbf{T}^{-1}[m]\|_2 \right\} = \rho(\bar{\mathbf{K}}), \end{aligned} \tag{5.54}$$

where $\rho(\bar{\mathbf{\Gamma}})$ and $\rho(\bar{\mathbf{K}})$ are the spectral radius of the constant gain matrix $\bar{\mathbf{\Gamma}}$ and the constant stiffness matrix $\bar{\mathbf{K}}$, respectively. The least upper bound of the dynamic matrix $\mathbf{A}[m]$ can be established using norms equivalency between the Euclidean and the infinity norms as,

$$\begin{aligned}\sup_m \|\mathbf{A}[m]\|_2 &\leq \sup_m \sqrt{u_a}\ \|\mathbf{A}[m]\|_\infty \\ &= \sqrt{u_a}\ \sup_m \left\{ \max_{1\leq i\leq u_a} \sum_{j=1}^{u_a} |a_{i,j}[m]| \right\},\end{aligned} \tag{5.55}$$

where $u_a = \bar{n}n(N+1)$ is the row-dimension of matrix $\mathbf{A}$. All row sums of $\mathbf{A}$ are equal to 1 from definition in Eq. (5.48), except the last bottom block row, which depends on block matrices $\mathbf{a}_1$ and $\mathbf{a}_2$ in Eq. (5.49). Thus,

$$\begin{aligned}\sup_m \|\mathbf{A}[m]\|_2 &\leq \sqrt{u_a} \left( 1 + \alpha\beta\delta_t \left\{ \sup_m \|\mathbf{\Gamma}[m]\mathbf{K}[m]\|_\infty \right\} \right. \\ &\quad \left. + \frac{2}{N} \left[ 1 + \beta \left\{ \sup_m \|\mathbf{\Gamma}[m]\mathbf{K}[m]\|_\infty \right\} \right] \right) \\ &\leq \sqrt{u_a} \left( 1 + \alpha\beta\delta_t\sqrt{u_a} \left\{ \sup_m \|\mathbf{\Gamma}[m]\mathbf{K}[m]\|_2 \right\} \right. \\ &\quad \left. + \frac{2}{N} \left[ 1 + \beta\sqrt{u_a} \left\{ \sup_m \|\mathbf{\Gamma}[m]\mathbf{K}[m]\|_2 \right\} \right] \right) \\ &= \sqrt{u_a} \left( 1 + \alpha\beta\delta_t\sqrt{u_a}\ \rho(\bar{\mathbf{\Gamma}})\rho(\bar{\mathbf{K}}) \right. \\ &\quad \left. + \frac{2(1+\beta\sqrt{u_a}\ \rho(\bar{\mathbf{\Gamma}})\rho(\bar{\mathbf{K}}))}{N} \right) = a_M < \infty,\end{aligned} \tag{5.56}$$

where the right hand side of the Eq. (5.56) is bounded because it depends on constant parameters $(\alpha, \beta, \delta_t, N, u_a)$ and the spectral radius $\rho(\bar{\mathbf{\Gamma}})$ of the constant gain matrix $\bar{\mathbf{\Gamma}}$, and the spectral radius $\rho(\bar{\mathbf{K}})$ of the constant stiffness matrix $\bar{\mathbf{K}}$, resulting in the claim of the lemma. ■

Necessary and sufficient conditions are established for frozen-time stability of the case with unit time-step delay $N = 1$ in the following lemma, followed by a lemma establishing sufficient conditions for the case with multiple time-step delay $N > 1$.

**Lemma 3 (Frozen-time stability for unit time-step delay)** *For the unit time delay case* $N = 1$*, any given parameter* $0 < \epsilon < 0.5$ *and time step* $m$*, the spectral radius* $\rho$ *(the maximum of the absolute value of the eigenvalues) of the dynamics matrix* $\mathbf{A}[m]$ *in Eq.* (5.47) *satisfies*

$$\rho\left(\mathbf{A}[m]\right) < 1 - 2\epsilon, \quad \forall m \tag{5.57}$$

*if and only if the DSR update gains* $(\alpha, \beta)$ *satisfy*

$$\begin{aligned} &(i) \quad \alpha > \frac{1}{\delta_t}\left(\frac{2\epsilon}{1-2\epsilon}\right)\left[1 - \frac{2\epsilon}{\beta\bar{\lambda}_{\mathbf{L}}}\right] \\ &(ii) \quad 0 < \beta < \frac{4(1-2\epsilon) + 4\epsilon^2}{\bar{\lambda}_{\mathbf{L}}(2(1-2\epsilon) + 2\epsilon + \alpha\delta_t(1-2\epsilon))} = \overline{\beta}, \end{aligned} \tag{5.58}$$

where $\delta_t$ is the sampling time period, and $\bar{\lambda}_{\mathbf{L}}$ is the the largest eigenvalue of the positive definite symmetric matrix $\bar{\mathbf{L}} = \bar{\mathbf{\Gamma}}\bar{\mathbf{K}}$.

*Proof:* The bound on eigenvalues for stability of the DSR update law can be established by finding the roots of the characteristic equation of the proposed DSR transport dynamics in Eq. (5.45). The characteristic equation can be found by taking $z$-transform of Eq. (5.45) with no disturbance, e.g., $\mathbf{Q}_n[m+1] = \mathbf{Q}_n[m] = \mathbf{Q}_n[m-N]$, which results in

$$\begin{aligned} \det\Bigg\{ &\mathbf{I}z^{N+1} - \left(\mathbf{I} - \alpha\beta\delta_t\mathbf{L}[m] + \frac{(\mathbf{I} - \beta\mathbf{L}[m])}{N}\right) z^N \\ &+ \frac{(\mathbf{I} - \beta\mathbf{L}[m])}{N}\Bigg\} = 0, \end{aligned} \tag{5.59}$$

where the eigenvalues of matrix $\mathbf{L}[m] = \mathbf{\Gamma}[m]\mathbf{K}[m]$ are the same as the eigenvalues of $\bar{\mathbf{L}} = \bar{\mathbf{\Gamma}}\bar{\mathbf{K}}$ because $\mathbf{L} = \mathbf{T}[m]\bar{\mathbf{\Gamma}}\bar{\mathbf{K}}\mathbf{T}^{-1}[m] = \mathbf{T}[m]\bar{\mathbf{L}}\mathbf{T}^{-1}[m]$ from Eqs. (5.36) and the transformation matrix $\mathbf{T}$ is orthogonal. Therefore, the characteristic equation can be rewritten using the Jordan form $\mathbf{L}_J$ of matrix $\bar{\mathbf{L}}$ as

$$\begin{aligned} \det\Bigg\{ &\mathbf{I}z^{N+1} - \left(\mathbf{I} - \alpha\beta\delta_t\mathbf{L}_J + \frac{(\mathbf{I} - \beta\mathbf{L}_J)}{N}\right) z^N \\ &+ \frac{(\mathbf{I} - \beta\mathbf{L}_J)}{N}\Bigg\} = 0. \end{aligned} \tag{5.60}$$

Therefore, for each root $\lambda_{\mathbf{L},k}$, $k \in \{1, 2, \ldots, \bar{n}n\}$, of the matrix $\bar{\mathbf{L}} = \bar{\mathbf{\Gamma}}\bar{\mathbf{K}}$, the roots of the characteristic equation

$$\begin{aligned} C_k(z) =& z^{N+1} - \left(1 - \alpha\beta\delta_t\lambda_{\mathbf{L},k} + \frac{[1 - \beta\lambda_{\mathbf{L},k}]}{N}\right) z^N \\ &+ \frac{[1 - \beta\lambda_{\mathbf{L},k}]}{N} = 0, \end{aligned} \tag{5.61}$$

should have magnitude less than $1-2\epsilon$. For the unit-step delay case $N = 1$, the characteristic Eq. (5.61) becomes second order and stability conditions on DSR parameters $(\alpha, \beta)$ can be established using the Jury test. In particular, ensuring that the roots of characteristic Eq. (5.61) are inside the disc with radius $1 - 2\epsilon < 1$ is equivalent to establishing that the roots of the following shifted characteristic equation

$$\begin{aligned} C(\hat{z}) =& (1 - 2\epsilon)^2\hat{z}^2 - (2 - \alpha\beta\delta_t\lambda_{\mathbf{L},k} - \beta\lambda_{\mathbf{L},k})(1 - 2\epsilon)\hat{z} \\ &+ (1 - \beta\lambda_{\mathbf{L},k}) = 0 \end{aligned} \tag{5.62}$$

are inside the unit circle, where

$$\hat{z} = \frac{1}{(1 - 2\epsilon)}z. \tag{5.63}$$

Then, the three necessary and sufficient conditions for roots of the shifted characteristic equation to be in the unit circle are, from the Jury test,

1. $C(\hat{z} = 1) > 0$, i.e.,

$$\alpha\beta\delta_t\lambda_{\mathbf{L},k}(1 - 2\epsilon) > 2\beta\lambda_{\mathbf{L},k}\epsilon - 4\epsilon^2 \tag{5.64}$$

or

$$\alpha > \frac{1}{\delta_t}\left(\frac{2\epsilon}{1 - 2\epsilon}\right)\left[1 - \frac{2\epsilon}{\beta\lambda_{\mathbf{L},k}}\right]. \tag{5.65}$$

2. $|C(\hat{z} = 0)| < 1$, i.e.,

$$\begin{aligned} |1 - \beta\lambda_{\mathbf{L},k}| < 1 \quad \text{or} \quad -1 < (1 - \beta\lambda_{\mathbf{L},k}) < 1 \\ \Rightarrow 0 < \beta < \frac{2}{\lambda_{\mathbf{L},k}}. \end{aligned} \tag{5.66}$$

3. $(-1)^2 C(\hat{z}=-1) > 0$, i.e.,

$$\begin{aligned} 4 - 8\epsilon + 4\epsilon^2 - \beta\lambda_{\mathbf{L},k}(2 + \alpha\delta_t - 2\alpha\delta_t\epsilon - 2\epsilon) > 0 \\ \beta < \left(\frac{2}{\lambda_{\mathbf{L},k}}\right)\left[\frac{2(1-2\epsilon)+2\epsilon^2}{(2(1-2\epsilon)+2\epsilon+\alpha\delta_t(1-2\epsilon))}\right] \\ < \left(\frac{2}{\lambda_{\mathbf{L},k}}\right) \end{aligned} \tag{5.67}$$

since the denominator of the term in square brackets is greater than the numerator as $2\epsilon > 2\epsilon^2$ and $1 - 2\epsilon > 0$.

The condition in Eq. (5.67) is more stringent than in Eq. (5.66) and need to be satisfied for all eigenvalues $\lambda_{\mathbf{L},k}$, which results in conditions of the lemma. ■

For the case with large DSR delay, $N > 1$, sufficient conditions on DSR parameters $(\alpha, \beta)$ are found in the following lemma.

**Lemma 4 (Frozen-time stability for large time-step delay)** *For the case of large steps delay $N > 1$, the dynamics matrix $\mathbf{A}[m]$ has the spectral radius of $\rho(\mathbf{A}[m]) = 1 - 2\epsilon < 1$ if the DSR parameters $\alpha$ and $\beta$ satisfy*

$$\begin{aligned} (i) \quad & \alpha > 0, \\ (ii) \quad & b_l < \beta < b_u, \end{aligned} \tag{5.68}$$

*where $\bar{\lambda}_{\mathbf{L}}$ is the largest eigenvalue of the matrix $\bar{\mathbf{L}} = \bar{\mathbf{\Gamma}}\bar{\mathbf{K}}$,*

$$\begin{aligned} b_l &= \frac{1}{\bar{\lambda}_{\mathbf{L}}}\left[\max\left\{1 - N(1-2\epsilon)^{N+1}, \frac{N(1+2\epsilon)+2}{2(\alpha\delta_t N + 1)}\right\}\right] \\ b_u &= \frac{1}{\bar{\lambda}_{\mathbf{L}}}\left[\min\left\{1 - N(2\epsilon-1)^{N+1}, \frac{N(3-2\epsilon)+2}{2(\alpha\delta_t N + 1)}\right\}\right]. \end{aligned} \tag{5.69}$$

*Proof:* The DSR parameter $\alpha > 0$ as it is given from the ideal dynamics, as shown in Eq. (5.38). An upper bound $\overline{F}$ on roots of a general polynomial $(\sum_{i=1}^{N+1} a_i z^i) = 0$ can be

found using the Fujiwara's bound [50]

$$\overline{F} := 2\max\Bigg\{ \left|\frac{a_N}{a_{N+1}}\right|, \left|\frac{a_{N-1}}{a_{N+1}}\right|^{1/2}, \ldots, \left|\frac{a_1}{a_{N+1}}\right|^{\frac{1}{N}}, \left|\frac{a_0}{2a_{N+1}}\right|^{\frac{1}{N+1}} \Bigg\}. \tag{5.70}$$

Therefore, Fujiwara's upper bound on roots of the characteristic equation in Eq. (5.61) is

$$2\max\left\{ \left|\frac{[1-\beta\lambda_{\mathbf{L},k}]}{2N}\right|^{\frac{1}{N+1}}, \left|\left(1-\alpha\beta\delta_t\lambda_{\mathbf{L},k}+\frac{[1-\beta\lambda_{\mathbf{L},k}]}{N}\right)\right| \right\}, \tag{5.71}$$

which needs to be less than $1-2\epsilon$. Thus, it leads to the following conditions:

1.
$$\begin{aligned} &\left|\frac{[1-\beta\lambda_{\mathbf{L},k}]}{N}\right|^{\frac{1}{N+1}} < 1-2\epsilon \\ &\Rightarrow \frac{1-N(1-2\epsilon)^{N+1}}{\lambda_{\mathbf{L},k}} < \beta < \frac{1-N(2\epsilon-1)^{N+1}}{\lambda_{\mathbf{L},k}} \end{aligned} \tag{5.72}$$

2.
$$\begin{aligned} &\left|-\left(1-\alpha\beta\delta_t\lambda_{\mathbf{L},k}+\frac{[1-\beta\lambda_{\mathbf{L},k}]}{N}\right)\right| < 1/2-\epsilon \\ &\Rightarrow \frac{N(1+2\epsilon)+2}{2\lambda_{\mathbf{L},k}(\alpha\delta_t N+1)} < \beta < \frac{N(3-2\epsilon)+2}{2\lambda_{\mathbf{L},k}(\alpha\delta_t N+1)}. \end{aligned} \tag{5.73}$$

The selection of $\beta$ needs to satisfy conditions in both Eq. (5.72) and Eq. (5.73) for all eigenvalues $\lambda_{\mathbf{L},k}$ of matrix $\mathbf{L}$ leading to the conditions of the lemma. ■

**Remark 15** *If the dynamic matrices* $\mathbf{A}[m]$ *are uniformly bounded, and if their eigenvalues are inside a disc of radius* $1-2\epsilon$ *centered on the origin, then there exists a constant* $c$ *such that [51]*

$$\|(\mathbf{A}[m])^r\|_2 \leq c(1-\epsilon)^r, \quad \forall\, m, r. \tag{5.74}$$

**Part 2 (Slowly varying system):** The following lemma shows that time-variation of the dynamics matrix $\mathbf{A}[m]$ can be arbitrarily small if the rotational-transport speed is sufficiently slow.

**Lemma 5 (Slowly varying conditions)** *Given $\epsilon_A > 0$,*

$$\begin{aligned} &\sup_m \|\mathbf{A}[m+1] - \mathbf{A}[m]\|_2 < \epsilon_A \\ \textit{if} \quad &\sup_m \|\mathbf{T}[m+1] - \mathbf{T}[m]\|_2 < \epsilon_T < s_\epsilon\, \epsilon_A, \end{aligned} \tag{5.75}$$

*where the scaling factor $s_\epsilon$ is given by*

$$s_\epsilon = \frac{1}{4\rho(\bar{\mathbf{\Gamma}})\rho(\bar{\mathbf{K}})\sqrt{\mu}}, \tag{5.76}$$

$$\mu = (\beta/N)^2 + (\alpha\beta\delta_t + \beta/N)^2, \tag{5.77}$$

*$\alpha, \beta$ are DSR parameters, $\delta_t$ is the sampling time period and $\rho(\bar{\mathbf{\Gamma}})$ and $\rho(\bar{\mathbf{K}})$ are spectral radii of the constant gain matrix $\bar{\mathbf{\Gamma}}$ and the stiffness matrix $\bar{\mathbf{K}}$, respectively.*

*Proof:* The time variation of $\mathbf{A}[m]$ is, from Eqs. (5.47)-(5.49),

$$\begin{aligned} \Delta_{\mathbf{A}}[m] &= \mathbf{A}[m+1] - \mathbf{A}[m] \\ &= \begin{bmatrix} \mathbf{0} & \mathbf{0} & \dots & \mathbf{0} \\ \vdots & & \ddots & \vdots \\ \mathbf{0} & \dots & & \mathbf{0} \\ \Delta_{\mathbf{a}_1}[m] & \mathbf{0} & \dots & \Delta_{\mathbf{a}_2}[m] \end{bmatrix}, \end{aligned} \tag{5.78}$$

where $\Delta_{\mathbf{a}_i}[m] = \mathbf{a}_i[m+1] - \mathbf{a}_i[m]$, $i \in \{1, 2\}$. Moreover,

$$\begin{aligned} \|\Delta_{\mathbf{A}}[m]\|_2^2 &= \rho(\Delta_{\mathbf{A}}^{\intercal}[m]\Delta_{\mathbf{A}}[m]) \\ &= \rho(\Delta_{\mathbf{a}_1}^{\intercal}[m]\Delta_{\mathbf{a}_1}[m] + \Delta_{\mathbf{a}_2}^{\intercal}[m]\Delta_{\mathbf{a}_2}[m]) \\ &\le \rho(\Delta_{\mathbf{a}_1}^{\intercal}[m]\Delta_{\mathbf{a}_1}[m]) + \rho(\Delta_{\mathbf{a}_2}^{\intercal}[m]\Delta_{\mathbf{a}_2}[m]) \\ &= \|\Delta_{\mathbf{a}_1}[m]\|_2^2 + \|\Delta_{\mathbf{a}_2}[m]\|_2^2. \end{aligned} \tag{5.79}$$

Then, by Eq. (5.49) $\|\Delta_{\mathbf{A}}[m]\|_2^2$ can be rewritten as,

$$\begin{aligned}\|\Delta_{\mathbf{A}}[m]\|_2^2 \leq & \left\|\frac{\beta}{N}(\mathbf{\Gamma}[m+1]\mathbf{K}[m+1]-\mathbf{\Gamma}[m]\mathbf{K}[m])\right\|_2^2 \\ & + \Big\| - \alpha\beta\delta_t(\mathbf{\Gamma}[m+1]\mathbf{K}[m+1]-\mathbf{\Gamma}[m]\mathbf{K}[m]) \\ & - \frac{\beta}{N}(\mathbf{\Gamma}[m+1]\mathbf{K}[m+1]-\mathbf{\Gamma}[m]\mathbf{K}[m])\Big\|_2^2 \\ = & \ \mu\ \|\mathbf{\Gamma}[m+1]\mathbf{K}[m+1]-\mathbf{\Gamma}[m]\mathbf{K}[m]\|_2^2 \\ = & \ \mu\ \|\mathbf{\Gamma}[m+1](\mathbf{K}[m+1]-\mathbf{K}[m]) \\ & + (\mathbf{\Gamma}[m+1]-\mathbf{\Gamma}[m])\mathbf{K}[m]\|_2^2.\end{aligned} \tag{5.80}$$

Taking the square root on both sides of Eq. (5.80), using the triangle inequality and Eq. (5.54) results in

$$\begin{aligned}\|\Delta_{\mathbf{A}}[m]\|_2 \leq & \sqrt{\mu}\ \|\mathbf{\Gamma}[m+1]\|_2\|(\mathbf{K}[m+1]-\mathbf{K}[m])\|_2 \\ & + \sqrt{\mu}\ \|(\mathbf{\Gamma}[m+1]-\mathbf{\Gamma}[m])\|_2\|\mathbf{K}[m]\|_2 \\ \leq & \sqrt{\mu}\ \rho(\bar{\mathbf{\Gamma}})\|(\mathbf{K}[m+1]-\mathbf{K}[m])\|_2 \\ & + \sqrt{\mu}\ \|(\mathbf{\Gamma}[m+1]-\mathbf{\Gamma}[m])\|_2\rho(\bar{\mathbf{K}}).\end{aligned} \tag{5.81}$$

Using Eq. (5.37), the difference in the stiffness matrices becomes

$$\begin{aligned}\mathbf{K}[m+1]-\mathbf{K}[m] = & (\mathbf{T}[m+1]-\mathbf{T}[m])\bar{\mathbf{K}}\mathbf{T}^{-1}[m] \\ & + \mathbf{T}[m+1]\bar{\mathbf{K}}(\mathbf{T}^{-1}[m+1]-\mathbf{T}^{-1}[m]),\end{aligned} \tag{5.82}$$

and therefore, from Eqs. (5.52)-(5.54), and the triangle inequality,

$$\begin{aligned}& \|\mathbf{K}[m+1]-\mathbf{K}[m]\|_2 \\ & \leq \|(\mathbf{T}[m+1]-\mathbf{T}[m])\|_2\|\bar{\mathbf{K}}\|_2\|\mathbf{T}^{-1}[m]\|_2 \\ & \quad + \|\mathbf{T}[m+1]\|_2\|\bar{\mathbf{K}}\|_2\|(\mathbf{T}^{-1}[m+1]-\mathbf{T}^{-1}[m])\|_2 \\ & \leq \rho(\bar{\mathbf{K}})\|(\mathbf{T}[m+1]-\mathbf{T}[m])\|_2 \\ & \quad + \rho(\bar{\mathbf{K}})\|(\mathbf{T}^{-1}[m+1]-\mathbf{T}^{-1}[m])\|_2.\end{aligned} \tag{5.83}$$

Similarly,

$$\begin{aligned}\mathbf{\Gamma}[m+1]-\mathbf{\Gamma}[m] = & (\mathbf{T}[m+1]-\mathbf{T}[m])\bar{\mathbf{\Gamma}}\mathbf{T}^{-1}[m] \\ & + \mathbf{T}[m+1]\bar{\mathbf{\Gamma}}(\mathbf{T}^{-1}[m+1]-\mathbf{T}^{-1}[m]),\end{aligned} \tag{5.84}$$

and the norm of the difference is bounded as

$$\begin{aligned} &\|\mathbf{\Gamma}[m+1]-\mathbf{\Gamma}[m]\|_2 \\ &\quad\leq \rho(\bar{\mathbf{\Gamma}})\|(\mathbf{T}[m+1]-\mathbf{T}[m])\|_2 \\ &\qquad+\rho(\bar{\mathbf{\Gamma}})\|(\mathbf{T}^{-1}[m+1]-\mathbf{T}^{-1}[m])\|_2. \end{aligned} \tag{5.85}$$

If the change in orientation, represented by the change in the orthogonal transformation matrices $\mathbf{T}$, is bounded uniformly in time by $\epsilon_T > 0$, i.e.,

$$\|\mathbf{T}[m+1]-\mathbf{T}[m]\|_2 < \epsilon_T. \tag{5.86}$$

then the change in the inverse transformation also has the same bound, since

$$\begin{aligned} &\|\mathbf{T}^{-1}[m+1]-\mathbf{T}^{-1}[m]\|_2^2 \\ &\qquad=\|\mathbf{T}^{\intercal}[m+1]-\mathbf{T}^{\intercal}[m]\|_2^2 \\ &\qquad=\rho\left((\mathbf{T}[m+1]-\mathbf{T}[m])(\mathbf{T}^{\intercal}[m+1]-\mathbf{T}^{\intercal}[m])\right) \\ &\qquad=\rho\left((\mathbf{T}^{\intercal}[m+1]-\mathbf{T}^{\intercal}[m])(\mathbf{T}[m+1]-\mathbf{T}[m])\right) \\ &\qquad=\|\mathbf{T}[m+1]-\mathbf{T}[m]\|_2^2 < \epsilon_T^2. \end{aligned} \tag{5.87}$$

Therefore, the norms of the differences in stiffness matrix $\mathbf{K}$ from Eq. (5.83) and gain matrix $\mathbf{\Gamma}$ from Eq. (5.85) become

$$\begin{aligned} \|\mathbf{K}[m+1]-\mathbf{K}[m]\|_2 &\leq 2\epsilon_T\rho(\bar{\mathbf{K}}) \\ \|\mathbf{\Gamma}[m+1]-\mathbf{\Gamma}[m]\|_2 &\leq 2\epsilon_T\rho(\bar{\mathbf{\Gamma}}) \end{aligned} \tag{5.88}$$

and substitution into Eq. (5.81) yields

$$\|\Delta_{\mathbf{A}}[m]\|_2 \leq 4\sqrt{\mu}\;\rho(\bar{\mathbf{\Gamma}})\rho(\bar{\mathbf{K}})\epsilon_T \tag{5.89}$$

and the lemma follows since the right hand side of Eq. (5.89) satisfies

$$4\sqrt{\mu}\;\rho(\bar{\mathbf{\Gamma}})\rho(\bar{\mathbf{K}})\epsilon_T < \epsilon_A \tag{5.90}$$

from Eq. (5.76). ■

**Part 3 (Lyapunov stability):** Stability of the time-varying dynamics in Eq. (5.50) is established in the following lemma.

**Lemma 6 (Stability using the Lyapunov method)** *The origin of the time-varying system in Eq.* (5.50) *is exponentially stable if the following two conditions are satisfied.*

1. *DSR parameters* $(\alpha, \beta)$ *are chosen to satisfy conditions in either Lemma 3 Eq.* (5.58) *or Lemma 4 Eq.* (5.68) ,

2. *The orientation variation is sufficiently slow, i.e., there exists* $0 < \eta < 1$ *such that*

$$\sup_m \|\mathbf{T}[m+1] - \mathbf{T}[m]\|_2 < s_\epsilon \bar{\epsilon}_A, \tag{5.91}$$

*where*

$$\bar{\epsilon}_A = \frac{(1-(1-\epsilon)^2)^2}{2c^4 a_M}(1-\eta),$$

*constants* $c$ *and* $\epsilon$ *are from Eq.* (5.74)*,* $a_M$ *is the upper bound of matrix* $\mathbf{A}$ *in Eq.* (5.51)*,* $s_\epsilon = \frac{1}{4\rho(\bar{\mathbf{\Gamma}})\rho(\bar{\mathbf{K}})\sqrt{\mu}}$ *as in Eq.* (5.76)*,* $\mu$ *is defined in Eq.* (5.77) *and* $\rho(\bar{\mathbf{\Gamma}})$ *and* $\rho(\bar{\mathbf{K}})$ *are spectral radius of constant gain matrix* $\bar{\mathbf{\Gamma}}$ *and constant stiffness* $\bar{\mathbf{K}}$ *respectively.*

*Proof:* The proof follows from Ref. [51], which showed exponential stability of time-varying discrete-time systems as in Eq. (5.50), provided the following three conditions are satisfied.

(i) The dynamic matrix $\mathbf{A}[m]$ is uniformly bounded, i.e., $\sup_m \|\mathbf{A}[m]\|_2 = a_M < \infty$.

(ii) Eigenvalues of $\mathbf{A}[m]$ are inside a disc of radius $1-2\epsilon$ centered at the origin of the complex plane resulting in $\|(\mathbf{A}[m])^r\|_2 \leq c(1-\epsilon)^r$ as in Eq. (5.74).

(iii) The system is sufficiently slowly-time varying, i.e., there exist $0 < \eta < 1$ such that

$$\sup_m \|\mathbf{A}[m+1] - \mathbf{A}[m]\|_2 < \frac{(1-(1-\epsilon)^2)^2}{2c^4 a_M}(1-\eta) = \bar{\epsilon}_A.$$

Condition (i) is satisfied from Lemma 2 Eq. (5.51), and condition (ii) is satisfied due to Condition 1 of the current Lemma 6, as shown by Lemmas 3 and 4. Lastly, condition (iii) is

satisfied due to Condition 2 of the current Lemma 6, from Lemma 5 Eq. (5.75). Briefly, the proof in [51] establishes that the Lyapunov function

$$V_m(\mathbf{S}) = \mathbf{S}^\intercal \mathbf{P}_m \mathbf{S}, \tag{5.92}$$

where $\mathbf{P}_m$ is the positive definite solution to

$$\mathbf{A}^\intercal[m-1]\mathbf{P}_m\mathbf{A}[m-1] - \mathbf{P}_m = -\mathbf{I} \tag{5.93}$$

bounded by

$$1 \leq \|\mathbf{P}_m\|_2 \leq \frac{c^2}{1-(1-\epsilon)^2} \ = a_{\mathbf{P}} \ \ \forall m \tag{5.94}$$

resulting in

$$\|\mathbf{S}\|_2^2 \leq V_m(\mathbf{S}) \leq a_{\mathbf{P}} \|\mathbf{S}\|_2^2. \tag{5.95}$$

Moreover, under conditions (i)-(iii), the Lyapunov function can be shown to decrease with time step $m$ [51],

$$V_{m+1}(\mathbf{S}[m+1]) - V_m(\mathbf{S}[m]) \leq -\eta \|\mathbf{S}[m]\|_2^2 \ \ \forall m, \tag{5.96}$$

Using Eq. (5.95), Eq. (5.96) can be written as,

$$\begin{aligned} \|\mathbf{S}[m+1]\|_2^2 \leq V_{m+1}(\mathbf{S}[m+1]) &\leq V_m(\mathbf{S}[m]) - \eta\|\mathbf{S}[m]\|_2^2 \\ &\leq \left(1 - \frac{\eta}{a_{\mathbf{P}}}\right) V_m(\mathbf{S}[m]) \\ &\leq \left(1 - \frac{\eta}{a_{\mathbf{P}}}\right)^{m+1} V_0(\mathbf{S}[0]) \\ &\leq \left(1 - \frac{\eta}{a_{\mathbf{P}}}\right)^{m+1} a_{\mathbf{P}} \|\mathbf{S}[0]\|_2^2, \end{aligned} \tag{5.97}$$

and the right hand side tends to zero as $m$ increases since $0 < \frac{\eta}{a_{\mathbf{P}}} < 1$, leading to exponential stability. ■

*Small deformation for slow transport*

The previous subsection showed that the time-varying transport dynamics is stable. The associated Lyapunov function can be used to show that the transport dynamics in Eq. (5.49) is bounded-input bounded-output stable. Towards this, the lemma below shows that the perturbation $\mathbf{U}$ of the transport dynamics in Eq. (5.49) is bounded by the transport speed.

**Lemma 7 (U is bounded)** *The perturbation* $\mathbf{U}[m]$ *is uniformly bounded in* $m$ *as,*

$$\|\mathbf{U}[m]\|_2 \leq 2\ (\epsilon_T q_n + 6\epsilon_L) = a_{\mathbf{U}} \quad \forall\ m, \tag{5.98}$$

*given a bounded desired speed of transport, e.g.,*

$$\sup_m \|\Delta_{\mathbf{q}_d}[m]\|_2 = \sup_m \|\mathbf{q}_d[m] - \mathbf{q}_d[m-1]\|_2 \leq \epsilon_q, \tag{5.99}$$

*where*

$$\epsilon_L = (1-\gamma_L)\gamma_L \|\mathbf{q}_d[0] - \mathbf{q}_L[0]\|_2 + \epsilon_q, \tag{5.100}$$

$\gamma_L$ *is the leader update gain in Eq.* (5.1)*,* $\epsilon_T$ *is the upper bound on the rate of change of the transformation matrix* $\mathbf{T}$ *in Eq.* (5.75) *and* $q_n = \|\bar{\mathbf{Q}}_n\|_2$ *is a constant that depends on object's geometry and nominal robot configuration defined in Eq.* (5.30)*.*

*Proof:* In particular using Eq. (5.34), the perturbation term $\mathbf{U}$ in Eq. (5.49) can be rewritten as,

$$\begin{aligned}
\mathbf{U}[m] &= \mathbf{Q}_n[m] - \mathbf{Q}_n[m+1] + \frac{\mathbf{Q}_n[m] - \mathbf{Q}_n[m-N]}{N} \\
&= (\mathbf{T}[m] - \mathbf{T}[m+1])\bar{\mathbf{Q}}_n + \mathbf{B}_1(\mathbf{q}_L[m] - \mathbf{q}_L[m+1]) \\
&\quad + \frac{1}{N}\Big\{(\mathbf{T}[m] - \mathbf{T}[m-N])\bar{\mathbf{Q}}_n + \mathbf{B}_1(\mathbf{q}_L[m] \\
&\quad - \mathbf{q}_L[m-N])\Big\}.
\end{aligned}$$

Then, using the triangle inequality results in,

$$\begin{aligned}\|\mathbf{U}[m]\|_2 \leq \|\mathbf{T}[m] - \mathbf{T}[m+1]\|_2\|\bar{\mathbf{Q}}_n\|_2 \\ + \|\mathbf{B}_1\|_2\|\mathbf{q}_L[m] - \mathbf{q}_L[m+1]\|_2 \\ + \frac{1}{N}\Big\{\|\mathbf{T}[m] - \mathbf{T}[m-N]\|_2\|\bar{\mathbf{Q}}_n\|_2 \\ + \|\mathbf{B}_1\|_2\|\mathbf{q}_L[m] - \mathbf{q}_L[m-N]\|_2\Big\}.\end{aligned} \tag{5.101}$$

The variation of the leader robot's state $\mathbf{q}_L$ can be written using Eq. (5.1), as

$$\begin{aligned}(\mathbf{q}_L[m+1] - \mathbf{q}_L[m]) =& (1-\gamma_L)\left(\mathbf{q}_L[m] - \mathbf{q}_L[m-1]\right) \\ &+ \gamma_L\left(\mathbf{q}_d[m] - \mathbf{q}_d[m-1]\right) \\ =& (1-\gamma_L)^m\left(\mathbf{q}_L[1] - \mathbf{q}_L[0]\right) \\ &+ \gamma_L\sum_{i=0}^{m-1}(1-\gamma_L)^i\Delta_{\mathbf{q}_d}[m-i]\end{aligned} \tag{5.102}$$

with $\Delta_{\mathbf{q}_d}[i] = \mathbf{q}_d[i] - \mathbf{q}_d[i-1]$. Since the variation of desired trajectory is bounded from the condition in Eq. (5.99), and because $(1-\gamma_L) < 1$ resulting in $(1-\gamma_L)^m \leq (1-\gamma_L)$ for $m > 0$, the variation of the leader robot's state $\mathbf{q}_L$ can be bounded as

$$\begin{aligned}\|\mathbf{q}_L[m+1] - \mathbf{q}_L[m]\|_2 \leq& (1-\gamma_L)\|\mathbf{q}_L[1] - \mathbf{q}_L[0]\|_2 \\ &+ \gamma_L\left(\frac{\epsilon_q}{\gamma_L}\right) \\ =& (1-\gamma_L)\|\mathbf{q}_L[1] - \mathbf{q}_L[0]\|_2 + \epsilon_q \\ =& (1-\gamma_L)\gamma_L\|\mathbf{q}_d[0] - \mathbf{q}_L[0]\|_2 + \epsilon_q \\ & \text{using Eq. (5.1)} \\ =& \epsilon_L \quad \text{from Eq. (5.100).}\end{aligned} \tag{5.103}$$

This bound in the variation of the leader's state for a single time step in Eq. (5.103) can be used to bound the variation over $N$ time steps as $N$ times the variation over a single time

step, i.e.,

$$\begin{aligned}
&\|\mathbf{q}_L[m] - \mathbf{q}_L[m-N]\|_2 \\
&\quad = \|\mathbf{q}_L[m] - \mathbf{q}_L[m-1] + \mathbf{q}_L[m-1] + \ldots \\
&\qquad - \mathbf{q}_L[m-N+1] + \mathbf{q}_L[m-N+1] - \mathbf{q}_L[m-N]\|_2 \\
&\quad \leq N\epsilon_L.
\end{aligned} \tag{5.104}$$

Similarly, the variation of transformation matrix, i.e., $\|\mathbf{T}[m]-\mathbf{T}[m-N]\|_2$ over $N$ time steps can be bounded by $N$ times the variation over a single time step from Eq. (5.75), as

$$\begin{aligned}
&\|\mathbf{T}[m] - \mathbf{T}[m-N]\|_2 \\
&\quad = \|\mathbf{T}[m] - \mathbf{T}[m-1] + \mathbf{T}[m-1] + \ldots \\
&\qquad - \mathbf{T}[m-N+1] + \mathbf{T}[m-N+1] - \mathbf{T}[m-N]\|_2 \\
&\quad \leq N\epsilon_T.
\end{aligned} \tag{5.105}$$

Then, substituting the upper bounds established in Eqs. (5.103)-(5.105) and Eq. (5.75) into Eq. (5.101) and using $\|\mathbf{B}_1\|_2 = \sqrt{\rho(\mathbf{B}_1^\intercal \mathbf{B}_1)} = \bar{n}$ from Eq. (5.21) results in,

$$\begin{aligned}
\|\mathbf{U}[m]\|_2 &\leq \epsilon_T q_n + \bar{n}\epsilon_L + \frac{1}{N}\left(N\epsilon_T q_n + \bar{n}N\epsilon_L\right) \\
&= 2\left(\epsilon_T q_n + \bar{n}\epsilon_L\right) = a_{\mathbf{U}}. \qquad \blacksquare
\end{aligned} \tag{5.106}$$

**Remark 16 (Small perturbation)** *As the transport speed decreases, its bound* $\epsilon_q$ *in Eq.* (5.99) *decreases resulting in decreasing* $\epsilon_L$ *in Eq.* (5.100) *if the desired* $\mathbf{q}_d[0]$ *and actual* $\mathbf{q}_L[0]$ *leader positions match at the start of the transport, i.e.,* $\mathbf{q}_d[0] = \mathbf{q}_L[0]$. *Decreasing transport speed also leads to decreasing orientation changes and therefore, smaller* $\epsilon_T$ *in Eq.* (5.75). *Hence, the size* $a_{\mathbf{U}}$ *of the perturbation term* $\|\mathbf{U}[m]\|_2$ *decreases with decreasing transport speed from Eq.* (5.98).

Reducing the transport speed also reduces the deformation, as established in the next lemma using the Lyapunov approach.

**Lemma 8 (Effect of the perturbation)** *With undeformed initial configuration,* $\mathbf{S}[0] = \mathbf{0}$*, the deformation state* $\mathbf{S}$ *of the perturbed dynamics in Eq.* (5.47) *becomes small for small perturbation* $\mathbf{U}$*, i.e.,*

$$\|\mathbf{S}[m+1]\|_2 \to 0, \quad \textit{if} \quad a_{\mathbf{U}} \to 0 \quad \forall\, m, \tag{5.107}$$

*where* $\|\mathbf{U}[m]\| \leq a_{\mathbf{U}}$ *as in Eq.* (5.98)*.*

*Proof:* From Eq. (5.47) and the definition of the Lyapunov function $V_m$ in Eq. (5.92),

$$\begin{aligned}
&V_{m+1}(\mathbf{S}[m+1]) - V_m(\mathbf{S}[m]) \\
&\quad = \mathbf{S}^\intercal[m+1]\mathbf{P}_{m+1}\mathbf{S}[m+1] - \mathbf{S}^\intercal[m]\mathbf{P}_m\mathbf{S}[m] \\
&\quad = \mathbf{S}^\intercal[m]\Big(\mathbf{A}^\intercal[m]\mathbf{P}_{m+1}\mathbf{A}[m] - \mathbf{P}_m\Big)\mathbf{S}[m] \\
&\qquad + \mathbf{U}^\intercal[m]\mathbf{B}^\intercal\mathbf{P}_{m+1}\mathbf{A}[m]\mathbf{S}[m] \\
&\qquad + \mathbf{S}^\intercal[m]\mathbf{A}^\intercal[m]\mathbf{P}_{m+1}\mathbf{B}\mathbf{U}[m] \\
&\qquad + \mathbf{U}^\intercal[m]\mathbf{B}^\intercal\mathbf{P}_{m+1}\mathbf{B}\mathbf{U}[m] \\
&\quad \leq \ -\eta\|\mathbf{S}[m]\|_2^2 \\
&\qquad + \mathbf{U}^\intercal[m]\mathbf{B}^\intercal\mathbf{P}_{m+1}\mathbf{A}[m]\mathbf{S}[m] \\
&\qquad + \mathbf{S}^\intercal[m]\mathbf{A}^\intercal[m]\mathbf{P}_{m+1}\mathbf{B}\mathbf{U}[m] \\
&\qquad + \mathbf{U}^\intercal[m]\mathbf{B}^\intercal\mathbf{P}_{m+1}\mathbf{B}\mathbf{U}[m],
\end{aligned} \tag{5.108}$$

using Eq. (5.96), for the case when input is zero $\mathbf{U}[m] = \mathbf{0}$ for all $m$. From Eq. (5.49), $\|\mathbf{B}\|_2 = \sqrt{\rho(\mathbf{B}^\intercal\mathbf{B})} = 1$. Then, substituting the upper bounds of $\mathbf{A}$ in Eq. (5.51) and $\mathbf{P}_{m+1}$

in Eq. (5.94) into Eq. (5.108), and completing the square as in [52] results in,

$$\begin{aligned}
&V_{m+1}(\mathbf{S}[m+1]) - V_m(\mathbf{S}[m]) \\
&\leq -\eta\|\mathbf{S}[m]\|_2^2 + 2a_{\mathbf{P}}a_M\|\mathbf{U}[m]\|_2\|\mathbf{S}[m]\|_2 + a_{\mathbf{P}}\|\mathbf{U}[m]\|_2^2 \\
&= -\epsilon_\eta\eta\|\mathbf{S}[m]\|_2^2 + \hat{a}_{\mathbf{P}}\|\mathbf{U}[m]\|_2^2 \\
&\quad - \left(\sqrt{(1-\epsilon_\eta)w\eta}\|\mathbf{S}[m]\|_2 - \frac{a_{\mathbf{P}}a_M}{\sqrt{(1-\epsilon_\eta)\eta}}\|\mathbf{U}[m]\|_2\right)^2 \\
&\leq -\epsilon_\eta\eta\|\mathbf{S}[m]\|_2^2 + \hat{a}_{\mathbf{P}}\|\mathbf{U}[m]\|_2^2 \\
&\leq -\hat{\eta}V_m(\mathbf{S}[m]) + \hat{a}_{\mathbf{P}}\|\mathbf{U}[m]\|_2^2 \qquad \text{using Eq. (5.95)} \\
&\leq -\hat{\eta}V_m(\mathbf{S}[m]) + \hat{a}_{\mathbf{P}}a_{\mathbf{U}}^2 \qquad \text{using Eq. (5.98) ,}
\end{aligned} \tag{5.109}$$

where

$$\hat{\eta} = \epsilon_\eta\eta, \qquad \hat{a}_{\mathbf{P}} = \frac{(a_{\mathbf{P}}a_M)^2}{(1-\epsilon_\eta)\eta} + a_{\mathbf{P}}. \tag{5.110}$$

Rearranging the above equation, and iterating yields,

$$\begin{aligned}
V_{m+1}(\mathbf{S}[m+1]) &\leq (1-\hat{\eta})\, V_m(\mathbf{S}[m]) + \hat{a}_{\mathbf{P}}a_{\mathbf{U}}^2 \\
&= (1-\hat{\eta})^{m+1}\, V_0(\mathbf{S}[0]) \\
&\quad + \hat{a}_{\mathbf{P}}a_{\mathbf{U}}^2 \sum_{i=0}^{m} (1-\hat{\eta})^i\,,
\end{aligned} \tag{5.111}$$

which is a convergent series since $(1-\hat{\eta}) < 1$. Hence,

$$\begin{aligned}
\|\mathbf{S}[m+1]\|_2^2 &\leq V_{m+1}(\mathbf{S}[m+1]) \\
&\leq (1-\hat{\eta})^{m+1}\, V_0(\mathbf{S}[0]) + \frac{\hat{a}_{\mathbf{P}}a_{\mathbf{U}}^2}{\hat{\eta}} \\
&\leq (1-\hat{\eta})^{m+1}\, a_{\mathbf{P}}\|\mathbf{S}[0]\|_2^2 + \frac{\hat{a}_{\mathbf{P}}a_{\mathbf{U}}^2}{\hat{\eta}}.
\end{aligned} \tag{5.112}$$

The bound on deformation $\mathbf{S}$ directly depends on the bound $a_{\mathbf{U}}$ on the perturbation term when the initial deformation is zero, $\mathbf{S}[0] = \mathbf{0}$, i.e.,

$$\|\mathbf{S}[m+1]\|_2^2 \leq \frac{\hat{a}_{\mathbf{P}}a_{\mathbf{U}}^2}{\hat{\eta}}. \tag{5.113}$$

Therefore,

$$\|\mathbf{S}[m+1]\|_2 \to 0, \quad \text{as} \quad a_{\mathbf{U}} \to 0, \tag{5.114}$$

which leads to the claim of the lemma. ■

### *5.2.5 Special case: diagonalizable dynamics*

Although more general, the slowly-time-varying Lyapunov-based approach for stability can be conservative. A less conservative condition that only requires frozen-time stability is established below by exploiting the orientation change aspect of the time variations when the dynamics in Eq. (5.50) is diagonalizable.

**Lemma 9 (Bounded-perturbation bounded-deformation)** *Let the constant matrix* $\bar{\mathbf{A}}$ *be diagonalizable, where*

$$\bar{\mathbf{A}} = \begin{bmatrix} \mathbf{0} & \mathbf{I} & \dots & \mathbf{0} \\ \vdots & & \ddots & \vdots \\ \mathbf{0} & \dots & & \mathbf{I} \\ \bar{\mathbf{a}}_1 & \mathbf{0} & \dots & \bar{\mathbf{a}}_2 \end{bmatrix} \tag{5.115}$$

*similar to Eq.* (5.48)*, with*

$$\begin{aligned} \bar{\mathbf{a}}_1 &= -\frac{(\mathbf{I} - \beta\bar{\mathbf{\Gamma}}\bar{\mathbf{K}})}{N}, \\ \bar{\mathbf{a}}_2 &= (\mathbf{I} - \alpha\beta\delta_t\bar{\mathbf{\Gamma}}\bar{\mathbf{K}}) + \frac{\mathbf{I} - \beta\bar{\mathbf{\Gamma}}\bar{\mathbf{K}}}{N}. \end{aligned} \tag{5.116}$$

*Then, if the spectral radius* $\rho(\bar{\mathbf{A}}) < 1$*, the time-varying dynamics in Eq.* (5.47) *is bounded-perturbation bounded-deformation stable, i.e.,*

$$\|\mathbf{S}[m+1]\|_2 \leq \rho(\bar{\mathbf{A}})^m \|\mathbf{S}[1]\|_2 + \frac{a_{\mathbf{U}}}{1 - \rho(\bar{\mathbf{A}})}, \tag{5.117}$$

*where the perturbation is bounded,* $\|\mathbf{U}[m]\|_2 \leq a_{\mathbf{U}}$*, as in Eq.* (5.98)*.*

*Proof:* The dynamic matrix $\mathbf{A}[m]$ in Eq. (5.50) only varies due to change in unitary transformation matrix $\mathbf{T}[m]$, since from Eq. (5.37),

$$\mathbf{A}[m] = \mathbf{T}_a[m]\bar{\mathbf{A}}\mathbf{T}_a^{-1}[m], \tag{5.118}$$

where $\mathbf{T}_a$ is unitary

$$\begin{aligned}\mathbf{T}_a[m] &= \left(\mathbf{I}_{(N+1)\times(N+1)} \otimes \mathbf{T}[m]\right), \\ \mathbf{T}_a^{-1}[m] &= \left(\mathbf{I}_{(N+1)\times(N+1)} \otimes \mathbf{T}^{-1}[m]\right),\end{aligned} \tag{5.119}$$

with

$$\|\mathbf{T}_a[m]\|_2 = \|\mathbf{T}_a^{-1}[m]\|_2 = 1. \tag{5.120}$$

Moreover, since the constant matrix $\bar{\mathbf{A}}$ is diagonalizable, there exists a constant unitary matrix $\mathbf{V}$ such that $\mathbf{V}^{-1} = \mathbf{V}^{\intercal}$,

$$\|\mathbf{V}[m]\|_2 = \|\mathbf{V}^{-1}[m]\|_2 = 1 \tag{5.121}$$

and

$$\bar{\mathbf{A}} = \mathbf{V}\bar{\mathbf{A}}_J\mathbf{V}^{-1}, \tag{5.122}$$

where $\bar{\mathbf{A}}_J$ is a diagonal matrix which entries consist of eigenvalues $\lambda_{\bar{\mathbf{A}},j}$, $j \in \{1, 2, \ldots, \bar{n}n(N+1)\}$ of the constant dynamic matrix $\bar{\mathbf{A}}$. The spectral radius $\rho(\bar{\mathbf{A}}_J) < 1$ from the lemma condition that the spectral radius $\rho(\bar{\mathbf{A}}) < 1$ resulting in

$$\|\bar{\mathbf{A}}_J\|_2 = \rho(\bar{\mathbf{A}}_J) = \rho(\bar{\mathbf{A}}). \tag{5.123}$$

The update equation in Eq. (5.47) can be rewritten using the transformation in Eq. (5.118) and the Jordan matrix in Eq. (5.122) as

$$\mathbf{S}[m+1] = \mathbf{T}_a[m]\mathbf{V}\bar{\mathbf{A}}_J\mathbf{V}^{-1}\mathbf{T}_a^{-1}[m]\mathbf{S}[m] + \mathbf{U}[m]. \tag{5.124}$$

Then, taking Euclidean norm on both sides of Eq. (5.124), and using the triangle inequality,

results in,

$$
\begin{aligned}
&\|\mathbf{S}[m+1]\|_2 \\
&\quad \leq \|\mathbf{T}_a[m]\mathbf{V}\bar{\mathbf{A}}_J\mathbf{V}^{-1}\mathbf{T}_a^{-1}[m]\mathbf{S}[m]\|_2 + \|\mathbf{U}[m]\|_2 \\
&\quad \leq \|\mathbf{T}_a[m]\|_2\|\mathbf{V}\|_2\|\bar{\mathbf{A}}_J\|_2\|\mathbf{V}^{-1}\|_2\|\mathbf{T}_a^{-1}[m]\|_2\|\mathbf{S}[m]\|_2 \\
&\qquad + \|\mathbf{U}[m]\|_2 \\
&\quad \leq \|\bar{\mathbf{A}}_J\|_2 \ \|\mathbf{S}[m]\|_2 \ + \|\mathbf{U}[m]\|_2 \\
&\qquad \text{using Eqs. (5.120), (5.121), (5.123)} \\
&\quad \leq \rho(\bar{\mathbf{A}}) \ \|\mathbf{S}[m]\|_2 \ + a_{\mathbf{U}} \\
&\qquad \text{using Eqs. (5.98), (5.123)} \\
&\quad \leq \rho(\bar{\mathbf{A}})^m \ \|\mathbf{S}[1]\|_2 \ + \sum_{j=0}^{m-1} \rho(\bar{\mathbf{A}})^j a_{\mathbf{U}} \\
&\leq \rho(\bar{\mathbf{A}})^m \|\mathbf{S}[1]\|_2 + \frac{a_{\mathbf{U}}}{1-\rho(\bar{\mathbf{A}})} \\
&\qquad \text{since } \rho(\bar{\mathbf{A}}) < 1 \ ,
\end{aligned}
\tag{5.125}
$$

which is the lemma's claim. ■

**Remark 17 (Stability)** *The spectral radius $\rho(\mathbf{A}[m])$ of the time-varying matrix $\mathbf{A}[m]$ is the same as the spectral radius $\rho(\bar{\mathbf{A}})$ of the constant matrix $\bar{\mathbf{A}}$ and therefore, frozen-time stability $\rho(\mathbf{A}[m]) < 1$ is sufficient for stability of the time-varying transport dynamics if the matrix $\bar{\mathbf{A}}$ is diagonalizable, from Lemma 9.*

The stiffness matrix $\bar{\mathbf{K}}$ is typically real and symmetric, and hence, diagonalizable. Moreover, the stiffness matrix $\bar{\mathbf{K}}$ is invertible (with non-zero eigenvalues) when the structure is held rigidly by the leader. Therefore, a constant diagonal gain in $\bar{\mathbf{\Gamma}}$ for each diagonal block of the stiffness matrix $\bar{\mathbf{K}}$ results in a real symmetric and invertible matrix $\bar{\mathbf{L}} = \bar{\mathbf{\Gamma}}\bar{\mathbf{K}}$, which is diagonalizable. The following lemma shows that the resulting matrix $\bar{\mathbf{A}}$ in Eq. (5.115) is diagonalizable with a unit time-step delay $N = 1$, leading to the less conservative condition in Lemma 9.

**Lemma 10 (Diagonalizable $\bar{\mathbf{A}}$)** *The constant matrix* $\bar{\mathbf{A}}$ *in Eq.* (5.115) *for unit time-step delay* $N = 1$*, given as,*

$$\bar{\mathbf{A}} = \begin{bmatrix} \mathbf{0} & \mathbf{I} \\ \bar{\mathbf{a}}_1 & \bar{\mathbf{a}}_2 \end{bmatrix}, \tag{5.126}$$

*is diagonalizable if the matrix* $\bar{\mathbf{L}} = \bar{\mathbf{\Gamma}}\bar{\mathbf{K}}$ *is invertible (with non-zero eigenvalues) and diagonalizable, where, from Eq.* (5.116)*,* $\bar{\mathbf{a}}_1 = -(\mathbf{I} - \beta\bar{\mathbf{L}})$ *and* $\bar{\mathbf{a}}_2 = (\mathbf{I} - \alpha\beta\delta_t\bar{\mathbf{L}}) + \mathbf{I} - \beta\bar{\mathbf{L}}$*.*

**Proof:** Since $\bar{\mathbf{L}}$ is diagonalizable, it has $\bar{n}n^*$ linearly-independent eigenvectors $V_{L,i}$ with eigenvalues $\lambda_{L,i}$ with $i = 1, 2, \ldots, \bar{n}n^*$. For each eigenvalue $\lambda_{L,i}$, there exists two eigenvalues $\lambda_{\bar{\mathbf{A}},i,j},\ j = 1, 2$ of the matrix $\bar{\mathbf{A}}$ with corresponding eigenvectors

$$V_{\bar{\mathbf{A}},i,j} \ = \begin{bmatrix} V_{L,i} \\ \lambda_{\bar{\mathbf{A}},i,j} V_{L,i} \end{bmatrix}, \tag{5.127}$$

if

$$\begin{bmatrix} \mathbf{0} & \mathbf{I} \\ \bar{\mathbf{a}}_1 & \bar{\mathbf{a}}_2 \end{bmatrix} \begin{bmatrix} V_{L,i} \\ \lambda_{\bar{\mathbf{A}},i,j} V_{L,i} \end{bmatrix} = \lambda_{\bar{\mathbf{A}},i,j} \begin{bmatrix} V_{L,i} \\ \lambda_{\bar{\mathbf{A}},i,j} V_{L,i} \end{bmatrix}. \tag{5.128}$$

Since the first set of $\bar{n}n^*$ equations are satisfied, the remaining equations can be rewritten using Eq. (5.116) as

$$\begin{aligned} &-(\mathbf{I} - \beta\bar{\mathbf{L}})V_{L,i} + \\ &\lambda_{\bar{\mathbf{A}},i,j} \left( (\mathbf{I} - \alpha\beta\delta_t\bar{\mathbf{L}}) + \mathbf{I} - \beta\bar{\mathbf{L}} \right) V_{L,i} \ = \lambda^2_{\bar{\mathbf{A}},i,j} V_{L,i}, \end{aligned} \tag{5.129}$$

which is equivalent to (since $V_{L,i}$ is an eigenvalue of $\bar{\mathbf{L}}$ with eigenvalue $\lambda_{L,i}$)

$$\begin{aligned} -(1 - \beta\lambda_{L,i}) + \lambda_{\bar{\mathbf{A}},i,j} \left( (1 - \alpha\beta\delta_t\lambda_{L,i}) + 1 - \beta\lambda_{L,i} \right) \\ = \lambda^2_{\bar{\mathbf{A}},i,j}. \end{aligned} \tag{5.130}$$

and is satisfied with eigenvalues $\lambda_{\bar{\mathbf{A}},i,j},\ j = 1, 2$ of the matrix $\bar{\mathbf{A}}$

$$\lambda_{\bar{\mathbf{A}},i,j} = \frac{\bar{a}_2^* \pm \sqrt{(\bar{a}_2^*)^2 + 4\beta\lambda_{L,i}}}{2} \tag{5.131}$$

$\bar{a}_2^* = (2 - \beta\lambda_{L,i}(\alpha\delta_t + 1))$. Note that the resulting eigenvalues $\lambda_{\bar{\mathbf{A}},i,j},\ j = 1, 2$ are real and distinct, i.e.,

$$\lambda_{\bar{\mathbf{A}},i,1} \neq \lambda_{\bar{\mathbf{A}},i,2}, \tag{5.132}$$

since eigenvalue $\lambda_{L,i} > 0$ and DSR gain $\beta > 0$ are both positive. If the eigenvectors of the matrix $\bar{\mathbf{A}}$ are linearly dependent then there exists constants $c_{i,j}$ such that

$$\sum_i c_{i,1} V_{\bar{\mathbf{A}},i,1} + \sum_i c_{i,2} V_{\bar{\mathbf{A}},i,2} = 0, \tag{5.133}$$

which can be rewritten using Eq. (5.127) as

$$\sum_i c_{i,1} V_{L,i} + \sum_i c_{i,2} V_{L,i} = 0 \tag{5.134}$$

$$\sum_i \lambda_{\bar{\mathbf{A}},i,1} c_{i,1} V_{L,i} + \sum_i \lambda_{\bar{\mathbf{A}},i,2} c_{i,2} V_{L,i} = 0 \tag{5.135}$$

Since eigenvectors $V_{L,i}$ of $\bar{\mathbf{L}}$ are linearly independent, Eq. (5.135) requires

$$c_{i,2} = -c_{i,1} \tag{5.136}$$

$$\lambda_{\bar{\mathbf{A}},i,1} c_{i,1} = -\lambda_{\bar{\mathbf{A}},i,2} c_{i,2} \tag{5.137}$$

resulting in (by substituting for $c_{i,2}$ into the second equation)

$$\lambda_{\bar{\mathbf{A}},i,1} c_{i,1} = \lambda_{\bar{\mathbf{A}},i,2} c_{i,1} \quad \text{or} \quad \lambda_{\bar{\mathbf{A}},i,1} = \lambda_{\bar{\mathbf{A}},i,2}, \tag{5.138}$$

which is not possible from Eq. (5.132). Therefore, the eigenvectors of matrix $\bar{\mathbf{A}}$ are linearly independent resulting in diagonalizability. ■

### *5.2.6 Stability without the DSR approach*

The standard transport dynamics without DSR in Eq. (5.35) has a similar time-varying form as the DSR dynamics in Eq. (5.47). Therefore, the stability of the standard without DSR approach in Eq. (5.35) can be established using the same approach as the case with DSR

described in the previous subsection. In particular, the main parameter (the control gain $\gamma$ in Eq. (5.2)) can be selected for frozen-time stability of the dynamics without the DSR approach as in Eq. (5.35) by ensuring that the eigenvalues of matrix $\mathbf{H}[m]$ are inside the disc with radius $1-2\epsilon$, i.e., from Eq. (5.36),

$$|1-\lambda_{\mathbf{L},k}| < (1-2\epsilon) \quad \text{for } k = 1, 2, \ldots, 6n, \tag{5.139}$$

where $\lambda_{\mathbf{L},k}$ is the $k^{th}$-eigenvalue of matrix $\bar{\mathbf{L}} = \bar{\mathbf{\Gamma}}\bar{\mathbf{K}}$. Since this condition needs to be satisfied for all eigenvalues of matrix $\bar{\mathbf{L}}$,

$$\underline{\gamma} = \frac{2\epsilon}{\underline{\lambda}_{\mathbf{L}}} < \gamma < \frac{2(1-\epsilon)}{\bar{\lambda}_{\mathbf{L}}} = \overline{\gamma}, \tag{5.140}$$

where $\underline{\lambda}_{\mathbf{L}}$ and $\bar{\lambda}_{\mathbf{L}}$ are the smallest and the largest eigenvalue of matrix $\bar{\mathbf{L}} = \bar{\mathbf{\Gamma}}\bar{\mathbf{K}}$ respectively, and $0 < \epsilon < 0.5$ is a constant. The settling time $T_s$ to reach a new desired position depends on the update gain $\gamma$ and the eigenvalue of matrix $\mathbf{L}$, which can be computed as

$$T_s \approx \frac{-4\delta_t}{ln(\lambda^*_{\mathbf{L}})} \quad \text{where} \quad \lambda^*_{\mathbf{L}} = \arg\max_{\mathbf{L},j} |1-\gamma\lambda_{\mathbf{L},j}|. \tag{5.141}$$

### *5.2.7 Selection of controller gains and algorithm*

The steps for selection of gains $(\alpha, \beta)$ in the DSR approach for a given desired trajectory $(\mathbf{q}_d)$ and transport time (given using settling time $T_s$) for an object transport task are provided in Algorithm 1.

## *5.3 Experiment Setup*

Experiments are used to comparatively evaluate the transport improvement with and without the use of DSR. In particular, experiments were performed for planar transport, with 2DOF ($\bar{n} = 2$), with and without DSR for three transport scenarios; (i) Case 1: translational transport along a straight-line trajectory of a linear object using mobile robots; (ii) Case 2: rotational transport along a curved-line trajectory of a linear object using mobile robots; and (iii) Case 3: circular transport of a cylindrical object using robotic manipulators.

**Algorithm 1** DSR algorithm for object transport

**Require:** Place robots in the initial configuration and tare the force values

**Initialize:**
Set sampling period $\delta_t$ and time-step delay $N$
Set desired transport trajectory for leader $\mathbf{q}_d$
Select update gain for the leader $\gamma_L$ in Eq. (5.1)
*—– Finding eigenvalues —–*
**for** $s \in \{x, y, z, \theta_x, \theta_y, \theta_z\}$ **do**
    Tare force sensors
    **for** $i \in \{1, 2, \ldots, n^*\}$ **do**
        Move robot $i$ by $\Delta\bar{p}_{s,i}$
        Record: $\bar{f}_{s,i}$
        Compute $\bar{k}_{s,i} = \frac{\bar{f}_{s,i}}{\Delta\bar{p}_{s,i}}$ and populate matrix $\bar{\mathbf{K}}$
    **end for**
**end for**
Compute eigenvalues of normalized stiffness $\bar{\mathbf{L}} = \bar{\mathbf{\Gamma}}\bar{\mathbf{K}}$
*—– Gain selection without DSR —–*
Select gain $\gamma$ satisfying bounds ($\underline{\gamma}$ and $\bar{\gamma}$) as in Eq. (5.140)
Estimate settling time $T_s$ experimentally, or compute using Eq. (5.141)
*—– Gain selection with DSR —–*
Compute update gain $\alpha = 4/T_s$
**if** time-step delay $N = 1$ **then**
    select DSR gain $\beta$ using Eq. (5.58)
**else**
    using Eq. (5.68)
**end if**
Select transport time $T$ (satisfying Eq. (5.91) if $\bar{\mathbf{L}}$ is not diagonalizable)
*—– Update for leaders and followers —–*
**for** $m \in \{1, 2, \ldots, T\}$ **do**
    Record: $\mathbf{q}_L[m]$
    Compute $\mathbf{q}_L[m+1]$ based on Eq. (5.1)
    **for** $i \in \{1, 2, \ldots, n^*\}$ **do**
        Store: $\mathbf{q}_i[m-1]$ and $\mathbf{f}_i[m-1]$
        Record: $\mathbf{q}_i[m]$ and $\mathbf{f}_i[m]$
        Compute $\mathbf{q}_i[m+1]$ using Eq. (5.44)
    **end for**
**end for**

### *5.3.1 Hardware description*

The mobile-robots system consists of four custom-built mobile robots carrying a highly-flexible spring, which helps to visualize the deformation during transport of flexible objects as shown in Fig. 5.2. Each robot $k$ is equipped with wheel encoders to measure its position $\hat{\mathbf{p}}_k = [\hat{p}_{x,k}, \hat{p}_{y,k}]^\intercal \in \mathbb{R}^2$ and orientation $\bar{\theta}_{z,k} \in \mathbb{R}$, a custom 2-axis force sensor to measure local reactions $\hat{\mathbf{f}}_k$, and a microcontroller for on-board computations. All sensor measurements are filtered using first-order low pass filter to avoid high frequency noise. Each robot also has LEDs to indicate large forces due to relative deformations of the object. The leader robot has an additional microcontroller with a Bluetooth module to enable human remote-control using a joystick. The flexible object (a coiled spring with $1.30cm$ diameter and $90cm$ length) is mechanically grasped by each robot. The desired trajectory $\mathbf{q}_d = [\mathbf{p}_d, \Theta_d]^\intercal \in \mathbb{R}^3$ is available only to the leader robot and the position updates are computed and achieved within a sampling time period $\delta_t = 0.03s$, using a velocity feedback control similarly as shown in [2].

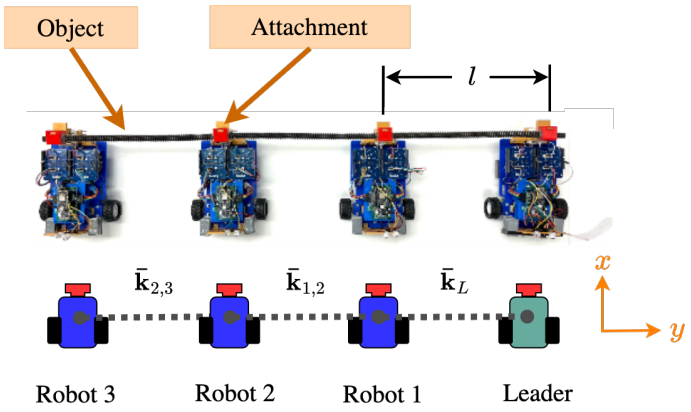


Figure 5.2: Experimental mobile-robots system carrying a flexible object. The length of each segment (element) of the spring between the robots is $l$. Each robot implicitly communicates with its neighbors through the object by sensing the force measured at the contact point.

The robotic-manipulators system consists of four ABB IRB 120 robots, consisting of one leader robot and three follower robots, carrying a circular flexible object made of UHMW plastic with thickness of $6.35mm$ and diameter of $610mm$ as shown in Fig. 5.3a. Each of the

follower robots is equipped with an ATI Mini 45 F/T sensor mounted near the end-effector to measure local forces $\bar{\mathbf{f}}_k$ between the robot and the object as shown in Fig. 5.3b. The force readings from the sensors are filtered using built-in first order low pass filters before being collected in a Python client, which is set up in a master PC. Individual socket communication channels between each follower ABB robot's controller and the Python client on PC are set up, to obtain state feedback of the robot end-effector position ($\bar{\mathbf{p}}_k = [\bar{p}_{x,k}, \bar{p}_{y,k}]^\intercal \in \mathbb{R}^2$), and communicate the corrective motion based on with and without DSR algorithms back to the robots. A communication channel also exists between the leader robot and the Python client to communicate desired trajectory to the leader robot. The computation is performed within a sampling time period of $\delta_t = 0.4s$.

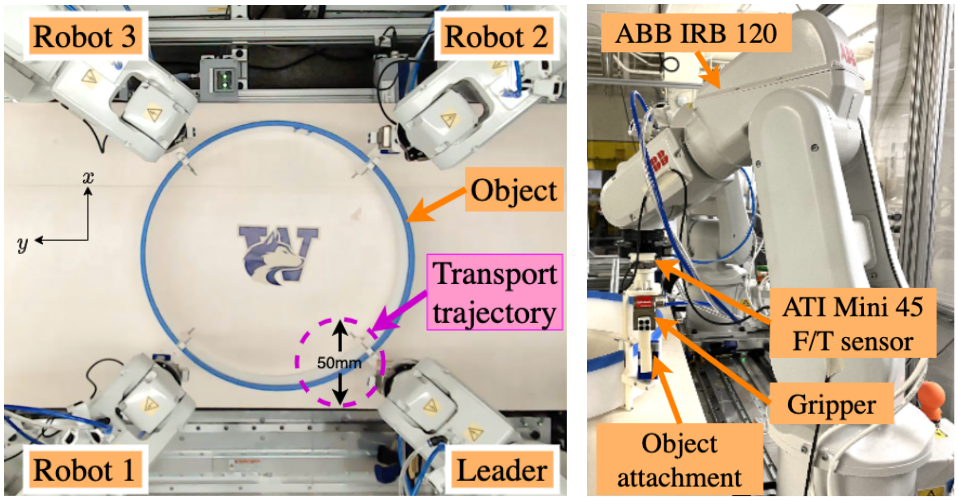


(a) System setup (b) Robot detail

Figure 5.3: Experimental robotic-manipulators system. (a) ABB IRB 120 robots transport a circular object (UHMW plastic) in a circular motion with $50mm$ diameter shown in pink dash-line. (b) Details of manipulator's end-effector with an ATI Mini 45 Force/Torque sensor attached.

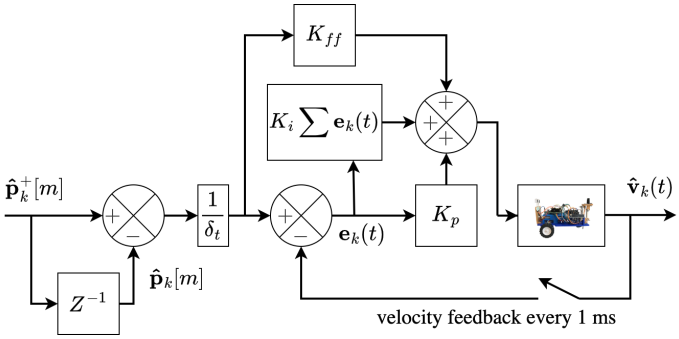


Figure 5.4: Velocity-based feedback control system of robot k to achieve the position $\hat{\mathbf{p}}_k^+[m]$ using proportional (gain $K_p$) and integral (gain $K_i$) feedback controller along with feed-forward control (gain $K_{ff}$).

### *5.3.2 Update parameters selection and implementation*

Algorithm 1 was used to select the control parameters with and without DSR. To begin, the normalized stiffness matrix $\bar{\mathbf{L}}$ was found. The estimated stiffness of the mobile-robots system shown in Fig. 5.2 has the decoupled form

$$\begin{bmatrix} \bar{\mathbf{F}}_x \\ \bar{\mathbf{F}}_y \end{bmatrix} = \begin{bmatrix} \bar{\mathbf{K}}_{x,x} & \mathbf{0} \\ \mathbf{0} & \bar{\mathbf{K}}_{y,y} \end{bmatrix} \begin{bmatrix} \bar{\mathbf{D}}_x \\ \bar{\mathbf{D}}_y \end{bmatrix} = \bar{\mathbf{K}}\bar{\mathbf{D}}. \tag{5.142}$$

where, $\bar{\mathbf{F}}_i = [\bar{f}_{i,1}, \bar{f}_{i,2}, \bar{f}_{i,3}]$ and $\bar{\mathbf{D}}_i = [\bar{d}_{i,1}, \bar{d}_{i,2}, \bar{d}_{i,3}]$ with $i \in \{x, y\}$. Then, the gain matrix $\bar{\mathbf{\Gamma}}$ in Eq. (5.15) was selected to normalize the stiffness matrix $\bar{\mathbf{K}}$, as

$$\bar{\mathbf{\Gamma}} = \begin{bmatrix} \bar{\mathbf{\Gamma}}_x & \mathbf{0} \\ \mathbf{0} & \bar{\mathbf{\Gamma}}_y \end{bmatrix} = \begin{bmatrix} \mathbf{I} & \mathbf{0} \\ \mathbf{0} & 0.075\,\mathbf{I} \end{bmatrix} \quad \in \mathbb{R}^6, \tag{5.143}$$

since the position update gain in the $\bar{y}$ direction is an order of magnitude smaller (due to higher stiffness) than the $\bar{x}$ direction in the leader's coordinate frame. This leads to the normalized stiffness matrix $\bar{\mathbf{L}} = \bar{\mathbf{\Gamma}}\bar{\mathbf{K}}$ in the algorithm.

For the experiment using the robotic-manipulators system shown in Fig. 5.3, the estimated stiffness matrix, found using Algorithm 1, has a more general coupled stiffness

$$\begin{bmatrix} \bar{\mathbf{F}}_x \\ \bar{\mathbf{F}}_y \end{bmatrix} = \begin{bmatrix} \bar{\mathbf{K}}_{x,x} & \bar{\mathbf{K}}_{x,y} \\ \bar{\mathbf{K}}_{y,x} & \bar{\mathbf{K}}_{y,y} \end{bmatrix} \begin{bmatrix} \bar{\mathbf{D}}_x \\ \bar{\mathbf{D}}_y \end{bmatrix} = \bar{\mathbf{K}}\bar{\mathbf{D}}. \tag{5.144}$$

Since the stiffness matrix $\bar{\mathbf{K}}$ in Eq. (5.144) has a coupled form, the gain matrix was selected to be identity $\bar{\mathbf{\Gamma}} = \mathbf{I}$ resulting in normalized stiffness $\bar{\mathbf{L}} = \bar{\mathbf{K}}$.

The normalized stiffness $\bar{\mathbf{L}}$ leads to the control parameters as described in the Algorithm 1. Specifically, the eigenvalues of the normalizing estimated stiffness matrix $\bar{\mathbf{L}}$ in Eq. (5.142) for the mobile-robots system and in Eq. (5.144) for the robotic-manipulators system are computed to establish bounds on update gain $\gamma$ using Eq. (5.140), and DSR parameters $\alpha, \beta$ as in Eq. (5.58). In each case the normalized stiffness is diagonalizable, and therefore, satisfies the conditions of Lemma 10 for frozen-time stability as in Remark 17. The selected gains with and without DSR approaches for both experimental systems, mobile-robots and robotic-manipulators, are shown in Table 5.1.

The decentralized updates with DSR were implemented in each follower robot $k$ with one delay step, i.e., $N = 1$. For the robotic-manipulators system, the decentralized update was implemented in the global coordinates as in Eq. (5.44). For the mobile-robots system (without access to the global frame) the DSR update in Eq. (5.44) was implemented using measurements in the local frame as,

$$\begin{aligned}\hat{\mathbf{q}}_k[m+1] =& \hat{\mathbf{q}}_k[m] - \alpha\beta\delta_t\hat{\mathbf{\Gamma}}_k\hat{\mathbf{f}}_k[m] + \{\hat{\mathbf{q}}_k[m] - \hat{\mathbf{q}}_k[m-1]\} \\ & - \beta\hat{\mathbf{\Gamma}}_k\left\{\hat{\mathbf{f}}_k[m] - \hat{\mathbf{f}}_k[m-1]\right\}.\end{aligned} \tag{5.145}$$

### *5.3.3 Evaluation metric*

*Maximum deformation*

The performance metric, used to quantify the results for both the approaches is the maximum deformation $D^*$ found using local reaction force measurements $\bar{\mathbf{F}}$ in the leader robot's coordinate frame $(\bar{x}, \bar{y}, \bar{z})$, i.e., from Eq. (5.142), and Eq. (5.144),

$$\bar{\mathbf{D}}[m] = \bar{\mathbf{K}}^{-1}\,\bar{\mathbf{F}}[m], \tag{5.146}$$

is the deformation at each follower robot at time step $m$. Then, the maximum deformation $D^*$ is computed by taking the Euclidean norm of deformation values of each robot along each

Table 5.1: Selection of parameters with and without DSR approaches, for all cases of experiment using mobile robots and robotic manipulators. The parameters are selected following Algorithm 1.

| **Case** | $\overline{\lambda}_{\mathbf{L}}$ | $\underline{\lambda}_{\mathbf{L}}$ | $\delta_t(s)$ | $\gamma_L$ | $\underline{\gamma}$ | $\overline{\gamma}$ | $\gamma$ | $T_s(s)$ | $\alpha$ | $\overline{\beta}$ | $\beta$ |
|---|---|---|---|---|---|---|---|---|---|---|---|
| Cases 1 & 2 | 0.16 | 0.01 | 0.03 | 0.90 | 2.00 | 12.38 | 2.38 | 5.00 | 0.80 | 12.23 | 10.65 |
| Case 3 | 0.79 | 0.007 | 0.40 | 1.00 | 0.11 | 2.53 | 0.15 | 224.8 | 0.017 | 2.18 | 2.00 |

axis, and finding the maximum value for all time $m$ among all the three follower robots, i.e.,

$$\begin{aligned} D^* &= \max_{k\in\{1,2,3\}} \left\{ \bar{\mathbf{d}}_M = \max_m \|\bar{\mathbf{d}}_k[m]\|_2 \right\}, \\ &\text{where} \quad \bar{\mathbf{d}}_k[m] = \begin{bmatrix} \bar{d}_{x,k}[m] & \bar{d}_{y,k}[m] \end{bmatrix}^{\mathsf{T}}. \end{aligned} \tag{5.147}$$

*Maximum Force*

Direct measurements of the local force at each robot is used as another metric, given by

$$\begin{aligned} f^* &= \max_{k\in\{1,2,3\}} \left\{ \bar{\mathbf{f}}_M = \max_m \|\bar{\mathbf{f}}_k[m]\|_2 \right\}, \\ &\text{where} \quad \bar{\mathbf{f}}_k[m] = \begin{bmatrix} \bar{f}_{x,k}[m] & \bar{f}_{y,k}[m] \end{bmatrix}^{\mathsf{T}}. \end{aligned} \tag{5.148}$$

### *5.3.4 Design of transport trajectories*

Two different types of transport are considered for the mobile-robots system: (i) pure translation without orientation change and (ii) rotational transport with orientation change as shown in Fig. 5.5. The robotic-manipulators system followed a circular trajectory as shown in Fig. 5.3a.

*Straight-line trajectory (pure translation)*

The leader robot follows a predefined straight trajectory of $50cm$ in the $x-$direction as shown in Fig. 5.5a with constant speed. The straight trajectory (orientation alignment of the leader) is achieved using a guiding track, highlighted in Fig. 5.5a. The track helps to

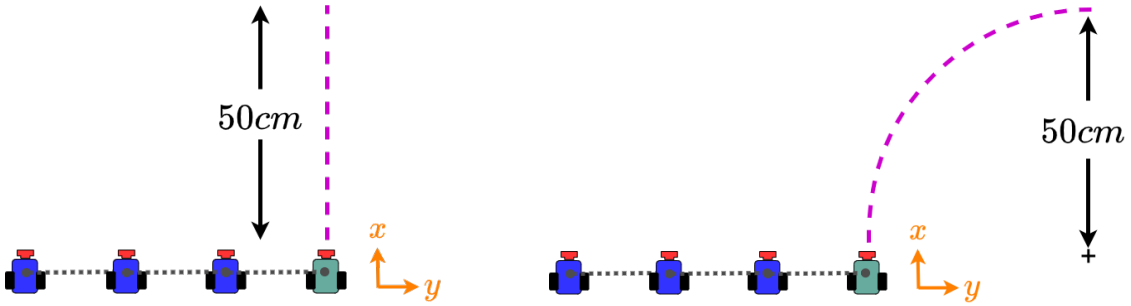


(a) Straight (b) Curved

Figure 5.5: Mobile-robots trajectories. (a) A straight-line trajectory (pink dash line) in the $x-$direction for the case of a fully autonomous leader (green) where the orientation of the leader is maintained by placing it on a track. (b) A curved-line trajectory with radius of $50cm$ (pink dash line), and human feedback correction of the leader's (green) orientation to maintain stay on the curved path.

correct for orientation errors arising from the use of wheel encoders and allows autonomous operation of the robots.

The speed of the leader robot $\mathbf{v}_L$ is selected numerically using simulations, to stay within a range of transport speeds such that the simulated maximum deformation $D^*$ is below the limit of $10cm$. Beyond this deformation (which depends on the amount of friction between the robot wheels and the ground), the robot gets dragged by its neighbors. Simulations indicate that the maximum deformation increases with transport speed as shown in Fig. 5.6a. Based on these results, the transport speed was selected as $\mathbf{v}_L = 5cm/s$.

*Curved-line trajectory with orientation change*

The leader robot is to be moved along a curved desired trajectory with $50cm$ radii and total orientation change of $90°$ that is marked on the floor, as illustrated in Fig. 5.5b. The leader robot's tracking of the circular trajectory is achieved using angular-velocity corrections from a human teleoperator. The speed of the leader robot $\mathbf{v}_L$ along the curved-line trajectory is fixed and selected numerically using simulations, shown in Fig. 5.6b. To maintain the allowable deformation below $10cm$, the speed is chosen as $\mathbf{v}_L = 2.5cm/s$.

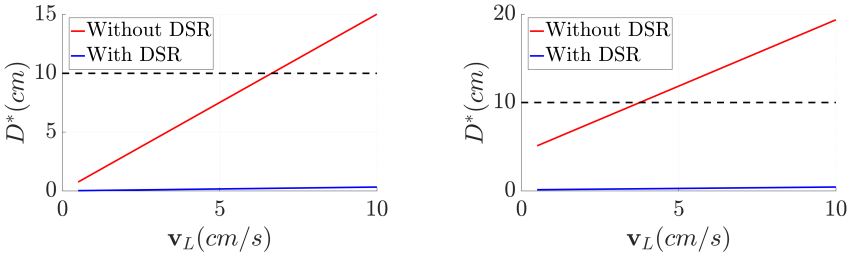


(a) Straight traj. (b) Curved traj.

Figure 5.6: Simulation results with and without DSR. Speed of transport versus maximum deformation $D^*$ as in Eq. (5.147) when moving with constant speed for (a) straight trajectory, and (b) curved trajectory. The speed of the leader robot (transport speed) $\mathbf{v}_L$ for experiments was selected such that the maximum deformation (predicted from simulation) is less than the allowable limit ($10cm$) – $5cm/s$ for the straight trajectory case and $2.5cm/s$ for the curved trajectory case.

*Trajectory for robotic manipulators*

The desired transport trajectory is chosen as a circular motion with $50mm$ diameter as shown in Fig. 5.3a, moving with a constant speed. The trajectory is achieved by prescribing a set of way-points in the global coordinate frame $(x, y)$ for the leader robot to track.

## 5.4 Experimental Results and Discussion

Comparative evaluations, with and without DSR are presented below to evaluate the transport improvement with DSR.

### *5.4.1 Deformation decreases with DSR during translation*

The deformation of the object during transport is inferred from force measurements using Eq. (5.147). The case with DSR approach shows a significant reduction in object's deformation during translation-only transport using the mobile-robots system, from $(9.61 \pm 0.61)cm$ to $(2.44 \pm 0.17)cm$, which is a $75 \pm 3\%$ in improvement as compared to the case without DSR as shown in Table 5.2. The improvement is also quantified using the measured reaction

force, where the mean maximum force $f^*$ as in Eq. (5.148) is reduced by $75 \pm 2\%$, from $(0.12 \pm 0.01)N$ without DSR to $(0.03 \pm 0.02)N$ with DSR as presented in Table 5.2. Note that this reduction of deformation and force with DSR is obtained while completing the task in similar time as the case without DSR. Plots of deformation and force at each robot's contact point in Figs. 5.7a-5.7b and Figs. 5.8a-5.8b respectively also show the similarity of improvement between deformation and force. The deformation in one of the experimental trials, in which the maximum deformation $D^*$ is the closes to mean value, is also presented in Fig. 5.9a, which visualizes the deformation reduction during transport with DSR compared to the case without DSR.

### *5.4.2 Deformation decreases with DSR during rotation*

In the presences of rotation, the change in orientation induces unintended deformation as well as time-varying dynamics. The results show that even with rotational effects, with the desired-position dependent on the part geometry, DSR reduces object's deformation significantly during transport. The maximum deformation $D^*$ (Eq. (5.147)) without DSR of $(9.66 \pm 0.79)cm$ is reduced to $(2.76 \pm 1.33)cm$ with DSR, while completing the task in the same time. This leads to $72 \pm 3\%$ reduction of maximum deformation with DSR as compared to the case without DSR as shown in Table 5.2. Again, the improvement is reflected in the measured reaction forces, where the mean maximum force $f^*$ as in Eq. (5.148) is reduced by $78 \pm 3\%$, from $(0.14 \pm 0.03)N$ without DSR to $(0.03 \pm 0.01)N$ with DSR as presented in Table 5.2.

Plots of deformation and force comparing the results show similar improvement for both metrics for both cases, with and without DSR are shown in Figs. 5.7c-5.7d and Figs. 5.8c-5.8d respectively. Furthermore, snapshots of the deformation with and without the DSR approach during one of the experimental trials, where the maximum deformation $D^*$ is the closest to the mean value, are shown in Fig. 5.9b to help visualize the deformation reduction with DSR.

**Case 1: Translational transport**

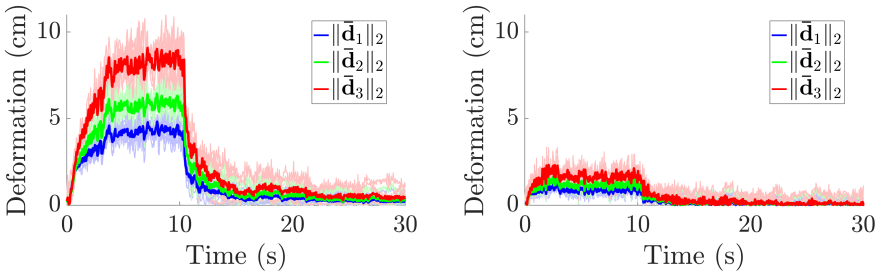


(a) Without DSR (b) With DSR

**Case 2: Rotational transport**

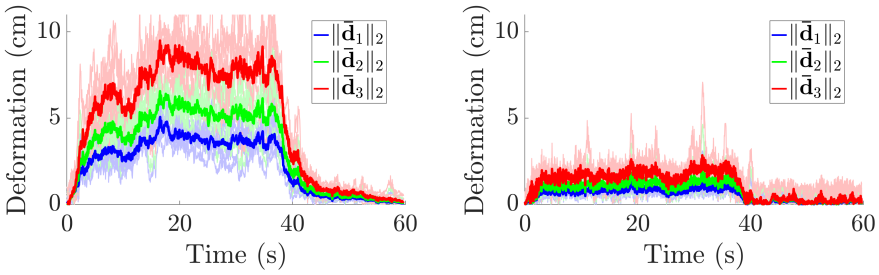


(c) Without DSR (d) With DSR

**Case 3: Circular transport**

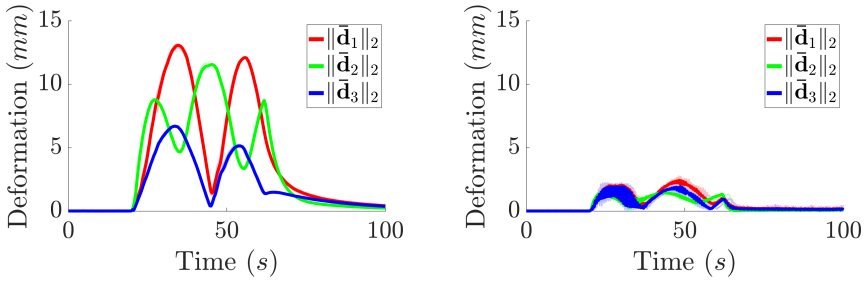


(e) Without DSR (f) With DSR

Figure 5.7: Comparative evaluation of experimentally inferred deformation $\|\bar{\mathbf{d}}_i\|_2$ as in Eq. (5.147) where $\bar{\mathbf{d}}_i = [\bar{d}_{x,i}, \bar{d}_{y,i}]$ for $i = \{1, 2, 3\}$: without DSR (left column, a,c,e), and with DSR (right column, b,d,f). The results are shown for 7 trials (shown in thin lines), and the means are shown in thick lines.

**Case 1: Translational transport**

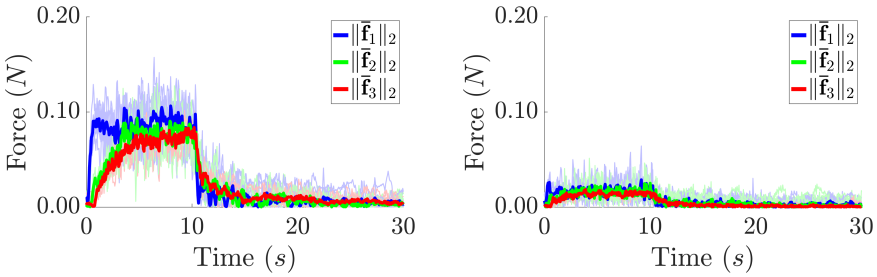


(a) Without DSR (b) With DSR

**Case 2: Rotational transport**

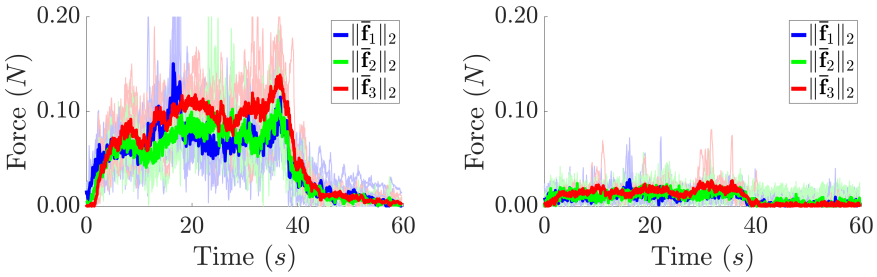


(c) Without DSR (d) With DSR

**Case 3: Circular transport**

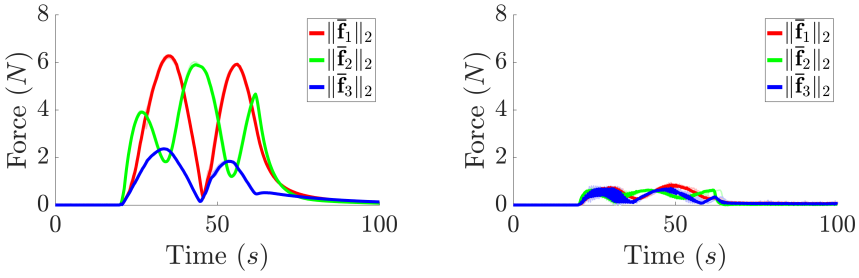


(e) Without DSR (f) With DSR

Figure 5.8: Comparative evaluation of experimentally measured force $\|\bar{\mathbf{f}}_i\|_2$ as in Eq. (5.148) where $\bar{\mathbf{f}}_i = [\bar{f}_{x,i}, \bar{f}_{y,i}]$ for $i = \{1, 2, 3\}$: without DSR (left column, a,c,e), and with DSR (right column, b,d,f). Results are shown for 7 trials (shown in thin lines), and the means are shown in thick lines.

### *5.4.3 Deformation decreases using DSR for robotic manipulators*

Substantial reduction in deformation is also observed in experiments using robotic manipulators when transporting the circular object. The maximum deformation $D^*$ in Eq. (5.147)

reduces with DSR from $(13.07 \pm 0.10)mm$ to $(2.53 \pm 0.18)mm$ without DSR, which is an improvement of $80 \pm 1\%$ as shown in Table 5.2. Similar improvement is also shown in force measurement where the mean maximum force $f^*$ as in Eq. (5.148) is reduced by $86 \pm 1\%$, from $(6.27 \pm 0.04)N$ without DSR to $(0.88 \pm 0.02)N$ with DSR as presented in Table 5.2. The significant reductions of deformation and force with the DSR approach also are seen in the time-domain plots in Figs. 5.7e-5.7f and Figs. 5.8e-5.8f. Note that the improvement is achieved without slowing down the transport speed. Additionally, Fig. 5.9c shows a snapshot from one of the trials to help visualize the comparison of deformation during transport with and without DSR.

Table 5.2: Improvement (reduction) in maximum deformation ( $D^*$) as in Eq. (5.147) and maximum force ( $f^*$) as in Eq. (5.148) for Case 1: translational transport, Case 2: rotational transport, and Case 3: circular transport, with and without DSR. Results presented for experiment with mean $\mu$ and standard deviation $\sigma$ over 7 experimental trials. Improvements are highlighted in green.

| | **CASE 1: TRANSLATIONAL** | | **CASE 2: ROTATIONAL** | | **CASE 3: CIRCULAR** | |
|---|---|---|---|---|---|---|
| **Metric** | **Method** | **Value** | **Method** | **Value** | **Method** | **Value** |
| | Without DSR | 0.12 ± 0.01 | Without DSR | 0.14 ± 0.03 | Without DSR | 6.27 ± 0.04 |
| **Force** | With DSR | 0.03 ± 0.02 | With DSR | 0.03 ± 0.01 | With DSR | 0.88 ± 0.02 |
| (N) | Improvement (%) | **75 ± 2 %** | Improvement (%) | **78 ± 3 %** | Improvement (%) | **86 ± 1 %** |
| | Without DSR | 96.1 ± 6.1 | Without DSR | 96.6 ± 7.9 | Without DSR | 13.07 ± 0.10 |
| **Deform.** | With DSR | 24.4 ± 1.7 | With DSR | 27.6 ± 13.3 | With DSR | 2.53 ± 0.18 |
| (mm) | Improvement (%) | **75 ± 3 %** | Improvement (%) | **72 ± 3 %** | Improvement (%) | **80 ± 1 %** |

## *5.5 Conclusion*

This chapter presented a decentralized robotic transport approach to reduce an object's deformation during transport. Experimental results show that the proposed delayed self-reinforcement (DSR) approach significantly reduces deformation during transport without increasing the transport time — even during rotational transport where the desired robot positions depend on the geometry of the object. Analysis methods were also developed to select robot control parameters to ensure stability of the time-varying transport dynamics

with the proposed DSR approach. Future effort will be focused on extending the work to include adaptive strategies for gain selection.

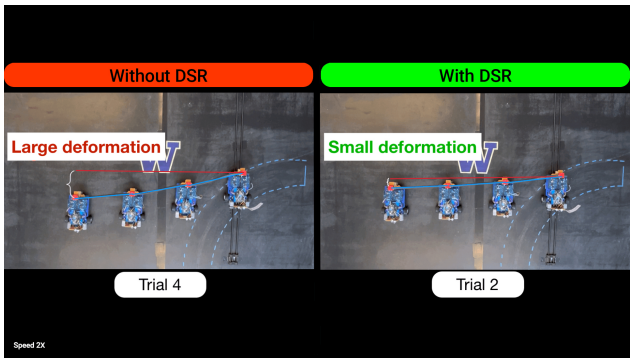


(a) Case 1: Translational transport

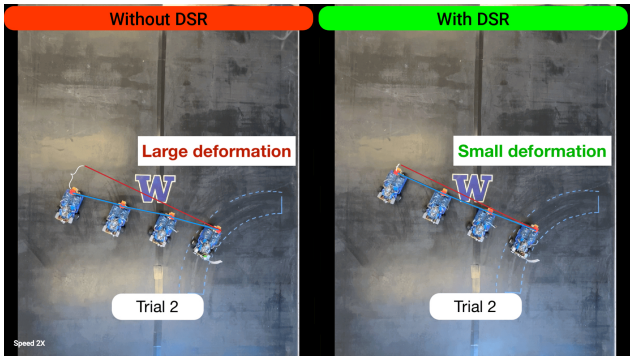


(b) Case 2: Rotational transport

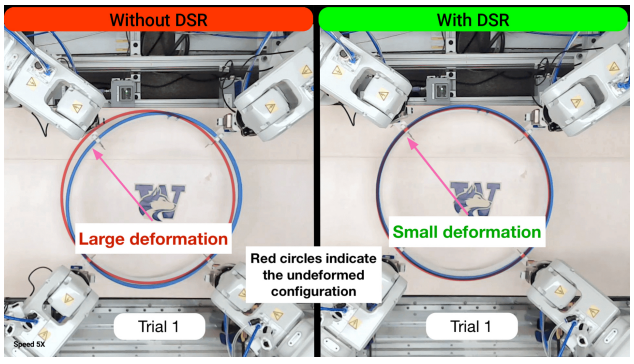


(c) Case 3: Circular transport

Figure 5.9: Snapshots of experiment showing deformation $\bar{\mathbf{D}}$ for both approaches, with and without DSR, when the robots are moving in (a) straight-line trajectory (Case 1), (b) curved-line trajectory (Case 2), and (c) circular trajectory (Case 3). The red lines and circles indicate the undeformed configuration based on the leader's orientation and the blue lines and circles show the deformation of the object. The snapshots, selected from one of the seven trials for each experimental case, have deformation values closest to the mean. For the full experiment video refer to the attached supporting media.

# Chapter 6

# MC3: DEVELOPMENT OF DECENTRALIZED PARAMETER SELECTION FOR TRANSPORT OF FLEXIBLE OBJECTS USING ROBOT NETWORKS

This chapter forms the main contribution 3 (**MC3**) of this dissertation. This work also is ready to be submitted to a peer-reviewed journal [20]. The main goal of this chapter is to develop a fully decentralized parameter-selection approach for transport tasks using robot networks. The proposed approach expands the DSR-based transport approach that solely utilizes previously stored sensed information from neighboring robots [47, 53]. Notably, the proposed approach decentralizes the selection of parameters by introducing a novel scaling factor to the robots' DSR-based update which can be obtained locally through random interactions between the robots and the object. An advantage of this approach is that it does not require prior knowledge of the dynamics or the network connectivity structure to determine a stable parameter range for any given network settling time $T_s$ that matches with the robots' capabilities. Hence, the proposed approach can be implemented to any network, e.g., to transport different types of objects, even with varying number of robots in the network. Furthermore, experimental results showcase the efficacy of the DSR-based transport with decentralized parameter selection, that show reduction in deformation during transport by 62% as compared to the standard case without DSR even when using centralized parameter selection.

## *6.1 Preliminaries and Problem Statement*

The object transport formulation which follows a leader-followers schematic is presented in the three dimensional (3D) translation coordinates. The robot network is a team of multiple

robots consisting of a leader robot which has access to the desired trajectory, and $n$-follower robots. The object is grasped by each robot as shown in Fig. 6.1, thus, reaction forces are generated by deformation at their respective contact points, measured using onboard force sensors used for feedback to compute the control actions.

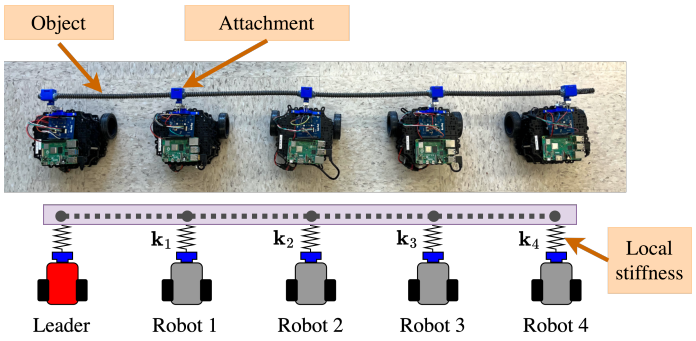


Figure 6.1: Top: Experiment setup with five TurtleBots transporting a flexible object (coiled spring). Bottom: Robot network schematic showing implicit communication between robots through the object. Each robot then only adjusts their motion based on the local force measurement at the contact point with the object.

### *6.1.1 Leader's update*

In the leader-followers transport mechanism, the role of a leader is to steer the object. The leader only tracks the desired trajectory and does not react to local force measurements. Thus, the leader robot updates its position $\mathbf{p}_L = [p_{Lx}, p_{Ly}, p_{Lz}]^\intercal \in \mathbb{R}^3$ based on the desired trajectory $\mathbf{p}_s = [p_{sx}, p_{sy}, p_{sz}]^\intercal \in \mathbb{R}^3$ as,

$$\mathbf{p}_L[m] = \mathbf{p}_s[m], \tag{6.1}$$

where $\mathbf{p}_L[m]$ and $\mathbf{p}_s[m]$ are the position of the leader robot and desired trajectory at time instant $[m] = (\delta_t m)$ respectively with sampling period $\delta_t$. Note that there is no force feedback in the leader's update law shown in Eq. (6.1).

### *6.1.2 Followers' decentralized update*

The follower robots assist the leader during transport by minimizing local deformation inferred through force measurements. In a decentralized setting, the follower robots do not have access to the desired trajectory, but update their position by using only local force measurement. Thus, the position update for each follower robot $i$ can be written as

$$\mathbf{p}_i[m+1] = \mathbf{p}_i[m] - \gamma \delta_t \mathbf{f}_i[m], \tag{6.2}$$

where $\gamma$ is the update gain, $\mathbf{p}_i = [p_{ix}, p_{iy}, p_{iz}]^\intercal \in \mathbb{R}^3$ is the position of robot $i$ and $\mathbf{f}_i = [f_{ix}, f_{iy}, f_{iz}]^\intercal \in \mathbb{R}^3$ is the local force measurement at contact point between robot $i$ and the object. Then, the update law for all $n$ - follower robots can be written in a matrix form as,

$$\mathbf{P}[m+1] = \mathbf{P}[m] - \gamma \delta_t \mathbf{F}[m], \tag{6.3}$$

where the concatenated robot positions and forces are

$$\begin{aligned} \mathbf{P} &= [\mathbf{p}_1, \mathbf{p}_2, \ldots, \mathbf{p}_n]^\intercal \quad \in \mathbb{R}^{3n}, \\ \mathbf{F} &= [\mathbf{f}_1, \mathbf{f}_2, \ldots, \mathbf{f}_n]^\intercal \quad \in \mathbb{R}^{3n}. \end{aligned} \tag{6.4}$$

Assuming that the deformation is small relative to the size of the object, the overall reaction forces $\mathbf{F}_r \in \mathbb{R}^{3(n+1)}$, which includes reaction force for the leader, due to the interaction between robots and the object can be written in terms of overall object stiffness $\mathbf{K}_o \in \mathbb{R}^{(3n+3)\times(3n+3)}$ and robots' positions $\mathbf{P}_r \in \mathbb{R}^{3n+3}$ as

$$\begin{aligned} \mathbf{F}_r &= \mathbf{K}_o \mathbf{P}_r \\ \begin{bmatrix} \mathbf{f}_L \\ \mathbf{F} \end{bmatrix} &= \begin{bmatrix} * & * \\ -\mathbf{B} & \mathbf{K} \end{bmatrix} \begin{bmatrix} \mathbf{p}_L \\ \mathbf{P} \end{bmatrix}, \end{aligned} \tag{6.5}$$

where $\mathbf{K} \in \mathbb{R}^{3n\times 3n}$ is the global stiffness matrix associated with the follower robots which depends on object's structural properties, $\mathbf{B} \in \mathbb{R}^{3n\times 3}$ is the connectivity matrix to the leader, the symbol $(*)$ indicates a non-empty entry of the matrix, $\mathbf{f}_L$ and $\mathbf{p}_L$ are the force

and position vectors of the leader robot respectively. Hence, the force-position relationship can be simplified for the followers as

$$\mathbf{F} = \mathbf{KP} - \mathbf{Bp}_L. \tag{6.6}$$

Then, using Eq. (6.6) to rewrite the update equation in Eq. (6.3) results in

$$\mathbf{P}[m+1] = (\mathbf{I} - \gamma\delta_t\mathbf{K})\mathbf{P}[m] + \gamma\delta_t\mathbf{B}\mathbf{p}_L[m]. \tag{6.7}$$

Note that the global stiffness matrix $\mathbf{K}$ also describes the network connectivity between robots, thus has a similar form as the pinned Laplacian matrix in [44], with real and positive eigenvalues.

**Lemma 11 (Stability of the standard approach)** *The transport dynamics in Eq.* (6.7) *is stable if and only if the update gain* $\gamma$ *is selected such that all eigenvalues of the matrix* $(\mathbf{I} - \gamma\delta_t\mathbf{K})$ *are inside the unit circle, which results in*

$$0 < \gamma < \left(\bar{\gamma} = \frac{2}{\bar{\lambda}_{\mathbf{K}}\delta_t}\right), \tag{6.8}$$

*where* $\bar{\lambda}_{\mathbf{K}}$ *is the largest eigenvalue of the stiffness matrix* $\mathbf{K}$.

*Proof:* The proof is shown in [2] and is omitted here for brevity.

### *6.1.3 Problem: decentralize parameter selection*

The update parameter $\gamma$ in Eq. (6.2) can be selected to achieve the desired network settling time $T_s$. In particular, the settling time $T_s$ to reach a desired step in position is given by

$$T_s \approx \frac{-4\delta_t}{\ln\left(\hat{\lambda}_{\mathbf{K}}\right)} \quad \text{where} \quad \hat{\lambda}_{\mathbf{K}} = \arg\max_{\lambda_{\mathbf{K},j}} |1 - \gamma\delta_t\lambda_{\mathbf{K},j}|. \tag{6.9}$$

Thus from Eq. (6.9) above, the update parameter $\gamma$ can be computed given desired network settling time $T_s$ as

$$\gamma = \frac{1 - \exp(-4\delta_t/T_s)}{\delta_t\ \underline{\lambda}_{\mathbf{K}}}, \tag{6.10}$$

where $\underline{\lambda}_{\mathbf{K}}$ is the smallest eigenvalue of the global stiffness matrix $\mathbf{K}$. Two problems identified from the standard decentralized approach are in the following.

1. Computing the update parameter $\gamma$ in Eq. (6.10) also depends on the smallest (slowest) eigenvalue $\underline{\lambda}_{\mathbf{K}}$ of the global stiffness matrix $\mathbf{K}$, which is difficult to obtain without centralized information regarding the properties of the global stiffness matrix $\mathbf{K}$.

2. Typically, faster settling time $T_s$ results in larger deformation and vice versa. Therefore, for a given settling time $T_s$ to compute $\gamma$, there is no further control over the deformations of the object during transport.

Hence, this article aims to develop an approach for parameter selection in fully decentralized manner without needing the knowledge of global stiffness matrix $\mathbf{K}$, while also reducing deformation during transport without increasing the network settling time $T_s$.

## *6.2 Decentralized parameter selection using estimated-DSR*

### *6.2.1 Followers' update with estimated-DSR*

The use of DSR method has been shown to reduce deformation significantly during transport [2]. The DSR-based transport dynamics is derived from the ideal dynamics where each follower has direct access to the leader's position, which can be written in the continuous time domain as

$$\begin{aligned}\dot{\mathbf{P}}(t) =& -\alpha\mathbf{P}(t) + \alpha\mathbf{B}_c\mathbf{p}_L(t)\\ =& -\alpha\mathbf{P}(t) + \alpha\mathbf{B}_c\mathbf{p}_L(t).\end{aligned} \tag{6.11}$$

where $\alpha > 0$ is the update gain and

$$\mathbf{B}_c = (\mathbf{1}_n \otimes \mathbf{I}_{3\times 3}) \in \mathbb{R}^{3n\times 3}, \tag{6.12}$$

describes connectivity to the leader with $\otimes$ indicating the Kronecker product. The ideal update law in Eq. (6.11) can be decentralized by multiplying both sides of Eq. (6.11) with a scaled normalized stiffness matrix $\beta\mathbf{L}$, where $\beta > 0$ is the DSR gain, which results in

$$\beta\mathbf{L}\dot{\mathbf{P}}(t) = -\alpha\beta\mathbf{L}\mathbf{P}(t) + \alpha\beta\mathbf{L}\mathbf{B}_c\mathbf{p}_L(t), \tag{6.13}$$

where the normalized stiffness matrix $\mathbf{L}$ is a scaled stiffness matrix $\mathbf{K}$ with ones along its diagonal, i.e.

$$\mathbf{L} = \mathbf{\Gamma K} = \begin{bmatrix} 1 & & * \\ & \ddots & \\ * & & 1 \end{bmatrix} \in \mathbb{R}^{3n \times 3n}, \tag{6.14}$$

where the scaling factor matrix $\mathbf{\Gamma}$ can be described as

$$\begin{aligned} \mathbf{\Gamma}_{\{j,j\}} &= (\mathbf{K}_{\{j,j\}})^{-1} \\ &= 0 \qquad \text{otherwise.} \end{aligned} \tag{6.15}$$

Then adding $\dot{\mathbf{P}}(t)$ to both sides of Eq. (6.13) and rearranging the terms to obtain,

$$\begin{aligned} \dot{\mathbf{P}}(t) =& -\alpha\beta\mathbf{LP}(t) + (\mathbf{I} - \beta\mathbf{L})\dot{\mathbf{P}}(t) + \alpha\beta\mathbf{LB}_c\mathbf{p}_L(t) \\ \approx& -\alpha\beta\mathbf{LP}(t) + (\mathbf{I} - \beta\mathbf{L})\frac{\mathbf{P}(t) - \mathbf{P}(t-\tau)}{\tau} \\ &+ \alpha\beta\mathbf{LB}_c\mathbf{p}_L(t), \end{aligned} \tag{6.16}$$

where the $\dot{\mathbf{P}}(t)$ term on the right hand side of Eq. (6.16) is approximated using a delay-based derivative as shown in [47]. Let the delay time step $\tau = \delta_t$, then the DSR-based update law in Eq. (6.16) can be written in the discrete time domain as,

$$\begin{aligned} \mathbf{P}[m+1] =& \mathbf{P}[m] - \alpha\beta\delta_t\mathbf{LP}[m] + \alpha\beta\delta_t\mathbf{B}_L\mathbf{p}_L[m] \\ &+ (\mathbf{I} - \beta\mathbf{L})(\mathbf{P}[m] - \mathbf{P}[m-1]), \end{aligned} \tag{6.17}$$

where $\mathbf{B}_L = \mathbf{\Gamma B} \in \mathbb{R}^{3n \times 3}$ contains zeroes but ones on entries associated with followers adjacent to the leader.

**Remark 18 (Decentralized implementation using local stiffness)** *In implementation, each robot $i$ still updates its position $\mathbf{p}_i$ using only force measurement $\mathbf{f}_i$ that is inversely scaled by its local stiffness, that is*

$$\begin{aligned} \mathbf{p}_i[m+1] =& \mathbf{p}_i[m] - \alpha\beta\delta_t\mathbf{\Gamma}_i\mathbf{f}_i[m] + (\mathbf{p}_i[m] - \mathbf{p}_i[m-1]) \\ &- \beta\mathbf{\Gamma}_i(\mathbf{f}_i[m] - \mathbf{f}_i[m-1]), \end{aligned} \tag{6.18}$$

*where* $\mathbf{\Gamma}_i \in \mathbb{R}^{3\times3}$ *is the scaling factor matrix that depends on diagonal entries of the local stiffness* $\mathbf{k}_i \in \mathbb{R}^{3\times3}$*, that is*

$$\begin{aligned}\mathbf{\Gamma}_{i\{s,s\}} &= \left(\mathbf{k}_{i\{s,s\}}\right)^{-1} \\ &= 0 \qquad \textit{otherwise.}\end{aligned} \tag{6.19}$$

*Note that the* $s^{th}$ *diagonal entry of the local stiffness* $\mathbf{k}_{i\{s,s\}}$ *corresponds to the local stiffness value in the* $s-$*axis where* $s \in \{x, y, z\}$ *at robot* $i$ *location. Therefore, the implementation remains decentralized since each robot only requires local information such as force, position, and local stiffness measurements to compute its update law in Eq.* (6.18)*.*

### *6.2.2 Stability of the estimated-DSR approach*

The stability of the proposed estimated-DSR can be established by finding the roots of the characteristic equation of the update law in Eq. (6.17), which can be written as,

$$\det\left(\mathbf{I}z^2 - \alpha\beta\delta_t\mathbf{L}_J + [\mathbf{I} - \beta\mathbf{L}_J]z + [\mathbf{I} - \beta\mathbf{L}_J]\right) = 0, \tag{6.20}$$

where $\mathbf{L}_J = \mathbf{J}^{-1}\mathbf{L}\mathbf{J}$ is the diagonalization of the normalized stiffness matrix $\mathbf{L}$. Note that since the stiffness matrix $\mathbf{K}$ has real and positive eigenvalues, the normalized stiffness matrix $\mathbf{L}$ also has real and positive eigenvalues (see [54]).

Then, for each eigenvalue $\lambda_{\mathbf{L},j}$ of the normalized stiffness matrix $\mathbf{L}$, the characteristic equation $C(z)$ can be rewritten as

$$C(z) = z^2 - (1 - \alpha\beta\delta_t\lambda_{\mathbf{L},j} + [1 - \beta\lambda_{\mathbf{L},j}])z + [1 - \beta\lambda_{\mathbf{L},j}] = 0. \tag{6.21}$$

The analytical conditions for stability are shown in the next lemma.

**Lemma 12** *The proposed approach with estimated-DSR is stable if and only if the selection update for parameters* $(\alpha, \beta)$ *satisfy the following conditions*

$$\begin{aligned}&(i) \quad 0 < \alpha \\ &(ii) \quad 0 < \beta < \left(\bar{\beta} = \frac{2}{\alpha\delta_t + 2}\right).\end{aligned} \tag{6.22}$$

*Proof:* The proof is divided into two steps:

**Step 1: establishing the stability conditions for eigenvalues**

The first step is to use Jury test to find the bound on update of parameters $(\alpha, \beta)$. The bounds can be established by finding the roots of the characteristic equation $C(z)$ in Eq. (6.21). In particular, the three necessary and sufficient conditions are in the following.

1. $C(z = 1) > 0$ :

$$\alpha\beta\delta_t\lambda_{\mathbf{L},j} > 0, \quad \rightarrow \quad \alpha > 0. \tag{6.23}$$

   This confirms the first condition of the lemma.

2. $|C(z = 0)| < 1$ :

$$\begin{aligned} |1 - \beta\lambda_{\mathbf{L},j}| < 1 \quad \text{or} \quad -1 < (1 - \beta\lambda_{\mathbf{L},j}) < 1, \\ 0 < \beta < \frac{2}{\lambda_{\mathbf{L},j}}. \end{aligned} \tag{6.24}$$

3. $(-1)^2 C(z = -1) > 0$ :

$$4 - \alpha\beta\delta_t\lambda_{\mathbf{L},j} - 2\beta\lambda_{\mathbf{L},j} > 0, \quad \rightarrow \quad \beta < \frac{4}{\lambda_{\mathbf{L},j}(\alpha\delta_t + 2)}. \tag{6.25}$$

The condition in Eq. (6.25) is used to establish the upper bound on the selection of $\beta$ since it is more stringent than Eq. (6.24).

**Step 2: decoupling the stability conditions from eigenvalues**

Since the condition needs to be satisfied for all eigenvalue of $\mathbf{L}$, then a more conservative condition on $\beta$ in Eq. (6.25) can be established using the upper bound of the eigenvalues of $\mathbf{L}$, which can be found using Gershgorin circle theorem [55]. The Gershgorin circle theorem implies that every eigenvalue $\lambda_{\mathbf{L},j}$ of the normalized stiffness matrix $\mathbf{L} \in \mathbb{R}^{3n\times 3n}$ satisfies the following condition,

$$|\lambda_{\mathbf{L},j} - \mathbf{L}_{j,k}| \leq \sum_{k\neq j} |\mathbf{L}_{j,k}| \qquad j, k \in \{1, 2, \ldots, n\}. \tag{6.26}$$

Typically, the normalized stiffness matrix $\mathbf{L}$ has a special form similar to the Laplacian matrix of a undirected graph (see [44]), that is the absolute row-sum of the off-diagonal terms is less than or equal to the diagonal term, e.g.,

$$\sum_{k \neq j} |\mathbf{L}_{j,k}| \leq \mathbf{L}_{j,j} \qquad j \in \{1, 2, \ldots, n\}. \tag{6.27}$$

Then, substituting Eq. (6.27) into the right-hand side of the Eq. (6.26) results in

$$|\lambda_{\mathbf{L},j} - \mathbf{L}_{j,j}| \leq \mathbf{L}_{j,j}, \tag{6.28}$$

which gives

$$\begin{aligned} -\mathbf{L}_{j,j} \leq (\lambda_{\mathbf{L},j} - \mathbf{L}_{j,j}) \leq \mathbf{L}_{j,j} \\ 0 \leq \lambda_{\mathbf{L},j} \leq 2\, \mathbf{L}_{j,j} \end{aligned} \tag{6.29}$$

Since the diagonal terms of the normalized stiffness matrix $\mathbf{L}$ are all ones from Eq. (6.14), i.e., $\mathbf{L}_{j,j}\ \forall\ j$, the bound on eigenvalues in Eq. (6.29) on $\mathbf{L}$ becomes,

$$0 \leq \lambda_{\mathbf{L},j} \leq 2. \tag{6.30}$$

Therefore, using the upper bound on eigenvalues of $\mathbf{L}$ above in Eq. (6.30), a more conservative stability condition for $\beta$ in Eq. (6.17) can be established as,

$$0 < \beta < \left( \frac{2}{\alpha \delta_t + 2} = \frac{4}{2(\alpha \delta_t + 2)} \right) \leq \frac{4}{(\max_j \lambda_{\mathbf{L},j})(\alpha \delta_t + 2)}, \tag{6.31}$$

which leads to the claim of the lemma.

**Remark 19 (Decentralized parameter selection)** *The update parameters selection with estimated-DSR approach is fully decentralized since the stable range of* $(\alpha, \beta)$ *as shown in Eq.* (6.17) *are independent of the global stiffness matrix* $\mathbf{K}$ *or its eigenvalues.*

**Remark 20 (Settling time with estimated-DSR)** *The parameter* $\alpha$ *of the ideal centralized update in Eq.* (6.11) *can be selected directly based on a specified network settling time* $T_s$*, e.g.,*

$$\alpha = \frac{4}{T_s}. \tag{6.32}$$

*Although, in general the $\alpha$ can be chosen individually for each robot based on their capabilities. However in implementation, the settling time $T_s$ of the network can be selected larger than the capability of the robots to ensure tracking of the desired trajectory as shown in Eq.* (2.1)*. Since the proposed DSR-based transport approach is an approximation of the ideal centralized dynamics in Eq.* (6.11)*, the parameter $\alpha$ in the decentralized update in Eq.* (6.18) *can be approximated using Eq.* (6.32)*.*

### *6.2.3 Measuring local stiffness*

The update law in Eq. (6.18) for robot $i$ requires the scaling factor $\mathbf{\Gamma}_i$ to normalize the force measurements $\mathbf{f}_i$. The scaling factor $\mathbf{\Gamma}_i$ only depends on the inverse of diagonal entries of the local stiffness matrix $\mathbf{k}_i$ as shown in Eq. (6.19). A way to obtain diagonal entries of the local stiffness $\mathbf{k}_i$ is through initial robot's interaction with the object. For instance, initially each robot $i$ can randomly displace from its undeformed configuration ($\mathbf{p}_i[0] = \mathbf{0}$ and $\mathbf{f}_i[0] = \mathbf{0}$) while keeping the leader fixed, in small amount along each axis of motion for a time period $T \in \{1, 2, \ldots, T_m\}$, e.g.,

$$p_{is}[T] = \epsilon \ (\mathcal{P} \in [-1, 1]), \quad s \in \{x, y, z\}, \tag{6.33}$$

where $\epsilon > 0$ is a scaling constant depends on the amplitude of the trajectory and $\mathcal{P} \in [-1, 1]$ indicates randomly generated trajectory with values between negative one and positive one. During the small random motions along the $s-$axis where $s \in \{x, y, z\}$, each robot $i$ records the reaction force $f_{is}$ and position $p_{is}$ measurements, e.g.,

$$\begin{aligned} \tilde{\mathbf{f}}_{is} &= \Big[f_{is}[1], f_{is}[2], \ldots, f_{is}[T_m]\Big], \\ \tilde{\mathbf{p}}_{is} &= \Big[p_{is}[1], p_{is}[2], \ldots, p_{is}[T_m]\Big]. \end{aligned} \tag{6.34}$$

In the case where initial random motions in Eq. (6.33) are performed by each robot $i$ sequentially, then the diagonal entry of the local stiffness $\mathbf{k}_{i\{s,s\}}$ can be easily found by using only one-time measurement from Eq. (6.6), for example,

$$\mathbf{k}_{i\{s,s\}} = \frac{f_{is}[1]}{p_{is}[1]}, \tag{6.35}$$

since the leader robot is not moving ($\mathbf{p}_L = \mathbf{0}$). However, this approach requires a centralized coordination amongst the robots to determine which robot will move next. Alternatively, all robots can perform initial random motions simultaneously or in random order without coordination. But, this approach introduces noise $\boldsymbol{\eta}_{is}$ to the force measurement $\tilde{\mathbf{f}}_{is}$ Eq. (6.34) of the robot $i$ due to motions from its adjacent neighbors, that is

$$\hat{\mathbf{f}}_{is} = \tilde{\mathbf{f}}_{is} + \boldsymbol{\eta}_{is}. \tag{6.36}$$

Then in this case, the diagonal entry of the local stiffness $\mathbf{k}_{i\{s,s\}}$ along the $s-$axis for robot $i$ can be inferred by finding a linear relationship between position $\tilde{\mathbf{p}}_{is}$ and force $\hat{\mathbf{f}}_{is}$ in Eq. (6.36) measurements in Eq. (6.34) using a fitting technique such as least squares, that is

$$\begin{aligned} \mathbf{k}_{i\{s,s\}} &= \arg\min_{\mathbf{k}_{i\{s,s\}}} \|\mathbf{k}_{i\{s,s\}}\tilde{\mathbf{p}}_{is} - \hat{\mathbf{f}}_{is}\|_2^2 \\ &= \arg\min_{\mathbf{k}_{i\{s,s\}}} \|\mathbf{k}_{i\{s,s\}}\tilde{\mathbf{p}}_{is} - \tilde{\mathbf{f}}_{is} - \boldsymbol{\eta}_{is}\|_2^2. \end{aligned} \tag{6.37}$$

Note that depending on the noise level $\boldsymbol{\eta}_{is}$, this estimation approach when all robots move simultaneously requires sufficient amount of time $T_m$ to obtain acceptable estimate of the local stiffness values. Nevertheless, initial interactions between the robots and the object can be used to measure local stiffness $\mathbf{k}_{i\{s,s\}}$ $s \in \{x, y, z\}$ for each robot $i$, which then can be used to compute the scaling factor matrix $\boldsymbol{\Gamma}_i$ in Eq. (6.19) in fully decentralized manner.

## *6.3 Experiment*

This section presents system description and parameter selection for the two different transport approaches discussed in this article, (i) without DSR and (ii) with estimated-DSR. The experiment was performed for transport tasks in a single-axis of motion ($x-$axis) .

### *6.3.1 Hardware setup*

The system consists of five TurtleBots which have the capability to measure position odometry $\mathbf{p}_i = p_{ix} \in \mathbb{R}$ and equipped with force sensor to measure reaction force $\mathbf{f}_i = f_{ix} \in \mathbb{R}$ at the contact point with the object. Each TurtleBot has an onboard microcomputer to

compute the update law, and the leader robot (shown in red in Fig. (6.1)) tracks the desired trajectory $\mathbf{p}_s = p_{sx}$ given by external computer through ROS (Robot Operating System) and achieved within the sampling period $\delta_t = 0.050s$. For this particular experiment, the desired trajectory $\mathbf{p}_s$ is chosen as a ramp in position to reach $50cm$ distance in task completion time $T_c = 25s$, or a constant speed of $2cm/s$ as shown in Fig. 6.2.

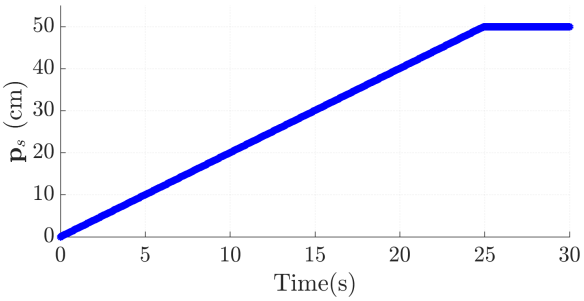


Figure 6.2: The desired trajectory $\mathbf{p}_s$ prescribed to the leader robot. The trajectory is chosen as a constant ramp in position with the slope of $2cm/s$ to reach $50cm$ distance of transport.

The object used for transport is a linear flexible object (coiled spring) with length of 120 cm to visualize the deformation during transport. The local stiffness values of the object are presented in Table 6.1. The schematic is shown in Fig. 6.1 with one leader and four follower robots, mechanically attached to the object.

Table 6.1: Comparison of Local stiffness values at each robot locationl $\mathbf{k}_{i\{x,x\}}$ for $i \in \{1, 2, 3, 4\}$ in the $x-$axis of motion, which are obtained in simulation, measured experimentally and estimated using the proposed approach with estimated-DSR. For the estimated stiffness, the mean value ($\mu$) and standard deviation ($\sigma$) across 7 trials are shown.

| | **Local stiffness values** (N/cm) | | | |
|---|---|---|---|---|
| | $\mathbf{k}_{1\{x,x\}}$ | $\mathbf{k}_{2\{x,x\}}$ | $\mathbf{k}_{3\{x,x\}}$ | $\mathbf{k}_{4\{x,x\}}$ |
| Sim. | 0.92 | 0.92 | 0.92 | 0.46 |
| Meas. | 0.95 | 0.89 | 0.90 | 0.46 |
| Est. | $1.28 \pm 0.34$ | $1.09 \pm 0.18$ | $0.88 \pm 0.29$ | $0.41 \pm 0.06$ |

### *6.3.2 Selection of update parameters*

The update parameters are selected to minimize the deformation for a specified transport settling time $T_s$ for a unit step change in leader's position $\mathbf{p}_L$. The parameter for the approach without DSR is selected in centralized manner based on the knowledge of object's stiffness, and for the approach with estimated-DSR, the update parameters are selected based on the local stiffness obtained through local measurements during the initial interactions with the object.

*Settling time*

The network settling time $T_s$ can be selected to match the capabilities of the robots, e.g., to ensure network convergence. Typically, the network settling time $T_s$ is much larger than the robot's $T_r$, as shown in Eq. (2.1). In this experiment, the settling time of the TurtleBot $T_r$ is measured experimentally, which is $0.03s$. Then, the update sampling time $\delta_t = 0.05s$ is selected to ensure that each robot has a sufficient time to compute and achieve the commanded input. Thus, to ensure convergence the network settling time $T_s$ is selected to be more than 200 times slower than the sampling time $\delta_t$, that is

$$T_s = \nu\delta_t = (200)\ 0.05s = 10s. \tag{6.38}$$

*Without DSR*

The update parameter $\gamma$ in Eq. (6.2) is selected such that the specified settling time $T_s = 10s$ can be reached for a desired step in leader's position $\mathbf{p}_L$. In particular, the gain $\gamma$ is computed using Eq. (6.10) with given settling time $T_s$ as,

$$\gamma = \frac{1 - \exp(-4(0.05))/10)}{0.05\ (0.05)} = 0.35, \tag{6.39}$$

where the smallest eigenvalue of the global stiffness matrix $\mathbf{K}$, $\underline{\lambda}_{\mathbf{K}} = 0.05$.

*With estimated-DSR*

The update parameters $(\alpha, \beta)$ for the proposed with estimated-DSR approach are computed based on the stability conditions in Eq. (6.22) and the measurement process described in Subsection 6.2.3 for computing the scaling factor $\mathbf{\Gamma}_i = \mathbf{\Gamma}_{i\{x,x\}} \in \mathbb{R}$ in Eq. (6.18). In this case, the parameter $\alpha$ is selected for the similar network settling time $T_s$ as the approach without DSR using Eq. (6.32), i.e.,

$$\alpha = \frac{4}{T_s} = \frac{4}{10} = 0.4. \tag{6.40}$$

The parameter $\beta$ is selected to reduce deformation as,

$$\beta = \arg\min_{\beta}(D^*) < \bar{\beta}, \tag{6.41}$$

Typically, the maximum deformation $D^*$ decreases as $\beta$ increases before reaching its stability upper bound $\bar{\beta}$ as shown in Fig. 6.3. Thus, the DSR parameter $\beta$ is computed using Eq. (6.22)

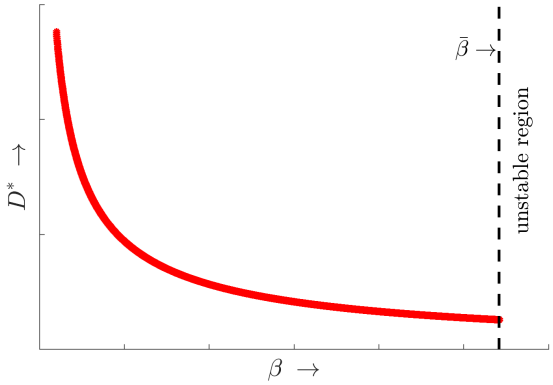


Figure 6.3: The effect of maximum deformation $D^*$ with respect to the DSR parameter $\beta$ given a fixed $\alpha$ which shows that the maximum deformation $D^*$ tends to decrease as $\beta$ increases. The transport dynamic is unstable as $\beta$ passes the upper bound $\bar{\beta}$ in Eq. (6.22) indicated by the dash-line.

at 75% before reaching the stability upper bound, that is

$$\beta = 75\% \left(\frac{2}{\alpha\delta_t + 2}\right) = \frac{(0.75)2}{(0.4)(0.05) + 2} = 0.74. \tag{6.42}$$

For the scaling factor $\mathbf{\Gamma}_i$, each robot measures its local stiffness $\mathbf{k}_i = \mathbf{k}_{i\{x,x\}} \in \mathbb{R}$ by following the process described in Subsection 6.2.3. In this experiment, each robot moved along a sinusoidal trajectory of $0.5cm$ amplitude with randomly generated frequency for time period $T_m = 20s$, e.g.,

$$p_{ix}[T] = 0.5 \ \sin(\omega_i \delta_t T), \quad T \in \{1, 2, \ldots, (20/\delta_t)\} \tag{6.43}$$

where $\omega_i$ is a randomly generated frequency for robot $i$. The position $\tilde{\mathbf{p}}_{ix}$ and force $\tilde{\mathbf{f}}_{ix}$ measurements of the robots as in Eq. (6.34) are shown in Fig. 6.4a - 6.4d. Then each robot infers its local stiffness $\mathbf{k}_{i\{x,x\}}$ by using least squares fitting in Eq. (6.37). The resulting fitted curves are shown in Fig. 6.4e - 6.4h and the numerical values of the estimated stiffness for each robot are shown in Table 6.1. Then, the values of the local stiffness $\mathbf{k}_{i\{x,x\}}$ are used to compute the scaling factor $\mathbf{\Gamma}_{i\{x,x\}}$ for each robot $i$ based on Eq. (6.19). The implementation of the approach with estimated-DSR follows Algorithm 2.

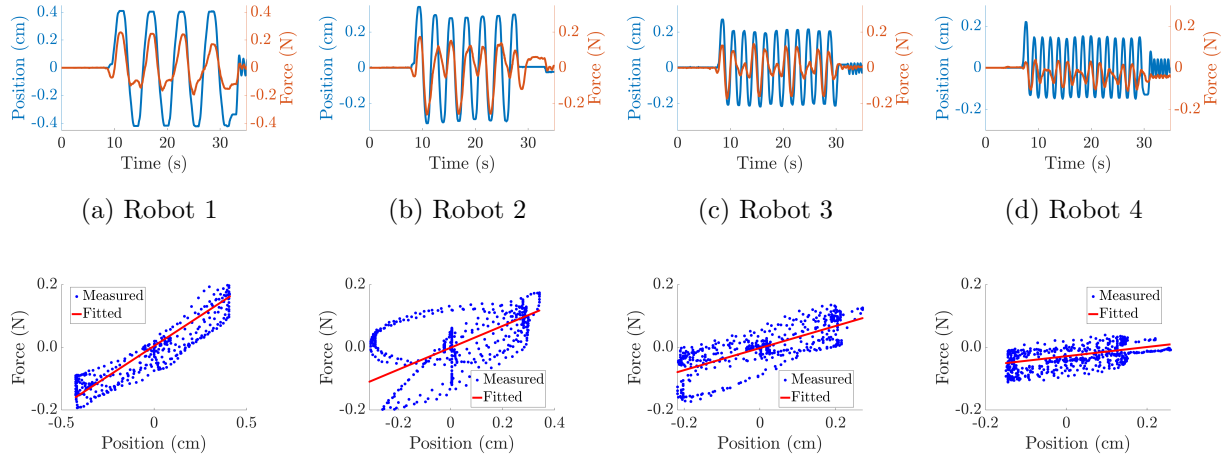


(a) Robot 1 (b) Robot 2 (c) Robot 3 (d) Robot 4

(e) Robot 1 (f) Robot 2 (g) Robot 3 (h) Robot 4

Figure 6.4: Top: Position responses of each robot during the stiffness estimation. Each robot moves in random fashion for $T_m = 20s$ while collecting the force measurement. Bottom: the relation between robot's $i \in \{1, 2, 3, 4\}$ position $\tilde{\mathbf{p}}_i$ and force $\tilde{\mathbf{f}}_i$ measurements. The local stiffness $\mathbf{k}_i$ is inferred by fitting a linear curve between the force measured and displacement during the estimation period $T_m$ as shown in Eq. (6.37).

### *6.3.3 Performance metric*

The deformation $\mathbf{D}$ during transport can be inferred from the force measurement, i.e.,

$$\mathbf{D}[m] = \mathbf{K}^{-1}\mathbf{F}[m] = \mathbf{P}[m] - \mathbf{B}_c\mathbf{p}_L[m] \tag{6.44}$$

from Eq. (6.6). Then for each robot $i$, individual deformation $\mathbf{d}_i = [d_x, d_y, d_z]^\intercal \in \mathbb{R}^3$ can be written as

$$\mathbf{d}_i[m] = \mathbf{p}_i[m] - \mathbf{p}_L[m]. \tag{6.45}$$

Then the maximum deformation $D^*$, used to quantify the transport performance, is computed by taking the Euclidean norm of the deformation $\mathbf{d}_i$ of each robot, and finding the maximum value for all time $m$ over all robots $i$, that is

$$D^* = \max_i \left\{ \max_m \|\mathbf{d}_i[m]\|_2 \right\}. \tag{6.46}$$

## *6.4 Results and Discussion*

Results and comparative evaluation of different transport approaches, without DSR and with estimated-DSR, are discussed below.

### *6.4.1 Decentralized parameter selection using local stiffness*

The process of obtaining local stiffness $\mathbf{k}_{i\{x,x\}}$ for each robot $i$ shown in the experiment uses sinusoidal motions with random frequencies. Although in general, the robots motions can follow any random trajectory as shown in Eq. (6.33). Results in Table 6.1 show that the estimated local stiffness values are similar to actual measured values. For example, the estimated local stiffness $\mathbf{k}_{1\{x,x\}}$ is $1.28 \pm 0.34$ N/cm is close to the actual measured value of 0.95 N/cm. The same can be observed for robot 2, 3 and 4 where the estimated local stiffness values $\mathbf{k}_{2\{x,x\}} = 1.09 \pm 0.18$ N/cm, $\mathbf{k}_{3\{x,x\}} = 0.88 \pm 0.29$ N/cm, and $\mathbf{k}_{4\{x,x\}} = 0.41 \pm 0.06$ N/cm, are relatively close to the actual measured vales of 0.89 N/cm, 0.90 N/cm, and 0.46 N/cm respectively. The values where the standard deviation are high, for example $\mathbf{k}_{2\{x,x\}}$

and $\mathbf{k}_{3\{x,x\}}$, indicate that more random motions by the neighboring robots that can add noise to the force measurements $\tilde{\mathbf{f}}_{2x}$ and $\tilde{\mathbf{f}}_{3x}$ since robot 2 and 3 are connected to two neighbors, as compared to robot 5. While the estimated local stiffness values shown are close the actual measured values, the accuracy of the estimation can be improved by running the estimation process for longer time period $T_m$.

### *6.4.2 DSR reduces deformation for the same settling time*

The approach with estimated-DSR reduces deformation during transport substantially as compared to the approach without DSR for the same network settling time $T_s$. As shown in Table 6.2, the deformation reduces from 6.10 cm without DSR to 1.45 cm with estimated-DSR in simulation and from 7.46±0.33 cm to 2.81±0.62 cm in experiment which are 76% and 62% of reduction in deformation respectively for the same transport time. The reduction in deformation indicates that even with decentralized parameter selection, the approach with estimated DSR still effective as compared to the approach without DSR when using centralized parameter selection. The reduction of deformation can also be visualized in Fig. 6.5, which show that the experimental results match the prediction in simulation. In addition, with estimated-DSR still ensures that each robot converges to desired trajectory within the specified network settling time $T_s = 10s$, as demonstrated in Fig. 6.6 using a step response simulation. Snapshots of the experiment are shown in Fig. 6.7.

## *6.5 Conclusion*

In this chapter, a fully decentralized approach for flexible object transport is proposed. In particular, the approach with estimated-DSR uses only local stiffness measurement to select update parameters in decentralized manner without any knowledge of the object's properties and centralized information. Therefore, the proposed approach can be implemented to any robot networks for potentially transporting different types of objects. Moreover, results in simulation and experiment show that using the proposed approach, deformation during transport is reduced significantly as compared to the standard approach without DSR by

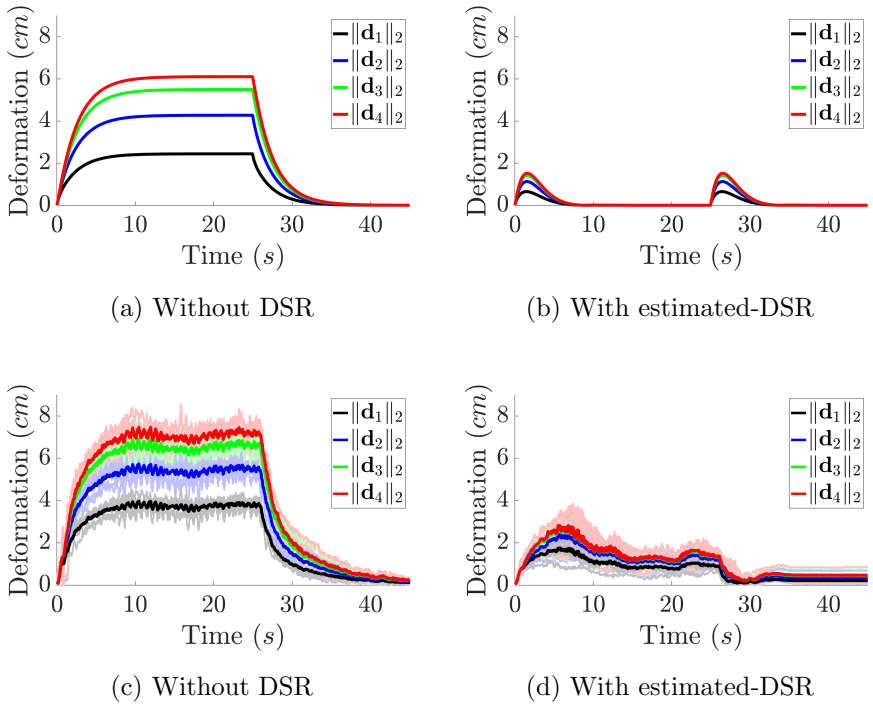


(a) Without DSR (b) With estimated-DSR

(c) Without DSR (d) With estimated-DSR

Figure 6.5: Comparative results of deformation $\|\mathbf{d}_i\|_2$ for i $\in \{1, 2, 3, 4\}$, inferred using Eq. (6.46) over time for simulation (a, b) and experiment (c, d).

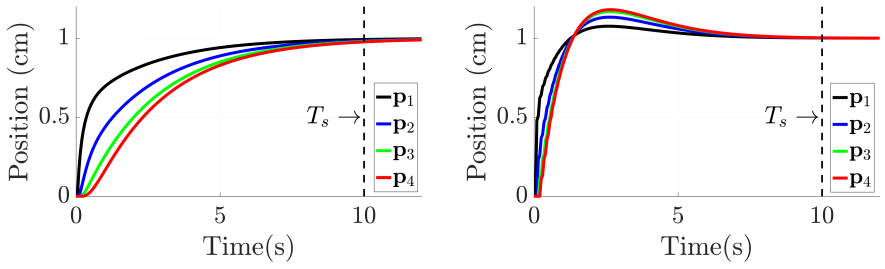


(a) Without DSR (b) With estimated-DSR

Figure 6.6: Position of the follower robots $\mathbf{p}_i$ for i $\in \{1, 2, 3, 4\}$ in response to a step in the leader's position in simulation, to show that the network settling time $T_s = 10s$ indicated by the dash line, is achieved using both approaches without DSR and with estimated-DSR.

Table 6.2: Improvement (reduction) in maximum deformation ( $D^*$) as in Eq. (6.46), using two transport methods: (i) without DSR and (ii) with estimated-DSR. Results presented for experiment with mean ($\mu$) and standard deviation ($\sigma$) over 7 experimental trials.

| **SIMULATION** | | |
|---|---|---|
| **Method** | **Deform.** (cm) | **Improve.** (%) |
| Without DSR | 6.10 | - |
| With estimated-DSR | 1.45 | 76% |
| **EXPERIMENT** | | |
| **Method** | **Deform.** (cm) | **Improve.**(%) |
| Without DSR | 7.46 $\pm$ 0.33 | - |
| With estimated-DSR | 2.81 $\pm$ 0.62 | 62 $\pm$ 8.3 % |

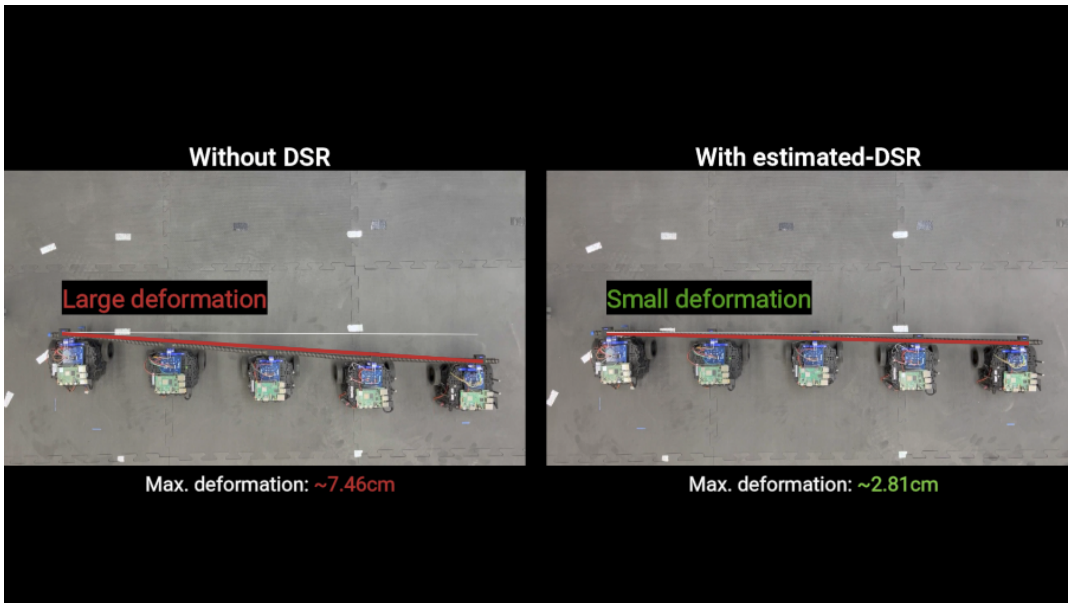


Figure 6.7: Snapshots of experiment showing deformation **D** for all transport approaches, without DSR and with estimated-DSR. The snapshots, selected from one of the seven trials for each experimental case, have deformation values closest to the mean. For the full experiment video refer to the attached supporting media.

62%. Future efforts are focused on extending the proposed approach to transport objects with much higher stiffness.

**Algorithm 2** Decentralized transport with estimated-DSR

**Require:** Place robots in the initial configuration and tare the force values

**Initialize:**
Set sampling period $\delta_t > T_r$ based on Eq. (2.1)
Set desired transport trajectory for leader $\mathbf{p}_s$
—– *Local stiffness measurements* —–
**for** $s \in \{x, y, z\}$ **do**
    Tare force sensors
    **for** $i \in \{1, 2, \ldots, n\}$ **do**
        **for** $T \in \{1, 2, \ldots, T_m\}$ **do**
            Move robot $i$ following random trajectory as in Eq. (6.33)
            Record: $f_{is}[T]$ and $p_{is}[T]$
        **end for**
        Stack force and position measurements into $\tilde{\mathbf{f}}_{is}$ and $\tilde{\mathbf{p}}_{is}$ as in Eq. (6.34)
        Compute local stiffness $\mathbf{k}_{i\{s,s\}}$ using Eq. (6.37)
        Compute the normalizing scaling factor $\mathbf{\Gamma}_i$ in Eq. (6.19)
    **end for**
**end for**
Select network settling time $T_s >> \delta_t$ based on Eq. (2.1)
—– *Gain selection with DSR* —–
Compute update gain $\alpha = 4/T_s$ as in Eq. (6.32)
Select DSR gain $\beta$ using Eq. (6.22)
—– *Update for leaders and followers* —–
**for** $m \in \{1, 2, \ldots, T\}$ **do**
    Compute $\mathbf{p}_L[m]$ based on Eq. (6.1)
    **for** $i \in \{1, 2, \ldots, n\}$ **do**
        Store: $\mathbf{p}_i[m-1]$ and $\mathbf{f}_i[m-1]$
        Record: $\mathbf{p}_i[m]$ and $\mathbf{f}_i[m]$
        Compute $\mathbf{p}_i[m+1]$ using Eq. (6.18)
    **end for**
**end for**

# Chapter 7

# SUMMARY AND FUTURE WORK

This chapter briefly provides a summary of the main contributions, and discusses some of the future works which can be pursued based on the results of the dissertation.

## *7.1 Summary*

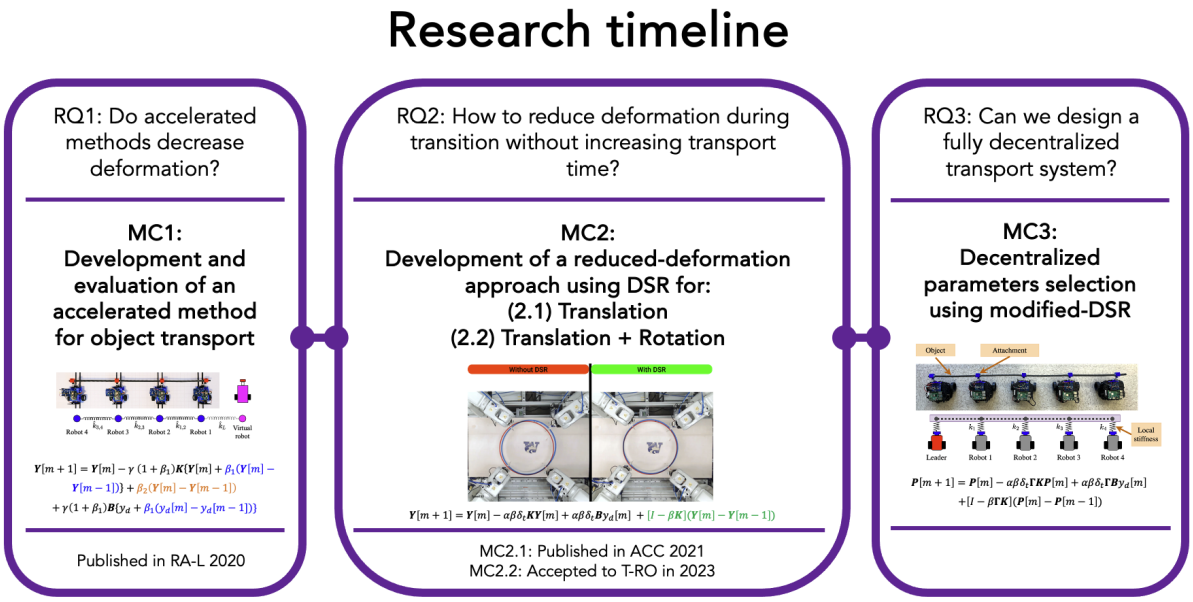


Figure 7.1: Research timeline showing the main contributions of the dissertation and resulting publications.

Summary of the main contributions of the dissertation is shown in Fig. 7.1. Details of the contributions are presented in the following.

1. Chapter 3 evaluates the use of accelerated method in decentralized robot networks to reduce deformation during transport. This chapter forms the main contribution 1

(**MC1**) of this dissertation, that is to use accelerated - delayed self reinforcement (A-DSR) to achieve faster transport using robot networks, and has been published in [1]. This work proposes the use of accelerated-gradient-based approaches, which have been used to speed up gradient-based optimization [19], to speed up transport using robot teams. Nevertheless, it is important that the increase in transport speed does not lead to excessive deformation. For example, when transporting flexible objects, such as large uncured-composite aircraft wings in a manufacturing setting, large deformations can lead to damage. Therefore in this chapter, an approach was proposed to improve the performance of flexible-object transport with a decentralized robot team. In particular, the approach used accelerated delayed self-reinforcement (A-DSR) of local force measurements to reduce the deformation during transport with the same completion time as the baseline approach without A-DSR. Moreover, A-DSR allowed reduction in completion time for the same maximum deformation. Simulation results were provided to verify the theoretical findings of the proposed approach. Finally, experimental results using four robots transporting a flexible object (spring) were presented to demonstrate the applicability of the proposed A-DSR approach.

2. Chapter 4 proposes a transport approach which uses delayed self-reinforcement (DSR) to reduce deformation during transport without increasing transport time. This chapter forms the main contribution 2.1 (**MC2.1**) of this dissertation, that is to use delayed self reinforcement (DSR) to achieve cohesive transport using robot networks, and has been published in [2]. In this chapter, an approach was presented to reduce deformation of objects during transport with decentralized robot networks. The approach used only local force measurements without additional communication, and conditions for stability were established. The proposed cohesive DSR approach was evaluated using simulation and the results closely matched the experimental results. Overall, the proposed approach led to 85% reduction in the deformation of the experimental system without increasing the time to transport the object to a new position.

3. Chapter 5 is an evolution of prior work in [2] and has been accepted to a peer-reviewed journal in [3], which presented experimental results that DSR can reduce deformation during purely translational transport where the motion of the robots is cohesive, i.e., each robot moves in the same manner in Chapter 4. This chapter presents a decentralized robotic transport approach to reduce an object's deformation during transport. Experimental results show that the proposed delayed self-reinforcement (DSR) approach significantly reduces deformation during transport without increasing the transport time — even during rotational transport where the desired robot positions depend on the geometry of the object. Analysis methods were also developed to select robot control parameters to ensure stability of the time-varying transport dynamics with the proposed DSR approach.

4. Chapter 6 develops a fully decentralized approach for transport task which includes selecting the update parameters. Typical decentralized approaches require certain level of centralized coordination or information when designing the transport system with robot network, for instance to select the update parameters. Such an approach overthrows the decentralized behavior being sought after bio-mimetic strategies and is not viable for large networks with varying number of robots. Thus in this chapter, a fully decentralized approach for flexible object transport is proposed. In particular, the approach with estimated-DSR uses only local stiffness measurement to select update parameters in decentralized manner without any knowledge of the object's properties and centralized information. Therefore, the proposed approach can be implemented to any robot networks for potentially transporting different types of objects. Moreover, results in simulation and experiment show that using the proposed approach, deformation during transport is reduced significantly as compared to the standard approach without DSR by 62%.

## *7.2 Future Work*

This section discusses potential future directions that can be pursued in regards to flexible-object transport using robot networks based on the results of this dissertation.

1. The proposed DSR-based transport approach presented in this dissertation mainly focuses on flexible-objects transport. While flexible-objects pose a challenge due to large deformation and nonlinear behavior, transporting rigid objects might pose a different challenge in regard to formulating the update law. Thus, further work can be extended to investigate the applicability of the DSR-based transport approach for rigid-objects transport.

2. The proposed DSR-based transport approach presented in this dissertation is applied to autonomous transports, i.e., the leader is autonomous. Nevertheless, certain applications might require human assistance during transport. Generally, human input introduces noise and may exhibit nonlinear dynamics. Therefore, assessing the integration of human input into the transport system with DSR is needed.

# BIBLIOGRAPHY

[1] Yoshua Gombo, Anuj Tiwari, and Santosh Devasia. Accelerated-Gradient-Based Flexible-Object Transport With Decentralized Robot Teams. *IEEE Robot. Autom. Lett.*, 6(1):151–158, January 2021.

[2] Yoshua Gombo, Anuj Tiwari, and Santosh Devasia. Communication-free Cohesive Flexible-Object Transport using Decentralized Robot Networks. In *2021 American Control Conference (ACC)*, pages 106–111, New Orleans, LA, USA, May 2021. IEEE.

[3] Yoshua Gombo, Anuj Tiwari, Mohamed Safwat, Henry Chang, and Santosh Devasia. Delayed self-reinforcement to reduce deformation during decentralized flexible-object transport. *IEEE Transactions on Robotics*, Accepted.

[4] Anuj Tiwari and Santosh Devasia. Cohesive velocity transitions in robotic platoons using nesterov-type accelerated delayed self reinforcement (a-dsr). In *2019 Sixth Indian Control Conference (ICC)*, pages 104–109. IEEE, 2019.

[5] J. Alonso-Mora, R. Knepper, R. Siegwart, and D. Rus. Local motion planning for collaborative multi-robot manipulation of deformable objects. In *2015 IEEE International Conference on Robotics and Automation (ICRA)*, pages 5495–5502, May 2015.

[6] Andrea Tagliabue, Mina Samir Kamel, Juan Nieto, and Roland Siegwart. Robust collaborative object transportation using multiple mavs. 11 2017.

[7] Z. Wang and M. Schwager. Kinematic multi-robot manipulation with no communication using force feedback. In *2016 IEEE International Conference on Robotics and Automation (ICRA)*, pages 427–432, May 2016.

[8] H. Bai and J. T. Wen. Cooperative load transport: A formation-control perspective. *IEEE Transactions on Robotics*, 26(4):742–750, Aug 2010.

[9] Behrokh Khoshnevis and George Bekey. Centralized sensing and control of multiple mobile robots. *Computers & Industrial Engineering*, 35(3):503 – 506, 1998. Selected Papers from the 22nd ICC and IE Conference.

[10] Kar-Han Tan and M. A. Lewis. Virtual structures for high-precision cooperative mobile robotic control. In *Proceedings of IEEE/RSJ International Conference on Intelligent Robots and Systems. IROS '96*, volume 1, pages 132–139 vol.1, Nov 1996.

[11] G. Montemayor and J. T. Wen. Decentralized collaborative load transport by multiple robots. In *Proceedings of the 2005 IEEE International Conference on Robotics and Automation*, pages 372–377, April 2005.

[12] A. Tsiamis, C. K. Verginis, C. P. Bechlioulis, and K. J. Kyriakopoulos. Cooperative manipulation exploiting only implicit communication. In *2015 IEEE/RSJ International Conference on Intelligent Robots and Systems (IROS)*, pages 864–869, Sep. 2015.

[13] A. Petitti, A. Franchi, D. Di Paola, and A. Rizzo. Decentralized motion control for cooperative manipulation with a team of networked mobile manipulators. In *2016 IEEE International Conference on Robotics and Automation (ICRA)*, pages 441–446, May 2016.

[14] Brian E. Jackson, Taylor A. Howell, Kunal Shah, Mac Schwager, and Zachary Manchester. Scalable Cooperative Transport of Cable-Suspended Loads With UAVs Using Distributed Trajectory Optimization. *IEEE Robot. Autom. Lett.*, 5(2):3368–3374, April 2020.

[15] Jianing Chen, Melvin Gauci, Wei Li, Andreas Kolling, and Roderich Gros. Occlusion-Based Cooperative Transport with a Swarm of Miniature Mobile Robots. *IEEE Trans. Robot.*, 31(2):307–321, April 2015.

[16] P. Culbertson and M. Schwager. Decentralized adaptive control for collaborative manipulation. In *2018 IEEE International Conference on Robotics and Automation (ICRA)*, pages 278–285, May 2018.

[17] J. E. Inglett and E. J. Rodríguez-Seda. Object transportation by cooperative robots. In *SoutheastCon 2017*, pages 1–6, March 2017.

[18] Aviram Gelblum, Itai Pinkoviezky, Ehud Fonio, Abhijit Ghosh, Nir Gov, and Ofer Feinerman. Ant groups optimally amplify the effect of transiently informed individuals. *Nature Communications*, 6(1):7729, 2015.

[19] Y. E. Nesterov. A Method of Solving a Convex Programming Problem with Convergence Rate of $O(1/k^2)$. *Soviet Mathematics Doklady*, 27(3):372–376, 1983.

[20] Yoshua Gombo, Anuj Tiwari, Mohamed Safwat, Henry Chang, and Santosh Devasia. Communication-free decentralized controller design for flexible object transport. 2023.

[21] T. G. Sugar and V. Kumar. Control of cooperating mobile manipulators. *IEEE Transactions on Robotics and Automation*, 18(1):94–103, Feb 2002.

[22] M.N. Ahmadabadi and E. Nakano. A "constrain and move" approach to distributed object manipulation. *IEEE Transactions on Robotics and Automation*, 17(2):157–172, April 2001.

[23] Charis J. Stamouli, Charalampos P. Bechlioulis, and Kostas J. Kyriakopoulos. Multi-Agent Formation Control Based on Distributed Estimation With Prescribed Performance. *IEEE Robot. Autom. Lett.*, 5(2):2929–2934, April 2020.

[24] T. Arai, E. Pagello, and L. E. Parker. Guest editorial advances in multirobot systems. *IEEE Transactions on Robotics and Automation*, 18(5):655–661, Oct 2002.

[25] Antonio Franchi, Antonio Petitti, and Alessandro Rizzo. Distributed Estimation of State and Parameters in Multiagent Cooperative Load Manipulation. *IEEE Trans. Control Netw. Syst.*, 6(2):690–701, June 2019.

[26] Sandesh Thapa, He Bai, and J.Á. Acosta. Cooperative aerial load transport with force control. *IFAC-PapersOnLine*, 51(12):38 – 43, 2018. IFAC Workshop on Networked and Autonomous Air and Space Systems NAASS 2018.

[27] Stefan Flixeder, Tobias Glück, and Andreas Kugi. Modeling and Force Control for the Collaborative Manipulation of Deformable Strip-Like Materials. *IFAC-PapersOnLine*, 49(21):95–102, 2016.

[28] Zhang Peng and Li Yuanchun. Position/force control of two manipulators handling a flexible payload based on finite-element model. In *2007 IEEE International Conference on Robotics and Biomimetics (ROBIO)*, pages 2178–2182, Sanya, China, December 2007. IEEE.

[29] Dong Sun, James K. Mills, and Yunhui Liu. Position Control of Robot Manipulators Manipulating a Flexible Payload. *The International Journal of Robotics Research*, 18(3):319–332, March 1999.

[30] Giuseppe Loianno and Vijay Kumar. Cooperative Transportation Using Small Quadrotors Using Monocular Vision and Inertial Sensing. *IEEE Robot. Autom. Lett.*, 3(2):680–687, April 2018.

[31] S. Devasia. Faster Response in Bounded-Update-Rate, Discrete-time Networks using Delayed Self-Reinforcement. *International Journal of Control*, Accepted, 2019, DOI: 10.1080/00207179.2019.1644537.

[32] Ruggero Carli, Fabio Fagnani, Alberto Speranzon, and Sandro Zampieri. Communication constraints in the average consensus problem. *Automatica*, 44(3):671–684, Mar 2008.

[33] B. Van Scoy, R. A. Freeman, and K. M. Lynch. The fastest known globally convergent first-order method for minimizing strongly convex functions. *IEEE Control Systems Letters*, 2(1):49–54, Jan 2018.

[34] S. Thapa, R. V. Self, R. Kamalapurkar, and H. Bai. Cooperative manipulation of an unknown payload with concurrent mass and drag force estimation. *IEEE Control Systems Letters*, 3(4):907–912, Oct 2019.

[35] Preston Culbertson, Jean-Jacques Slotine, and Mac Schwager. Decentralized Adaptive Control for Collaborative Manipulation of Rigid Bodies. *IEEE Trans. Robot.*, pages 1–15, 2021.

[36] Tomer Czaczkes and Ratnieks Nouvellet. Cooperative food transport in the neotropical ant, pheidole oxyops. *Insectes Sociaux*, 58:153, 05 2010.

[37] H. F. McCreery and M. D. Breed. Cooperative transport in ants: a review of proximate mechanisms. *Insectes Sociaux*, 61(2):99–110, May 2014.

[38] Andreas Björnsson, Marie Jonsson, and Kerstin Johansen. Automated material handling in composite manufacturing using pick-and-place systems – a review. *Robotics and Computer-Integrated Manufacturing*, 51:222–229, June 2018.

[39] Hamed Farivarnejad and Spring Berman. Multirobot Control Strategies for Collective Transport. *Annu. Rev. Control Robot. Auton. Syst.*, 5(1):annurev–control–042920–095844, May 2022.

[40] Spring Berman, Quentin Lindsey, Mahmut Selman Sakar, Vijay Kumar, and Stephen Pratt. Study of Group Food Retrieval by Ants as a Model for Multi-robot Collective Transport Strategies. *Robotics: Science and Systems VI*, page 8, 2011.

[41] Zijian Wang, Sumeet Singh, Marco Pavone, and Mac Schwager. Cooperative Object Transport in 3D with Multiple Quadrotors Using No Peer Communication. In *2018 IEEE International Conference on Robotics and Automation (ICRA)*, pages 1064–1071, Brisbane, QLD, May 2018. IEEE.

[42] Michael A. Neumann and Christopher A. Kitts. A Hybrid Multirobot Control Architecture for Object Transport. *IEEE/ASME Trans. Mechatron.*, 21(6):2983–2988, December 2016.

[43] Elio Tuci, Muhanad H. M. Alkilabi, and Otar Akanyeti. Cooperative object transport in multi-robot systems: A review of the state-of-the-art. *Frontiers in Robotics and AI*, 5:59, 2018.

[44] R. Olfati-Saber, J.A. Fax, and R.M. Murray. Consensus and cooperation in networked multi-agent systems. *Proceedings of the IEEE*, 95(1):215–233, Jan 2007.

[45] D. E. Rumelhart, G. E. Hinton, and R. J. Williams. *Learning Internal Representations by Error Propagation, pp. 318-362, in D. E. Rumelhart and J. L. McClelland (eds.) Parallel Distributed Processing, Vol. 1* . MIT Press, Cambridge, MA, 1986.

[46] Pin-Xian Wu, Cheng-Cheng Yang, and Teng-Hu Cheng. Cooperative Transportation of UAVs Without Inter-UAV Communication. *arXiv:2111.03283 [cs, eess]*, November 2021. arXiv: 2111.03283.

[47] Santosh Devasia. Cohesive networks using delayed self reinforcement. *Automatica*, 112:108699, 2020.

[48] Bruno Siciliano and Oussama Khatib, editors. *Springer Handbook of Robotics*. Springer Handbooks. Springer, 2016.

[49] Jose Sanchez, Kamal Mohy El Dine, Juan Antonio Corrales, Belhassen-Chedli Bouzgarrou, and Youcef Mezouar. Blind Manipulation of Deformable Objects Based on Force Sensing and Finite Element Modeling. *Front. Robot. AI*, 7:73, June 2020.

[50] Prashant Batra. A property of the nearly optimal root-bound. *Journal of Computational and Applied Mathematics*, 167(2):489–491, June 2004.

[51] C.A. Desoer. Slowly varying discrete system xi+1=aixi. *Electronics Letters*, 6(11):339 – 340, 1970.

[52] Zhong-Ping Jiang and Yuan Wang. Input-to-state stability for discrete-time nonlinear systems. *Automatica*, 37(6):857–869, 2001.

[53] Anuj Tiwari, Santosh Devasia, and James J. Riley. Low-distortion information propagation with noise suppression in swarm networks. *Proc. Natl. Acad. Sci. U.S.A.*, 120(11):e2219948120, March 2023.

[54] Sven Kurras. Variants of the graph laplacian with applications in machine learning. *Thesis, University of Hamburg*, 2017.

[55] S. A. Gershgorin. Über die Abgrenzung der Eigenwerte einer Matrix. *Bull. Acad. Sci. URSS*, 1931(6):749–754, 1931.

[56] Santosh Devasia. Rapid Information Transfer in Swarms Under Update-Rate-Bounds Using Delayed Self-Reinforcement. *Journal of Dynamic Systems, Measurement, and Control*, 141(8), 03 2019.

[57] Spring Berman, Quentin Lindsey, Mahmut Sakar, Vijay Kumar, and Stephen Pratt. Study of Group Food Retrieval by Ants as a Model for Multi-robot Collective Transport Strategies. 06 2010.

[58] H. Farivarnejad, S. Wilson, and S. Berman. Decentralized sliding mode control for autonomous collective transport by multi-robot systems. In *2016 IEEE 55th Conference on Decision and Control (CDC)*, pages 1826–1833, Dec 2016.

[59] He Bai and J. T. Wen. Motion coordination through cooperative payload transport. In *2009 American Control Conference*, pages 1310–1315, June 2009.

[60] K. Kosuge, T. Oosumi, Y. Hirata, H. Asama, H. Kaetsu, and K. Kawabata. Handling of a single object by multiple autonomous mobile robots in coordination with body force sensor. In *Proceedings. 1998 IEEE/RSJ International Conference on Intelligent Robots and Systems. Innovations in Theory, Practice and Applications (Cat. No.98CH36190)*, volume 3, pages 1419–1424 vol.3, Oct 1998.

[61] Fouad F. Khalil and Pierre Payeur. *Dexterous Robotic Manipulation of Deformable Objects with Multi-Sensory Feedback - a Review*. 03 2010.

[62] Jose Sanchez, Juan Antonio Corrales Ramon, B. Chedli BOUZGARROU, and Y Mezouar. Robotic manipulation and sensing of deformable objects in domestic and industrial applications: A survey. *The International Journal of Robotics Research*, 37:688 – 716, 06 2018.

[63] Félix Nadon, Angel Valencia, and Pierre Payeur. Multi-modal sensing and robotic manipulation of non-rigid objects: A survey. 11 2018.

[64] Yansheng Zhang, Farokh B. Bastani, and I-Ling Yen. Self-stabilizing structure forming algorithms for distributed multi-robot systems. volume 4808, pages 754–766, 12 2007.

[65] Manju Rani and Naveen Kumar. A new hybrid position/force control scheme for coordinated multiple mobile manipulators. *Arabian Journal for Science and Engineering*, 44, 09 2018.

[66] M. Lawitzky, A. Mörtl, and S. Hirche. Load sharing in human-robot cooperative manipulation. In *19th International Symposium in Robot and Human Interactive Communication*, pages 185–191, Sep. 2010.

[67] D. J. Stilwell and J. S. Bay. Toward the development of a material transport system using swarms of ant-like robots. In *[1993] Proceedings IEEE International Conference on Robotics and Automation*, pages 766–771 vol.1, May 1993.

[68] Guang-Zhong Yang, Jim Bellingham, Pierre E. Dupont, Peer Fischer, Luciano Floridi, Robert Full, Neil Jacobstein, Vijay Kumar, Marcia McNutt, Robert Merrifield, Brad Nelson, Brian Scassellati, Mariarosaria Taddeo, Russell Taylor, Manuela Veloso, Zhong Lin Wang, and Robert Wood. The grand challenges of science robotics. *Science Robotics*, 3:eaar7650, 01 2018.

[69] Y. C. Hou, K. S. M. Sahari, and D. N. T. How. Modeling of flexible deformable object for robotic manipulation. In *2016 IEEE International Symposium on Robotics and Intelligent Sensors (IRIS)*, pages 92–95, Dec 2016.

[70] Y. Cao, W. Yu, W. Ren, and G. Chen. An overview of recent progress in the study of distributed multi-agent coordination. *IEEE Transactions on Industrial Informatics*, 9(1):427–438, Feb 2013.

[71] A. Gautam and S. Mohan. A review of research in multi-robot systems. In *2012 IEEE 7th International Conference on Industrial and Information Systems (ICIIS)*, pages 1–5, Aug 2012.

[72] Zhi Yan, Nicolas Jouandeau, and Arab Ali Cherif. A survey and analysis of multi-robot coordination. *International Journal of Advanced Robotic Systems*, 10(12):399, 2013.

[73] Y. Kume, Y. Hirata, Zhi-Dong Wang, and K. Kosuge. Decentralized control of multiple mobile manipulators handling a single object in coordination. In *IEEE/RSJ International Conference on Intelligent Robots and Systems*, volume 3, pages 2758–2763 vol.3, Sep. 2002.

[74] Rachael Darmanin and Marvin Bugeja. A review on multi-robot systems categorised by application domain. 07 2017.

[75] Ali Dorri, Salil Kanhere, and Raja Jurdak. Multi-agent systems: A survey. *IEEE Access*, pages 1–1, 04 2018.

[76] Zhi Yan, Nicolas Jouandeau, and Arab Ali. A survey and analysis of multi-robot coordination. *International Journal of Advanced Robotic Systems*, 10:1, 12 2013.

[77] Eric Bonabeau, Marco Dorigo, and Guy Theraulaz. *Swarm Intelligence : From Natural to Artificial Systems / E. Bonabeau, M. Dorigo, G. Theraulaz.* Oxford University Press, 01 2001.

[78] Michael Rubenstein, Adrian Cabrera, Justin Werfel, Golnaz Habibi, James McLurkin, and Radhika Nagpal. Collective transport of complex objects by simple robots: Theory and experiments. In *Proceedings of the 2013 International Conference on Autonomous*

*Agents and Multi-agent Systems*, AAMAS '13, pages 47–54, Richland, SC, 2013. International Foundation for Autonomous Agents and Multiagent Systems.

[79] Charalampos P. Bechlioulis and Kostas J. Kyriakopoulos. Collaborative multi-robot transportation in obstacle-cluttered environments via implicit communication. *Frontiers in Robotics and AI*, 5:90, 2018.

[80] Lidia Furno, Mikkel Cornelius Nielsen, and Mogens Blanke. Centralised versus decentralised control reconfiguration for collaborating underwater robots. *IFAC-PapersOnLine*, 48(21):732 – 739, 2015. 9th IFAC Symposium on Fault Detection, Supervision andSafety for Technical Processes SAFEPROCESS 2015.

[81] Z. Xu, M. Schröter, D. Necsulescu, L. Ma, and K. Schilling. Formation control of car-like autonomous vehicles under communication delay. In *Proceedings of the 31st Chinese Control Conference*, pages 6376–6383, July 2012.

[82] Andrés Jiménez, Vicente García Díaz, and Sandro Bolaños. A decentralized framework for multi-agent robotic systems. *Sensors*, 18:417, 02 2018.

[83] S. Devasia. Accelerated consensus for multi-agent networks through delayed self reinforcement. In *2019 IEEE International Conference on Industrial Cyber Physical Systems (ICPS)*, pages 319–324, May 2019.

[84] Vicente Parra-Vega, Anand Sanchez, Carlos Izaguirre, Octavio Garcia, and Francisco Ruiz-Sanchez. Toward aerial grasping and manipulation with multiple uavs. *Journal of Intelligent and Robotic Systems*, 70:575–593, April 2013.

[85] Ning Qian. On the momentum term in gradient descent learning algorithms. *Neural Networks*, 12(1):145 – 151, 1999.

[86] D. Jakovetić, J. M. F. Xavier, and J. M. F. Moura. Convergence rates of distributed nesterov-like gradient methods on random networks. *IEEE Transactions on Signal Processing*, 62(4):868–882, Feb 2014.

[87] Yongcan Cao and Wei Ren. Multi-Agent Consensus Using Both Current and Outdated States with Fixed and Undirected Interaction. *Journal of Intelligent & Robotic Systems*, 58(1):95–106, April 2010.

[88] J. Bu, M. Fazel, and M. Mesbahi. Accelerated consensus with linear rate of convergence. In *2018 Annual American Control Conference (ACC)*, pages 4931–4936, June 2018.

[89] Hossein Moradian and Solmaz S Kia. Accelerated average consensus algorithm using outdated feedback. In *2019 18th European Control Conference (ECC)*, pages 50–55. IEEE, 2019.

[90] Hossein Moradian and Solmaz Kia. Accelerated average consensus algorithm using outdated feedback. In *2019 European Control Conference ECC, June 25-28, Napoli, Italy*, 2019.

[91] Anuj Tiwari. Cohessive network state transition for human controlled robotic multi agent systems. *PhD Thesis, University of Washington*, 2021, (expected).

[92] O. A. Bauchau and J. I. Craig. *Euler-Bernoulli beam theory*, pages 173–221. Springer Netherlands, Dordrecht, 2009.

[93] J.K. Mills and J.G.-L. Ing. Robotic fixtureless assembly of sheet metal parts using dynamic finite element models: modelling and simulation. In *Proceedings of 1995 IEEE International Conference on Robotics and Automation*, volume 3, pages 2530–2537, Nagoya, Japan, 1995. IEEE.

[94] F. Ficuciello, A. Migliozzi, E. Coevoet, A. Petit, and C. Duriez. FEM-Based Deformation Control for Dexterous Manipulation of 3D Soft Objects. In *2018 IEEE/RSJ International Conference on Intelligent Robots and Systems (IROS)*, pages 4007–4013, Madrid, October 2018. IEEE.

[95] Barbara Frank, Rudiger Schmedding, Cyrill Stachniss, Matthias Teschner, and Wolfram Burgard. Learning the elasticity parameters of deformable objects with a manipulation robot. In *2010 IEEE/RSJ International Conference on Intelligent Robots and Systems*, pages 1877–1883, Taipei, October 2010. IEEE.

[96] Fumio Hamano. Derivative of rotation matrix direct matrix derivation of well known formula, 2013.

[97] Mariah L. Schrum, Michael Johnson, Muyleng Ghuy, and Matthew C. Gombolay. Four Years in Review: Statistical Practices of Likert Scales in Human-Robot Interaction Studies. In *Companion of the 2020 ACM/IEEE International Conference on Human-Robot Interaction*, pages 43–52, Cambridge United Kingdom, March 2020. ACM.

[98] Oddgeir Friborg, Monica Martinussen, and Jan H. Rosenvinge. Likert-based vs. semantic differential-based scorings of positive psychological constructs: A psychometric comparison of two versions of a scale measuring resilience. *Personality and Individual Differences*, 40(5):873–884, April 2006.

[99] Amanda Ross and Victor L. Willson. *Paired Samples T-Test*, pages 17–19. SensePublishers, Rotterdam, 2017.

[100] Barry Johnson. Continuity of transformations which leave invariant certain translation invariant subspaces. *Pacific J. Math.*, 20(2):223–230, February 1967.

[101] Hassan K Khalil. *Nonlinear systems; 3rd ed.* Prentice-Hall, Upper Saddle River, NJ, 2002. The book can be consulted by contacting: PH-AID: Wallet, Lionel.

[102] Anuj Tiwari and Santosh Devasia. Decentralized Cohesive Response During Transitions for Higher-Order Agents Under Network Delays. *IEEE Trans. Automat. Contr.*, pages 1–7, 2022.

[103] Holly P. Hirst and Wade T. Macey. Bounding the roots of polynomials. *The College Mathematics Journal*, 28(4):292–295, 1997.

[104] John D. Renton. The beam-like behavior of space trusses. *AIAA Journal*, 22(2):273–280, February 1984.

[105] Nicole E. Carey and Justin Werfel. Collective Transport of Unconstrained Objects via Implicit Coordination and Adaptive Compliance. In *2021 IEEE International Conference on Robotics and Automation (ICRA)*, pages 12603–12609, Xi'an, China, May 2021. IEEE.

[106] Yudong Lin, Anuj Tiwari, Brian Fabien, and Santosh Devasia. Constant-spacing connected platoons with robustness to communication delays. *IEEE Transactions on Intelligent Transportation Systems*, pages 1–13, 2023.

[107] Anuj Tiwari and Santosh Devasia. Decentralized cohesive response during transitions for higher-order agents under network delays. *IEEE Transactions on Automatic Control*, 67(11):6303–6309, 2022.